

Marquette University

e-Publications@Marquette

Master's Theses (2009 -)

Dissertations, Theses, and Professional
Projects

Nematic Liquid Crystal Carbon Nanotube Composite Materials for Designing RF Switching Devices

Jeffrey Josse
Marquette University

Follow this and additional works at: https://epublications.marquette.edu/theses_open



Part of the [Engineering Commons](#)

Recommended Citation

Josse, Jeffrey, "Nematic Liquid Crystal Carbon Nanotube Composite Materials for Designing RF Switching Devices" (2022). *Master's Theses (2009 -)*. 692.

https://epublications.marquette.edu/theses_open/692

NEMATIC LIQUID CRYSTAL CARBON NANOTUBE COMPOSITE MATERIALS FOR DESIGNING RF SWITCHING DEVICES

by

Jeffrey Josse

A Thesis submitted to the Faculty of the Graduate School,
Marquette University,
in Partial Fulfillment of the Requirements for
the Degree of Master of Science (Electrical and Computer Engineering)

Milwaukee, Wisconsin

May 2022

ABSTRACT

NEMATIC LIQUID CRYSTAL CARBON NANOTUBE COMPOSITE MATERIALS FOR DESIGNING RF SWITCHING DEVICES

Jeffrey Josse

Marquette University, 2021

Radio frequency microelectromechanical systems (RF MEMS) devices are microdevices used to switch or modify signals from the RF to millimeter wave (mmWave) frequency range. Liquid crystals (LCs) are widely used as electro-optic modulators for display devices. An electric field-induced electrical conductivity modulation of pure LC media is quite low which makes it difficult to use for RF MEMS switching applications. Currently, RF MEMS devices are characterized as an excellent option between solid-state and electromechanical RF switches to provide high isolation, low insertion loss, low power usage, excellent return loss, and large frequency band. However, commercial usage is low due to their lower switching speed, reliability, and repeatability.

This research presents an electrical conductivity enhancement through the use of carbon nanotube (CNT) doping of LCs to realize a high-performance RF LC-CNT switching device. This thesis presents simulations of an RF switch using a coplanar waveguide (CPW) with a LC-CNT composite called 4-Cyano-4'-pentylbiphenyl multi-walled nanotube (5CB-MWNT) that is suitable for RF applications. The electrical conductivity modulation and RF switch performance of the 5CB-MWNT composite is determined using Finite Element Analysis (FEA). The simulations will present data on the coplanar waveguide's s -parameters at the input and output ports S_{11} and S_{21} to measure return and insertion loss respectively, two key parameters for determining any RF switch's performance.

Furthermore, this thesis presents applications for improving tunable phased antenna arrays using the LC-CNT composite to allow for beam steering with high-gain and directivity to provide a broad 3D scannable coverage of an area. Tunable antennas are an important characteristic for 5G applications to achieve an optimal telecommunication system to prevent overcrowding of antennas and reduce overall system costs. This research investigates various device geometries with 5CB-MWNT to realize the best performing RF device for RF applications and 5G telecommunication systems.

This research presents return and insertion loss data for three coplanar waveguide device configurations. The best results are shown using the standard CPW configuration. The return loss for the LC-CNT device showed a 5 dB improvement from -7.5 dB to -12.5 dB when using the LC-CNT signal line device. The insertion loss for this configuration showed a much more consistent 0 to -0.3 dB insertion loss value with much less noise when using the LC-CNT device compared to the -0.3 to -1 dB insertion loss value with heavy noise when using the Au signal line device. The other two configurations return and insertion loss showed no loss in performance when using the LC-CNT switching mechanism. This is ideal due to the benefits that the LC-CNT switching mechanism provides like device reliability and increased switching speeds.

Acknowledgements

Throughout the writing of this thesis, I have received a tremendous amount of support and guidance. The completion of my thesis would not have been possible without the continuous support of my advisor Dr. Ronald A. Coutu.

I am also extremely grateful for The Greater Milwaukee Foundation's Frank Rogers Bacon Research Assistantship, with their incredibly generous support over the years allowing me to focus on my schoolwork and thesis without having to worry about my life financially among other things. Without this financial support I cannot imagine me succeeding and making it as far in my work as I did with all things considered.

I cannot begin to express my deepest gratitude to my dad who, as a professor with many years of experience offered constant guidance, acted as an amazing resource to help me at any and every moment throughout my undergraduate and graduate career. My dad was so supportive every step of the way inside *and* outside of school to help me grow tremendously as a researcher and made me the person I am today. He helped me to learn so much about life inside and outside of school to improve my character and well-being and I wouldn't have made it this far without him.

I would also like to extend my sincere regards to Dr. Majeed M. Hayat who offered great support in many ways to help finish my thesis in a timely manner. I would like to give a sincere and special thank you to my committee members Dr. Ronald A. Coutu, Jr. Dr. Susan C. Schneider, and Dr. James E. Richie. Special thank you for your time, patience, and effort to help review my thesis and offer very insightful comments and suggestions. This insight helped me greatly as a researcher and writer for the future.

I would like to extend my gratitude to my lab and school mates Farhana Anwar, Nicholas Post, and Rafee Mahbub who were always available and provided very valuable help and resources regarding schoolwork and my thesis. Providing me with lots of reassurances on my decisions and goals as a graduate student encouraging me to complete my degree knowing that I can rely on them for help at any time.

Lastly, a very special thanks to my mom, family, friends, and loved ones who have offered so much continuous support along the way. Without them life outside of school would not have been manageable and they gave me a place of comfort to relax and fall back on when overwhelmed with my work and research. In turn, this support always provided me the much-needed headspace to continue pushing forward and succeed.

Table of Contents

Acknowledgements.....	i
LIST OF FIGURES.....	iv
LIST OF TABLES.....	viii
I. INTRODUCTION.....	1
II. BACKGROUND.....	3
2.1 Liquid Crystals.....	3
2.1.1 Liquid Crystal Phases.....	5
2.1.2 Liquid Crystal Composites.....	8
2.1.3 Optical Uses.....	18
2.2 RF Switches.....	22
2.2.1 Existing RF Switch Devices and Theory.....	23
2.2.2 Common RF Switch Materials.....	34
2.3 Coplanar Waveguides.....	37
2.3.1 Existing Coplanar Waveguide Devices and Theory.....	38
2.3.2 Common Coplanar Waveguide Materials.....	41
2.4 RF and Telecommunication Systems.....	44
2.4.1 Applications in Antenna Systems.....	46
2.4.2 RF and 5G Technology Systems.....	48
2.4.3 LC-CNT Tunable Array Application.....	49
2.5 Microelectromechanical Systems.....	52
2.5.1 Fabrication Processes.....	54
2.5.2 Material Selection for MEMS Processing.....	59
2.6 Fabrication Techniques for Microelectronics and MEMS.....	60
2.6.1 Photolithography.....	60
2.6.2 Etching.....	62
2.6.3 Deposition, Bonding, and Packaging.....	62
III. METHODOLOGY.....	66
3.1 Device structure.....	66
3.2 Working Principle of Device.....	67
3.2.1 RF Switch Operation.....	68
3.3 Design.....	69
3.4 Simulation Methods HFWorks.....	72

3.4.1 Finite Element Method	72
3.4.2 Finite Element Analysis	74
IV. RESULTS AND DISCUSSION.....	76
4.1 Design of Coplanar Waveguide in HFWorks	76
4.1.1 Material Selection in HFWorks	76
4.1.2 Coplanar Waveguide Design Types.....	80
4.1.3 Coplanar Waveguide Design Dimensions	82
4.2 HFWorks RF Finite Element Analysis.....	83
4.2.1 S-Parameters.....	86
4.2.4 Design Comparisons.....	95
4.2.5 Simulation Limitations	97
V. CONCLUSION.....	99
5.1 Summary	99
5.2 Future Works	100
BIBLIOGRAPHY	101

LIST OF FIGURES

Figure 1. States of matter in molecular form – with liquid crystals as an intermediate phase between solids and liquids by order of increasing temperature [5].	3
Figure 2. Diagram depicting basic optical property LC usage in LCDs on phones [6].	5
Figure 3. State of matter phase for LCs: (a) Liquid phase molecules orientation; (b) LCs nematic phase orientation – long axes of LC molecules aligned, but the ends are not aligned [9].	6
Figure 4. Diagram of molecule orientation in chiral LC phases: (a) Chiral Nematic phase; (b) Smectic C* (chiral) phase; (c) Chiral nematic phase showing chiral pitch [13,14].	7
Figure 5. Enlarged view of a TN liquid crystal cell denoting: (a) OFF state; (b) ON state with applied electric field [18].	9
Figure 6. Optical transmittance T vs applied voltage U(V) in 5CB/MWCNT cell with C=0.05 wt.%. The solid/dotted line denote the 60V ramp up and down respectively. The cell is shown before voltage is applied (1), 30V (2), and after voltage is off 0V (3) [20].	11
Figure 7. Electro-optical memory efficiency M and electric conductivity σ vs concentration of MWCNT C. Pure EBBA LC sample (dotted line) and EBBA/MWCNT sample (solid line). The photos show the aggregates of MWCNT at different C [20].	12
Figure 8. The most common n and p-type dopants used to create extrinsic semiconductors [31].	15
Figure 9. Electrical conductivity σ versus concentration of CNT mixture C wt.% for LC-MWCNT composite [39].	17
Figure 10. Electrical conductivity σ versus temperature of CNT mixture T measured based on heating (\rightarrow) and cooling (\leftarrow) of LC-MWCNT mixture [39]	17
Figure 11. IPS panel configuration where LC molecules are horizontally aligned with the plane of the display to allow the same picture from all viewing angles [43].	19
Figure 12. Bragg's law diagram where incident waves on a crystal surface with angle of incidence and scattering θ with path difference $d=n$ causing constructive interference resulting in color change [47].	21
Figure 13. Diagram of a single pole triple throw RF switching device with 3 inputs and 3 possible outputs for each input with switches [49].	22
Figure 14. Shows three electromechanical circuit configurations: (a) Single pole single throw (SPST); (b) Single pole double throw (SPDT); (c) Double pole single throw (DPST) [49].	25

Figure 15. Common PIN diode circuit schematics: (a) SPDT series PIN diode switch; (b) SPDT shunt PIN diode switch; (c) SPDT series-shunt PIN diode switch [51].	27
Figure 16. Schematic of a SPDT FET switch configuration [51].	28
Figure 17. Capacitive RF MEMS switch construction layers used by manufacturing company Omron [51].	29
Figure 18. A comparison of output power/insertion loss vs input power performance for a RF MEMS switch and GaAs MMIC FET switch [51].	30
Figure 19. A graphene RF/microwave NEMS switch device design with coplanar waveguide implementation [51].	31
Figure 20. A CPW device design of an electrostatically actuated switch with a capacitive shunt switch using a CPW and RF grounded contact [60].	32
Figure 21. Maturity Index for 2020 showing the maturity level of various metal manufacturing technologies. This diagram shows how commercialized a typical processing technology would be [67].	35
Figure 22. Coplanar waveguide structure showing general dimensions of importance (W , S , H , and ϵ_p) for conductor width, slot/gap width, substrate height, and effective permittivity respectively for EMF mitigation [81].	38
Figure 23. Three common coplanar waveguide configurations – CPW with one signal line and two ground plane conductors; a CPWG with one signal line, two upper layer ground conductors, and one bottom layer ground conductor; a GCPWG same configuration as CPWG with vias connecting the upper and lower ground planes [85].	39
Figure 24. Planar transmission line configurations: (a) microstrip planar transmission line structure; (b) CPWG structure with center signal line and two upper ground planes with one lower ground plane [96].	43
Figure 25. An example of an ideal via hole in a planar transmission line configuration that connects the upper and lower ground planes of a CPW device [96,97].	43
Figure 26. Telecommunication system process flow graph enabled by the semiconductor era. This diagram shows the basic transmitter analog-to-digital conversion process encoding a signal that is transmitted by an antenna. That signal is then received by another antenna, then decoded using the digital-to analog conversion processes shown [102].	45
Figure 27. Diagram of an emitting and receiving antenna telecommunication system. In the guiding device transmission line section is where a CPW device would be implemented. The guiding device is the key to a high performing telecommunication system.	46

Figure 28. An example diagram of a wireless link telecommunication system between a transmitting and receiving antenna with area and gain of transmitter and receiver labeled. As well as length of the transmission signal between both apertures.....	47
Figure 29. Design of general CPW structure for LC-CNT composite cell used for RF switching device. LC-CNT cell acts as switching mechanism with applied electric field.....	51
Figure 30. Functioning principle of a LC-CNT doped tunable phase array showing changes in permittivity will create a change in resonance frequency causing the shift in phase you see between ϵ_{r1} and ϵ_{r3} [116].....	52
Figure 31. Etching types for bulk micromachining: (a) anisotropic wet etching results; (b) isotropic wet etching; (c) DRIE [119].	55
Figure 32. Example of various planes in crystal unit cell used for anisotropic etching [120].....	56
Figure 33. Example of surface micromachining process to create membrane [121].	57
Figure 34. Example of HARM process using LIGA method [118].	59
Figure 35. Fabrication method with positive and negative photoresist patterns using photolithography [118].....	61
Figure 36. A diagram of the important role that packaging holds for commercial MEMS devices [118].....	63
Figure 37. Three common types of packaging for MEMS devices [118].	64
Figure 38. Design of general CPW structure for RF LC-CNT switching device. This device has a LC-CNT cell in the middle of the signal line to control the switching mechanism of the RF device. This is the model that this work is based around.	67
Figure 39. Various constraints of CPW device to alter RF switch parameters with W , L , and T being the width, length, and thickness of the conductors respectively. Where G and H are the width of the gaps between conductors and height of the substrate respectively. Lastly, 1 and 2 represent where the signal is fed through from port 1 to 2. [124].	69
Figure 40. Design of simulated CPW structure for LC-CNT RF switching device with Au ground lines, and Au or LC-CNT composite signal line for measurement comparison.....	70
Figure 41. A miniaturized 3D mesh analysis model of an RF coplanar waveguide shunt switch [139].....	73
Figure 42. Global mesh tolerance and frequency sweep settings used for s-parameter simulations.....	75
Figure 43. Shows the design structure of the standard simulated CPW configuration with typical dimensions used in this work. ' W_{sc}/W_{gc} , l , and t_c ' includes length, width and thickness of the	

signal and ground conductors respectively. 'h' is the height of the substrate, and 'w _{gap} ' is the width of gaps between substrates.....	80
Figure 44. Shows the design structure of the simulated CPWG configuration with the same dimensions as the standard CPW and FG-CPWG devices. This includes the length, width, and thickness of the conductors (top and bottom plane). Width of gaps between conductors, and height of substrate.....	81
Figure 45. Shows the design structure of the simulated FG-CPWG configuration without vias with different gap and top plane ground conductor widths compared to the CPW and CPWG configurations – dimensions are otherwise the same. This includes the length, and thickness of the conductors (top and bottom plane), and the height of substrate.	82
Figure 46. Shows the global mesh tolerance size versus electric field values to find the value where measurements remain consistent to avoid any errors due to too coarse of a mesh.	85
Figure 47. Example of the fine mesh created using 0.25 mm global tolerance for the various CPW device configurations.....	86
Figure 48. Comparison of return loss for standard Au signal line device and 5CB-MWNT signal line device. S-parameters simulated for CPW configuration.....	87
Figure 49. Comparison of insertion loss for standard Au signal line device and 5CB-MWNT signal line device. S-parameters simulated for CPW configuration.....	88
Figure 50. Comparison of return loss for standard Au signal line device and 5CB-MWNT signal line device. S-parameters simulated for CPWG configuration.	89
Figure 51. Comparison of insertion loss for standard Au signal line device and 5CB-MWNT signal line device. S-parameters simulated for CPWG configuration.	90
Figure 52. Comparison of return loss for standard Au signal line device and 5CB-MWNT signal line device. S-parameters simulated for FG-CPWG configuration.....	91
Figure 53. Comparison of insertion loss for standard Au signal line device and 5CB-MWNT signal line device. S-parameters simulated for FG-CPWG configuration.....	92
Figure 54. Comparison of return loss for standard Au signal line device and 5CB-MWNT signal line device in OFF state. S-parameters simulated for CPW configuration.....	93
Figure 55. Comparison of insertion loss for standard Au signal line device and 5CB-MWNT signal line device in OFF state. S-parameters simulated for CPW configuration.....	94

LIST OF TABLES

Table 1. Performance and characteristics comparison of electromechanical relay (EMR) vs solid-state PIN diode and FET vs MEMS RF and microwave switches [60].	33
Table 2. Advantages and disadvantages of a RF MEMS switch parameters design [60].	33
Table 3. Key material properties of the possible RF MEMS switch materials showing various material parameters as it relates to performance of RF MEMS switches [68,74].	37
Table 4. Various commercial applications of MEMS devices in various fields [118].	54
Table 5. Characteristics and values for various LC and chiral dopant media as it relates to material selection for 5CB-MWNT in this research [128].	71
Table 6. Properties and parameter values of various LC and chiral dopant as it relates to material selection for 5CB-MWNT in this research [129].	71
Table 7. Silicon material parameters used for device substrate.	77
Table 8. 5CB-MWNT composite material parameters used for Si substrate doping.	78
Table 9. Gold material parameters used for device signal and ground lines.	79
Table 10. General mesh characteristics for waveguide devices.	84
Table 11. Average device losses for Au and 5CB-MWNT signal lines. Signal lines were entirely Au or 5CB-MWNT due to simulation constraints discussed in 4.2.5. Overall, the total losses were fairly high between both materials. Enough to contribute to the larger insertion loss results for the antenna study.	96

I. INTRODUCTION

Microelectromechanical systems (MEMS) have a wide variety of high frequency applications with their ability to produce radio frequency (RF) electronic devices ranging from high frequency (HF) to ultra-high frequencies (UHF) [1]. An RF switch is a device that is able to route HF and UHF (tens of MHz to tens of GHz) through transmission lines. RF switches are used commonly in wireless telecommunication system technology namely with cellular and satellite communications. With this comes a need for RF switches to have most importantly, low insertion loss, high switching speed, and good reversibility. To achieve these device parameters a material needs to be investigated that shows a sharp change in resistivity in response to an external stimuli to realize this type of high-performance RF switch [2]. Liquid crystals (LCs) are a kind of adaptive optics commonly used in various electro-optical, imaging and display technologies due to their tunability.

In this research, the conductivity modulation of LC-CNT composites is used in RF switching applications. An application that is investigated in this research is a power and cost-efficient steerable LC-based phased array for 5G telecommunication systems. This is done using a coplanar waveguide (CPW) device that can provide us with UHF responses, we can ensure that there are no parasitic discontinuities in the ground plane [3]. With a CPW we can use a LC-CNT composite as the switching mechanism in order to achieve a high-speed switching response with high isolation in the UHF range where 5G frequency bands operate.

A second similar application with a RF LC-CNT switching device would be satellite communication in aerospace engineering. The goal of an RF switch is optimizing the communication functionality by reliably routing RF signals. Additionally, aerospace-based

communications have a need for tunable antennas that would be able to support multiple frequency bands and bandwidths. Tunable antennas are achievable through creating an omnidirectional antenna, where RF switches are the essential building blocks for these tunable arrays [4].

The following chapter will discuss the background of liquid crystals, along with existing theory, design, and background on RF Switches, Coplanar Waveguides, and tunable antennas or arrays. It will also provide the background information necessary to design and simulate an RF switching device using a LC-CNT composite as the switching mechanism that can achieve the desired applications. Chapter 3 will briefly discuss the fabrication process behind the proposed device via MEMS fabrication processes, material selection criteria and theory, micromachining process steps, and common RF switches. Chapter 4 will discuss the design and simulation that will be done via the finite element method (FEM) through a software called HFWORKS a simulation addon inside SOLIDWORKS that enables 3D field simulation for RF, microwave, and wireless applications. It also allows for antenna calculation along with tuning elements, and waveguides. Chapter 5 includes simulation procedure, design calculations and results. The procedures behind the actual device and collected data will be discussed in detail here. Lastly, in Chapter 6, the summary and conclusion will discuss possible modified design proposals and compare with our and others' existing designs.

II. BACKGROUND

This chapter offers background information about liquid crystals and nanoparticle composites and their properties. RF switch and coplanar waveguide theory, material, and design are discussed. With this in mind, a brief overview of RF applications with 5G technology and telecommunication systems will also be discussed. MEMS fabrication processes along with material selection are discussed. Then finally, common MEMS fabrication techniques used for microelectronics such as photolithography, deep reactive ion etching (DRIE) and bonding/packaging will be discussed briefly.

2.1 Liquid Crystals

Liquid crystal is an intermediate phase that is between isotropic structure liquid and crystal structure solid, and is distinct from the solid, liquid, or gas state of matter. This intermediate phase of LCs is also called a mesophase (Figure 1) [5]. Liquid crystals can flow like a liquid; however, its molecules can be aligned in a crystal lattice-like structure.

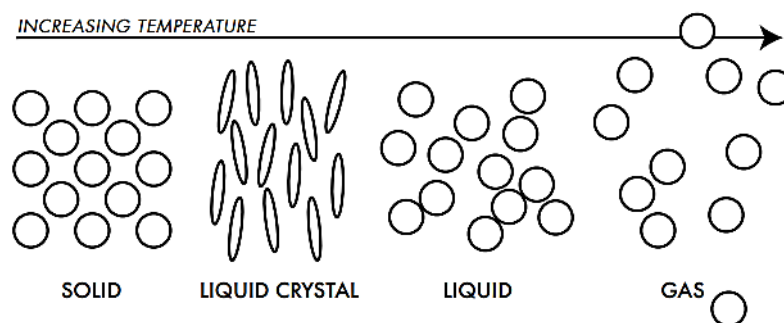


Figure 1. States of matter in molecular form – with liquid crystals as an intermediate phase between solids and liquids by order of increasing temperature [5].

Within LCs naturally occurring mesophase there are many different types of distinct LC phases that are determined by the various electro-optic properties the LCs offer. These electro-optic properties are why LCs can be used in devices that use liquid crystal displays (LCDs) (Figure 2) [6]. These also have a wide variety of temperature applications based on these distinct LC phases such as thermometers, semiconductor analysis, and tunable lenses for adaptive optics [7]. These distinct LC phases come from how the LC molecules are able to be oriented in various directions.

LC material is not always in its naturally occurring mesophase just as water can be ice or water vapor. Naturally, LCs have anisotropic geometry and have a common rod or disc like shape. Rod shaped LC molecules have anisotropic geometry which allows for preferential alignment in a desired direction [8]. LC molecules in a group can have either isotropic or anisotropic orientations which is also known as the nematic LC phase. This molecule orientation one of the most defining features of an LC molecule - its ability to exhibit different magnetic, electrical, and optical properties based on its orientation.

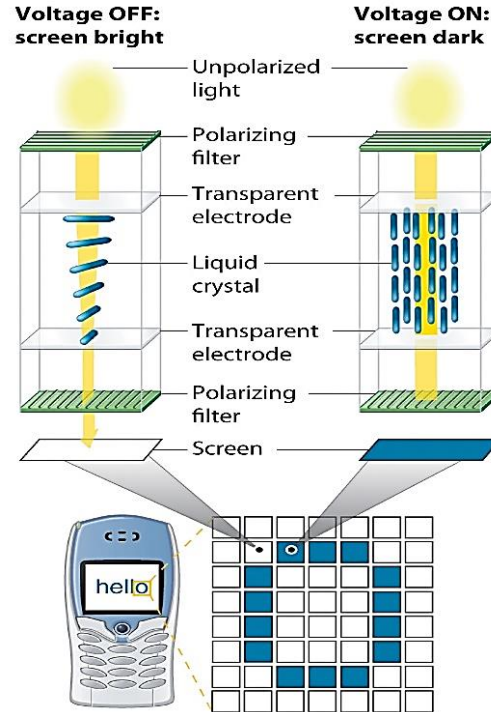


Figure 2. Diagram depicting basic optical property LC usage in LCDs on phones [6].

2.1.1 Liquid Crystal Phases

The nematic LC phase is one of the most common and important LC phases. In this phase the LCs 'self-align' anisotropically but with no positional order along the horizontal axis of the molecule's. During this nematic phase the LCs molecules are free to move while each molecules center of mass is randomly distributed along the vertical axis in no particular layer, similar to a liquid but retaining the anisotropic orientation (Figure 3) [9].

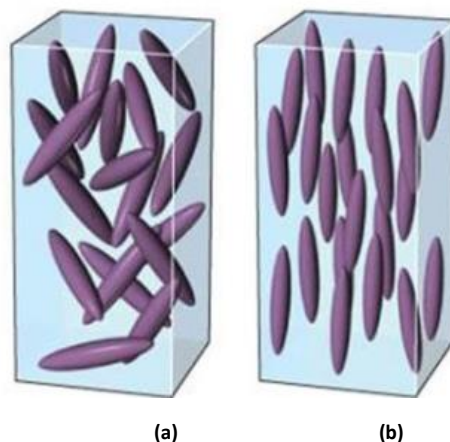


Figure 3. State of matter phase for LCs: (a) Liquid phase molecules orientation; (b) LCs nematic phase orientation – long axes of LC molecules aligned, but the ends are not aligned [9].

In this nematic phase molecules have fluidity similar to isotropic molecules in a liquid, however comparatively the LCs can easily be reoriented by an external magnetic or electric field unlike the isotropic liquid. When this reorientation occurs, aligned nematic molecules gain the optical properties of uniaxial crystals – a transparent crystalline material where the refractive index of the optic axis is different from the other two crystal axes which is what makes LCs very useful in devices with liquid-crystal displays (LCD) [10-12]. Due to LCs unique electrical and physical properties they are widely used in scientific and technical applications, where most of the research is focused on the electro-optic (EO) properties. The reason behind their wide usage is due to EO properties being associated with the orientation or ‘switching’ of LC molecules in an electric field which can be affected by external stimuli. This ‘switching’ does not require light to be emitted and only redirects the passing of light through the electrodes and polarizers. In turn this makes EO switches extremely useful for non-display type applications, such as tunable color filters, tunable lenses, optical computing, and most importantly telecommunication for steerable antennas and antenna arrays [7].

Another common and arguably more important LC phase used for their EO effect is the chiral or twisted nematic phase also known as the cholesteric or smectic C phase (Figure 4) [13,14]. The twisted nematic phase displays chirality (handedness). In this phase there is a twisting of the molecules perpendicular to the rod shape molecules original horizontal axis. The molecules have positional ordering in a layered structure as is the same with other smectic phases. In the twisted nematic phase, the LC molecules are all tilted by a finite angle in respect to the axis parallel to the original horizontal axis in what is known as the chiral pitch. The chiral pitch is the distance 'p' (figure(4c)) in which the LC molecules go through a complete 360° twist, however the structure of a chiral nematic phase repeats every half pitch (figure(4c)). The pitch increases or decreases typically with temperature or the addition of a dopant when various molecules are added to the original LC structure [15]. This means an achiral (non-handedness) LC system may form the chiral nematic phase if properly doped with a chiral material. This doping will cause these systems to produce unique optical properties. When these achiral nematic phase LC systems are doped with chiral molecules (twist agents), the LC molecules adopt the helical orientation known as the chiral nematic (N*) phase which are the most commonly researched and scientifically used technologies of LCs [11].

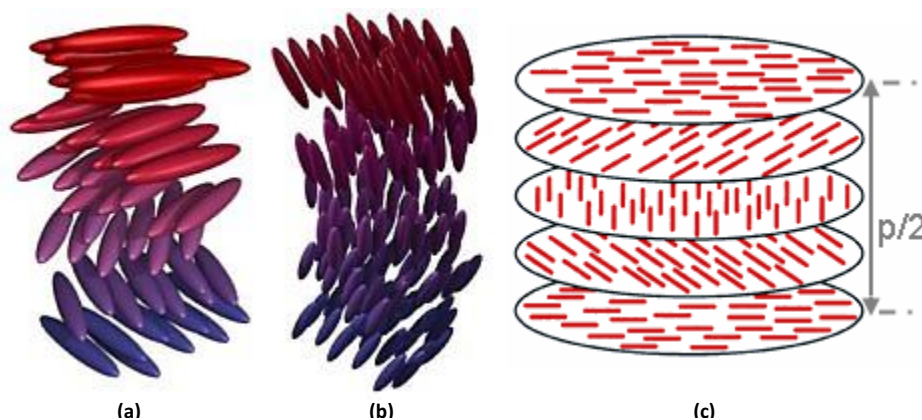


Figure 4. Diagram of molecule orientation in chiral LC phases: (a) Chiral Nematic phase; (b) Smectic C* (chiral) phase; (c) Chiral nematic phase showing chiral pitch [13,14].

2.1.2 Liquid Crystal Composites

It is very possible for chiral LC composites to create what are essentially achiral mesophases, dependent on the range of concentrations and molecular weights used. It has been observed that there is a formation of chiral mesophases from achiral LC molecules. In any given LC sample the various domains will have opposite handedness (achiral ordering). It is observed that within these domains the LC molecules have strong chiral ordering and have shown that the molecules stack and orient themselves in layers [16]. Another way to control chirality is to incorporate a chiral dopant which is where the 'twisted' nematic phase is born. These twisted nematic mixtures often contain a small amount of any given chiral dopant.

LCs find use in LCDs that rely on the various optical properties of LC molecules in the presence or absence of an electric field. The alignment of LCs is chosen so that its natural state (relaxed phase) is a twisted one known as the twisted nematic field effect. The twisted nematic field effect is the precise controlled realignment of liquid crystal molecules between various ordered molecular arrangements, while under the influence of an applied electric field (Figure 5) [12,17,18]. Twisted nematics (TN) panels became an important technology using LCs due to their low power consumption, and low operating voltages. The advantages of using TN are fast response times, and wide temperature ranges. Because of these advantages, new classes of liquid crystal materials were developed to keep up with the development and usage of TN into current capabilities we use and see every day [17,19].

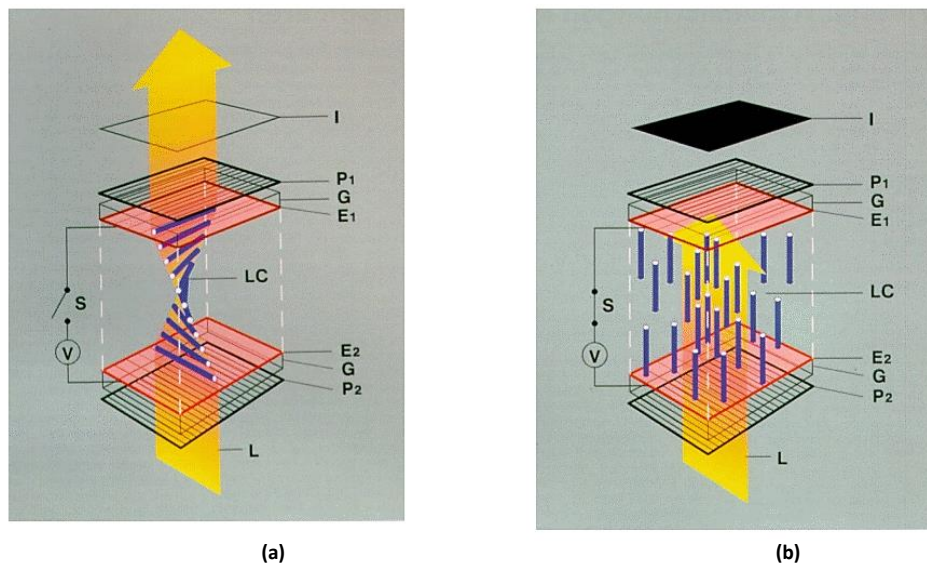


Figure 5. Enlarged view of a TN liquid crystal cell denoting: (a) OFF state; (b) ON state with applied electric field [18].

Various LC composites were investigated during this research to realize a high-performance RF switch by altering the electro-optic effects of liquid crystals. The main LC composite investigated in this research was the LC-CNT composite. Research has been aimed at altering the properties of LCs to improve EO effects for telecommunication in recent years by means of doping the LC matrix. Modifying the physical properties of LCs by introducing suitable nanomaterials into the LC host matrix may allow for improved device performance and lifetime, faster switching speeds, and better reversibility [7]. The goal of a LC-CNT composite is to reduce the threshold voltage, enhance the electrical conductivity and elastic constants. Completing any of the above goals will improve RF device performance when using an LC-CNT composite. It is shown that multi-walled carbon nanotubes (MWCNT) introduced into a LC matrix decreases the orientational order time (increase in switching speed), increases electrical conductivity, and lowers the threshold voltage [20]. However, nematic liquid crystal (NLC) composites are also

known to show irreversibility at high concentrations. This irreversibility is called the electro-optic memory effect – an effect caused by the incomplete relaxation of LC molecules back to their initial off state after the electric field is removed. This effect can persist for more than a month compared to a pure LC matrix [7,20,21]. This effect is to be considered when applying an electric field to LC molecules to reorient them as desired.

Parallel alignment of single-walled carbon nanotubes (SWCNT) or MWCNT can be achieved by dispersion of nanotubes into a self-orientating anisotropic fluid, such as NLC. By using this reorientation of liquid crystals, the nanotube's alignment can be controlled by an applied external electric field. By using SWCNT or MWCNT we can verify this reorientation behavior for two geometrically complementary systems. In turn this reorientation behavior using SWCNT or MWCNT demonstrates an electrically controlled CNT ON and OFF switch [22]. As seen in figure 6 the electro-optical cell configuration with two electrodes where the electric field is applied there is a 'brightening' of these areas after the electric field is introduced in picture 3 of the two electrodes. This suggests that the cell to some extent memorizes the optical state that was created with the electric field in picture 2 of the electrodes, showing that this sample exhibits the effect of electro-optical memory [20].

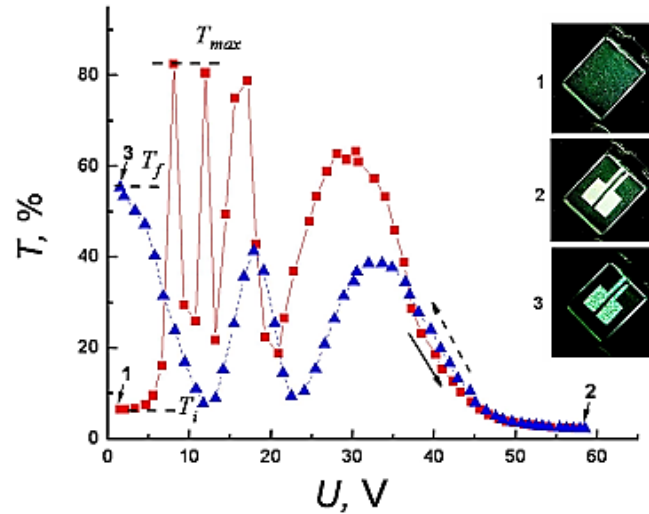


Figure 6. Optical transmittance T vs applied voltage U (V) in 5CB/MWCNT cell with $C=0.05$ wt.%. The solid/dotted line denote the 60V ramp up and down respectively. The cell is shown before voltage is applied (1), 30V (2), and after voltage is off 0V (3) [20].

The electro-optical memory effect is much stronger at higher concentrations of SWCNT and MWCNT. The effectiveness of electro-optical memory sharply increases with an increase in concentration of the sample and reaches maximum effectiveness at $C \approx 0.05$ wt. % and gradually decreases to zero with a further increase of CNT concentration with a sharp decline in electrical conductivity as well (figure 7) [20]. This development is important to note as the material parameters used for this work were defined based on a LC-CNT composite with 'C' greater than threshold in figure 6 and in figure 7 below. Using a LC+MWNT composite with greater than 0.05 wt. % is when the effectiveness of the memory effect has decreased drastically.

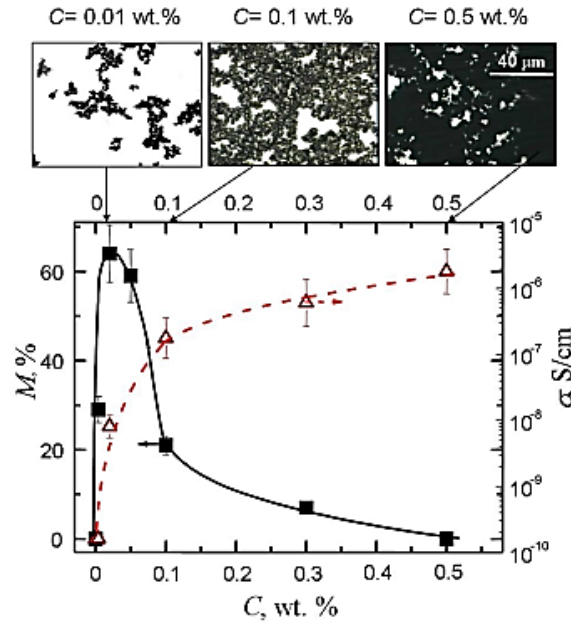


Figure 7. Electro-optical memory efficiency M and electric conductivity σ vs concentration of MWCNT C . Pure EBBA LC sample (dotted line) and EBBA/MWCNT sample (solid line). The photos show the aggregates of MWCNT at different C [20].

The electro-optic memory efficiency strongly depends on the history of a system, operating voltages, and how long the system was exposed to the electric field, t . Voltages that exceed the threshold voltage of switching V_{th} led to a stronger electro-optic memory, however, at low voltages $M \approx 0$ even when the electric field has been active for a long time (greater than 5 minutes). When the applied voltage $V > V_{th}$ the efficiency M increases as a function of saturation time t . This effect is exponential, as the higher the voltage applied the faster the saturation time is reached. The saturation value of M is approximately the same for $V > V_{th}$ [21,23]. Similar to concentration amount of the sample the applied voltage has a great effect on the effectiveness of the electro-optical memory effect. So, the amount of applied voltage was also taken into consideration for the simulations in this work.

To reduce or remove the electro-optic memory effect in this process there are several options. One; drastically lower the concentration of the pure LC media which leads to low conductivity. Two; applying a mechanical stress to the cell. Three; heating the cell above the temperature of the isotropic-nematic transition (OFF state) and subsequently cooling the cells to their nematic state. Four; applying a very high electric field $V > V_{th}$ voltage at a low frequency ($f < 1 \text{ Hz}$) [20,23].

Aside from reversibility and switching speed another point of interest is increasing the electrical conductivity of switching with LC-CNT done by electric field induced conductivity modulation. Pure LC is a dielectric material, meaning that an LC system will act as a capacitor. When an electric field is applied to an LC system there is only a displacement current – not an electric current of moving charges, but a time-varying electric field defined by the following formula:

$$D = \varepsilon_0 E + P \quad (1)$$

Equation (1) defines the electric displacement field D is defined where ε_0 , is the permittivity of free space, then E , is the electric field intensity, and P , is the polarization of the medium. Differentiating equation (1) with respect to time defines the displacement current quantity, $\frac{\partial D}{\partial t}$, which has two components in a dielectric:

$$J_D = \varepsilon_0 \frac{\partial E}{\partial t} + \frac{\partial P}{\partial t} \quad (2)$$

$$D = \varepsilon E, \varepsilon = \varepsilon_0 \varepsilon_r \quad (3)$$

In equation (2) for displacement current density, J_D , the first term $\varepsilon_0 \partial E / \partial t$ is shown in material and in free space mediums. It doesn't necessarily come from any *actual* movement of charges, but has an associated magnetic field, just as a current does due to charge motion.

Some works have applied 'displacement current' to just this first term. The second term $\partial P/\partial t$ comes from the change in polarization of the individual molecules of the dielectric material (LCs). This polarization occurs under the influence of an applied electric field when the charges in molecules have moved and the positive/negative charges in molecules separate. In the case of a simple dielectric material equation (3) holds true [24-26].

With the above equations and theory, the electrical conductance and capacitance of LC molecules can be modeled for high-voltage and low-voltage regions using the following equation:

$$C = \omega C_0 \varepsilon'_\gamma \quad G = \omega C_0 \varepsilon''_\gamma \quad \gamma = \begin{cases} \perp & \text{for } V < V_{th} \\ \parallel & \text{for } V \gg V_{th} \end{cases} \quad (4)$$

Here $C_0 = \varepsilon_0 A/d$ describes the capacitance where A is the area of the electrodes and d is the distance between those electrodes, $\omega = 2\pi f$ is angular frequency – whereas the frequency increases the current flowing through the capacitor increases commonly called capacitive reactance, and ε' and ε'' are the real and imaginary parts of the dielectric constant respectively [27,28]. The dielectric constant of a liquid crystal is shown as:

$$E = \varepsilon_\perp \cos^2\theta + \varepsilon_\parallel \sin^2\theta \quad (5)$$

In equation (4) It is shown that for voltages $V \ll V_{th}$ the dielectric constant of the cell is equal to the ε_\perp term as the LC director. The LC director is defined by the rod-shaped LC molecules with long axes that are aligned approximately to each other. A dimensionless unit vector n called the director is introduced to denote the preferred direction of orientation of LC molecules in a system at any given time [29]. For voltages $V \gg V_{th}$ the dielectric constant of the cell is equal to ε_\parallel where the LC director is then aligned parallel to the direction of the electric field creating the ON state for devices and switches [28,30].

Pure LC materials act as intrinsic semiconductors because there is no free charge carrier or conductive path between electrodes, which means the electrical conductivity modulation from external stimuli (i.e., temperature, and electric or magnetic field) is naturally very low. Undoped LCs therefore have a less desirable use for RF switching applications. The solution is to add a nanoparticle to the LC system to increase the resistivity ratio for switching [30,31].

To increase electrical conductivity, nanoparticle dopants can be added to create an extrinsic semiconductor. What makes extrinsic semiconductors in MEMS sensors so valuable in electronics and various device applications is that their high electrical conductivity can be continuously varied through the controlled addition of dopant atoms into the crystal lattice structure. This process is what allows the silicon device to be used to control electrical current in electronic devices controlling the OFF and ON states – namely switches [31]. In figure 8 we can see a list of elements that commonly create extrinsic semiconductors, one element of importance to note in this research is carbon:

	IIIA	IVA	VA	
	Boron 5 B 10.811	Carbon 6 C 12.011	Nitrogen 7 N 14.007	
P-type Dopants	Aluminum 13 Al 26.982	Silicon 14 Si 28.086	Phosphorus 15 P 30.974	N-type Dopants
	Gallium 31 Ga 69.723	Germanium 32 Ge 72.64	Arsenic 33 As 74.922	
	Indium 49 In 114.82	Tin 50 Sn 118.71	Antimony 51 Sb 121.76	
	↑ Elemental Semiconductors			

Figure 8. The most common n and p-type dopants used to create extrinsic semiconductors [31].

Through doping pure LCs that have naturally low electrical conductivity, a two to four order magnitude increase in electrical conductivity can be realized [28,30]. In an electric field, LC molecules orient themselves based on the voltage applied. During this orientation LC molecules can orient guest molecules with them through elastic potential energy interaction – when molecules begin twisting due to external stimuli, they start a ‘rubber band’ effect. Once that stimulus is removed, they return to their original position [30,32]. CNTs can alter the chemical and physical properties of the LC matrix changing its transition temperature, threshold voltage, dispersion quality, etc. These chemical and physical property alterations can lead to faster electro-optic responses by altering the dielectric anisotropy and changing the orientation of the LC systems nematic director. External stimuli like electrical, magnetic, thermal, and optical excitations interact directly with LC molecules and LC molecules elastically interact with nanoparticles, meaning there is no change in the nanoparticle properties themselves [30,32-36]. This is best as we do not want to alter the already ideal properties of the nanoparticles themselves.

When the concentration of a LC-CNT mixture reaches the percolation threshold the electrical conductivity increases by 2 to 4 orders of magnitude or higher (figure 9). The percolation threshold is when, during a mixture between a dielectric component and metallic (nanoparticle) component, the dielectric constant and conductivity of the mixture show a critical behavior. This percolation threshold transition creates a continuous path of conduction creating a very efficient extrinsic semiconductor [37-40].

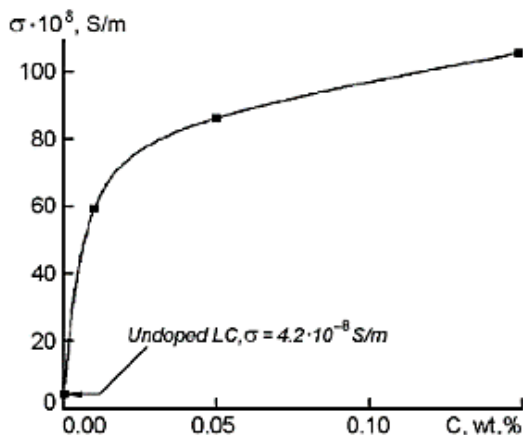


Figure 9. Electrical conductivity σ versus concentration of CNT mixture C wt.% for LC-MWCNT composite [39].

It is also shown that the electrical conductivity is affected by the temperature of the LC-CNT mixture as shown in figure 10 [39]. When the temperature increases so does the electrical conductivity, and vice versa. Ideally, you cannot increase or decrease the temperature too much because outside of the temperature range shown in figure 10, the LC molecules will begin to liquify or solidify respectively.

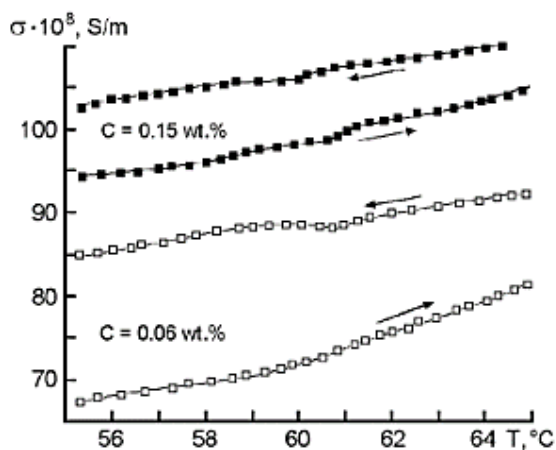


Figure 10. Electrical conductivity σ versus temperature of CNT mixture T measured based on heating (\rightarrow) and cooling (\leftarrow) of LC-MWCNT mixture [39]

If you superimpose any given mixtures heating and cooling phases, the hysteresis behavior is observed. It is seen that as the mixture concentration approaches the critical percolation threshold, the hysteresis of the sample increases as well. As the temperature increases towards the liquid phase transition temperature the discontinuity between heating and cooling phases as shown in figure 10, disappears. This is significant for LC-CNT composite because it shows that high temperatures affect the electrical conductivity order magnitude greatly and avoid hysteresis problems that cause the irreversibility due to the electro-optic memory effects for the switching device. Temperature also greatly effects the arrangement of LC molecules based on the orientation of their director [30,37-39].

2.1.3 Optical Uses

As previously mentioned, LCs have many various applications and their most common is optical usage that is based around their unique EO effects in the presence or absence of external stimuli (electric, magnetic field, temperature change etc.). In a typical LCD, the liquid crystal layer is sandwiched between two polarizers. Polarizers are optical filters that allow light waves of specific orientations (or polarizations) to pass through while blocking out all other light waves with different polarizations [41,42]. The alignment of the LC molecules is chosen so that its natural state is OFF based on the twisted nematic field effect. This common TN field effect has been used for optics seen in various TN displays for digital watches, TVs, and most commonly computer screens [17]. The TN phase reorients light waves that have passed through the first polarizer, twisting them to allow passage through the second polarizer. This reorientation of light causes an LCD to appear transparent. When the electric field is applied the LC molecules do not reorient the light waves anymore. The light waves instead get absorbed at the second polarizer. During this process the LCD begins to lose the transparency as the applied voltage

increases towards the threshold voltage, this is how an applied electric field causes an image on a screen. When pixels switch between transparent or opaque based on the applied electric field. A singular pixel is made of 3 subcategories of red, green, and blue (RGB) allowing for color on LCDs, with the use of color filters you're able to achieve the vivid LCDs we have today [12,41,42].

Along with TN panels there is another popular display device called in-plane switching (IPS) panels that were designed to eliminate some of the drawbacks of TN panels. These advantages include increased viewing angles, and color accuracy and consistency. As shown in figure 11 the setup is similar to TN panels with two polarizers sandwiching an LC layer, however the electrodes both lay in the bottom layer of the glass substrate on the left and right of the LC layer [43]. The LC molecules are aligned in a horizontal layer configuration which gives the LCs the ability to then shift horizontally. This shifting pattern of liquid crystals is the defining trait of IPS panels enabling their better viewing angles and color accuracy/consistency [44].

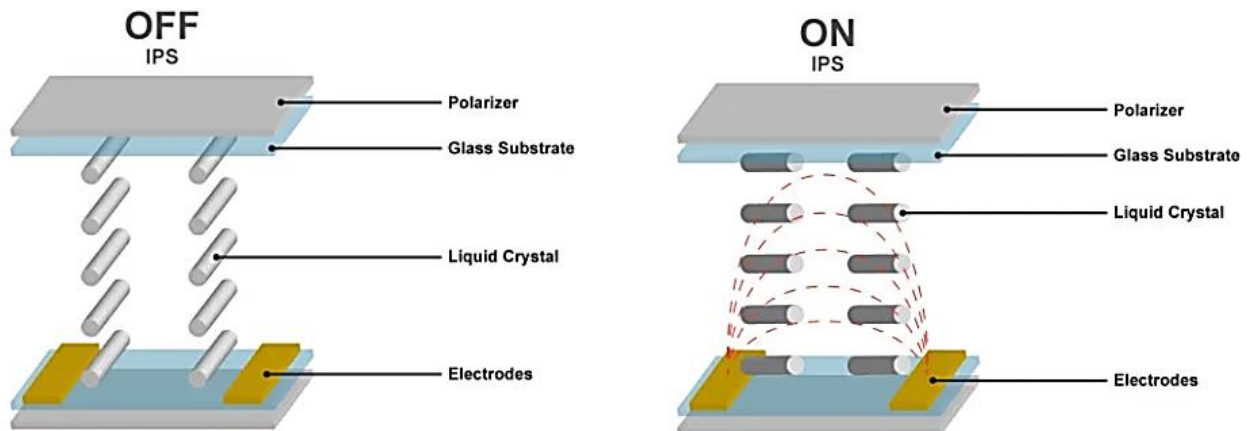


Figure 11. IPS panel configuration where LC molecules are horizontally aligned with the plane of the display to allow the same picture from all viewing angles [43].

The advantage of IPS panels means that it is very useful for graphic designers, photographers, and engineers using modeling software. The only potential downside with IPS monitors is possibly more motion blur and below average static contrast ratio due to the monitor's backlighting, however over the years these drawbacks have drastically improved and are usually only prevalent in older lower-end monitors [43,44].

As previously discussed, liquid crystals change phase orientation based on temperature. This means that LCs can be used as various types of thermometers. This is done using thermotropic (temperature dependent) chiral LCs whose chiral pitch changes greatly with temperature. It should be noted that a liquid crystal is a mesophase meaning if temperatures become too high the LC molecules will transition to an isotropic liquid phase, and if the temperature becomes too low the LC molecules will transition to a crystalline glass-like solid phase [5,7].

Thermotropic LCs have color transitions based on temperatures, so they have applications as aquarium, and pool thermometers, and beverage temperature indicators - color changing baby bottles, coffee mugs, kettles, etc. LCs also experience color transitions when stressed or strained, meaning LC sheet layers can be used to monitor heat flow, stress/strain distribution and affects, etc. When LCs are used as a fluid, they can detect electrically generated hot spots for failure analysis – a practice commonly used in the semiconductor industry [45,46]. LC color change is dependent on selective reflection of certain wavelengths of light based on the crystalline structure of the LC material as applied temperature change goes from crystalline glass-like solid at low temperature, to TN or chiral phase as an anisotropic LC, to the isotropic liquid phase at high temperature. Through this entire transition only the TN mesophase of LCs have the thermotropic property causing the effective applied temperature range to be quite restricted [45]. The TN phase has LC molecules oriented with their director's typically parallel in

layers where they frequently change orientation, this gives them periodic spacing. When light passes through an LC crystal structure it undergoes Bragg diffraction – based on Bragg’s law that gives the angles for scattering of light waves in a crystal lattice. As shown in figure 12, the law shows that when waves are incident onto the crystals surface, its angle of incidence θ will reflect with the same angle of scattering θ . When the path or plane difference of atoms in the crystal structure $d = n (\text{wavelength})$; where $n = 1,2,3, \dots$ whole number a constructive interference will occur, the wavelength with the largest constructive interference is reflected back which is then perceived as a spectral RGB color [47].

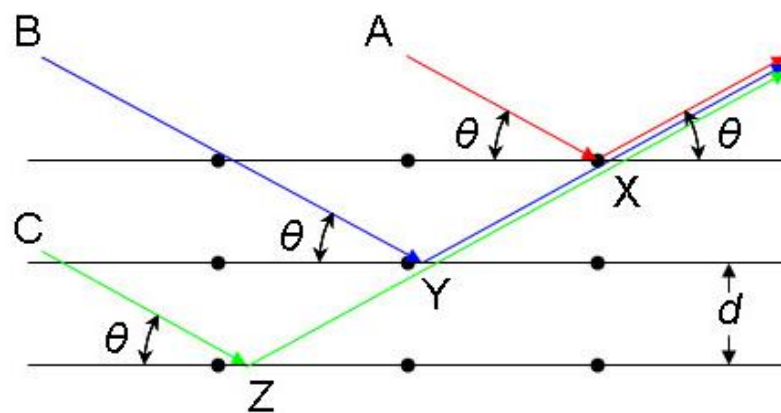


Figure 12. Bragg’s law diagram where incident waves on a crystal surface with angle of incidence and scattering θ with path difference $d=n$ causing constructive interference resulting in color change [47].

By changing the LC molecule’s temperature in an LC structure, the periodic spacing between molecules changes causing different reflected wavelengths. This allows the color of these thermochromic liquid crystals to always range from non-reflective (black) to spectral RGB colors back to black again, depending on the temperature. High temperatures will often reflect blue-ish colors, while lower temperatures will often reflect red-ish colors. Because blue light has

shorter wavelengths than red light, it indicates that the periodic spacing of LC molecules is increased by cooling or decreased by heating of material with thermochromic LCs [45-47].

2.2 RF Switches

A radio frequency (RF) switch, also known as a microwave switch, is a device used to route high frequency signals through various transmission branches. These devices are commonly used in RF and microwave test systems to route signals between instruments and the devices under test (DUT). RF switches are essential in a wide range of telecommunication systems – such as wireless communications (5G technology), radar systems, and satellite communications (aerospace and military uses) [48]. Using RF switches allows multiple tests to be performed without having to change the setup of instruments and DUT, which results in much higher efficiency due to removing the need to disconnect and reconnect devices in the system. The usage of RF switches to simplify complex signal routing can be realized in a switching matrix as shown in figure 13 [49].

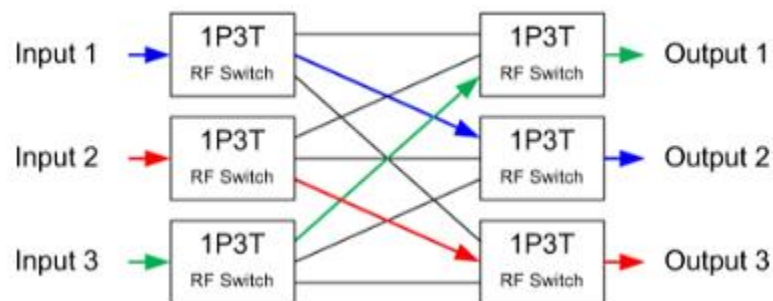


Figure 13. Diagram of a single pole triple throw RF switching device with 3 inputs and 3 possible outputs for each input with switches [49].

The example device is a common configuration of a single pole, triple throw (SPTT or 1:3) switch to route three different RF signals. Each colored route in the diagram shows the original path of each input signal. By tuning each switch, the various input signals can be rerouted to any given output shown via the black routes. Because these devices use only switches, RF switches require less additional components and are ideal devices due their low insertion loss, and high isolation [49,50].

2.2.1 Existing RF Switch Devices and Theory

RF switches have several parameters that are of importance to engineers when designing the devices:

Frequency range where devices operate around 100 MHz to 60 GHz for semiconductor devices in satellite communications. Applications that need to meet broad operating frequency ranges may sacrifice other critical parameters such as switching speed.

Insertion loss how much a device will attenuate a peak signal and increase the rising/falling edge times of switching, which affecting the switching speed. Low insertion loss is achieved by minimizing the number of poles and throws or selecting low insertion loss components for a specific system configuration.

Isolation is the level of signal attenuation from an unwanted signal that is detected at the input/output of interest. Isolating becomes more important at higher frequencies, so having a high isolation device will reduce the amount of influence signals receive from other ports/paths on the device. A high isolation also helps with the device's measurement accuracy or repeatability.

Repeatability is important for RF switches to guarantee the accuracy of the measurement. Low insertion loss and repeatability reduce the amount of randomness and

errors in a measurement, improving overall accuracy. In turn this can reduce device costs reducing the need to recalibrate the device and increase device lifetime.

Return loss is based on how much impedance mismatch there is between circuits which is why circuit matching is very important in RF designs. Impedance mismatch is important due to need to maximize power transfer or minimize reflected signals in the circuit during switching. If the impedance at the source does not match the load it will not allow maximum power transfer and may reflect some of it back that could reduce the lifetime of the device.

Switching speed is an important parameter that is simply defined as the time needed for switch to change states from OFF to ON or OFF to ON [48,49,51,52].

The key parameter to define RF switches for telecommunications applications is high switching speed. Typically, the switching speed is limited by material, design choice of the switching mechanisms of the electrical devices used, or tuning capability of the circuit components (i.e., resistor, capacitor, or inductor) [48].

Depending on the application and technology needed, RF switches have many different configurations for various applications. They are typically classified into two types of devices - electromechanical switches that rely on the physical movement of mechanical contacts to switch circuits ON or OFF, and solid-state switches that use semiconductor technology like transistors and diodes to switch circuits ON or OFF [49].

The most important S-parameters that are considered for this work are return and insertion loss. These parameters most commonly characterize the performance of RF switches. They are also the most easily measured and simulated parameters for properly determining RF device performance. For return loss you want a low return loss which means less reflected power. This is commonly given as a ratio of incident power to reflected power in decibels (dB). When the value of the return loss is high (e.g., 40 dB) the less power is reflected versus a lower

return loss value (e.g., 5 dB) then more power is reflected. This also means that the load for the transmission line is correctly matched and characteristic impedance of the transmission line is excellent. So, ideally if none of the signal was reflected then the return loss would be infinite.

For insertion loss, this is the amount of signal that is lost along the transmission line as the wave travels through. RF applications require low values of insertion loss which translate to a low amount of signal power being lost in the transmission line. This is also given as a ratio of transmitted power to received power in dB. So, ideally if there was absolutely zero signal and power lost in the transmission line, insertion loss would be zero [49,51].

Electromechanical Switches

Electromechanical (EM) RF switches use metal contacts that are physically in an open state where no current will flow through them meaning no signal can be routed through either, or a physically closed state, where current will flow, and signals can be routed through the switch. This type of switch is described by the number of circuits that can be physically connected – called poles; and the number of unique connections or positions that the switch can have – called throws. Three various electromechanical design configurations are shown below in figure 14 [49].

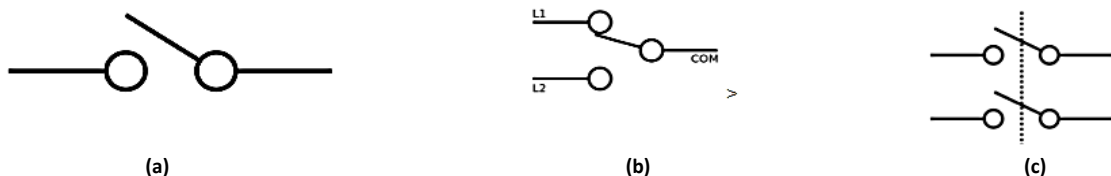


Figure 14. Shows three electromechanical circuit configurations: (a) Single pole single throw (SPST); (b) Single pole double throw (SPDT); (c) Double pole single throw (DPST) [49].

Electromechanical switches can be used from DC to low millimeter wave (mmWave) frequencies. Compared to other conventional RF switches, electromechanical switches advantages are low insertion loss, excellent isolation and power handling, and large frequency range. The disadvantages are low switching speeds, and limited device lifetime. So, the advantages come from the minimal crosstalk between input/output ports and signals, and the disadvantages come from the metal contacts physically switching causing contact bounce and electromagnetic interference [49,51].

Solid-State Switches

Solid-state switches are semiconductor type devices and operate from high (MHz) to super high frequencies (GHz). Because there are no moving parts there are no problems with contact bounce or physical wear meaning it can switch much faster and is much more reliable. Solid-state switches are much more resistant to shock, vibration, and other mechanical wear in general. So, compared to electromechanical switches the advantages of solid-state switches are very fast switching speeds, excellent repeatability, and very long device lifetime. The disadvantages are its high insertion loss, lower isolation, and smaller frequency band [49,51].

Solid state switches typically use three primary types of semiconductor technologies in their design to do signal switching:

PIN Diodes

PIN diodes were the first widely used solid-state switching device. They act as variable resistors operating at RF and microwave frequencies. They are current controlled devices meaning they rely on changing amounts of input current that will either increase resistance to an OFF state or decrease resistance to an ON state. These operations are controlled by biasing

components that control currents/voltages to RF devices called a bias tee [49,51]. Managing RF bandwidth, insertion loss, impedance matching at the two RF ports, and maximum current are very important factors to a bias tee [53]. Figure 15 shows three common PIN diode circuit schematics in the form of SPDT configurations with the bias tees.

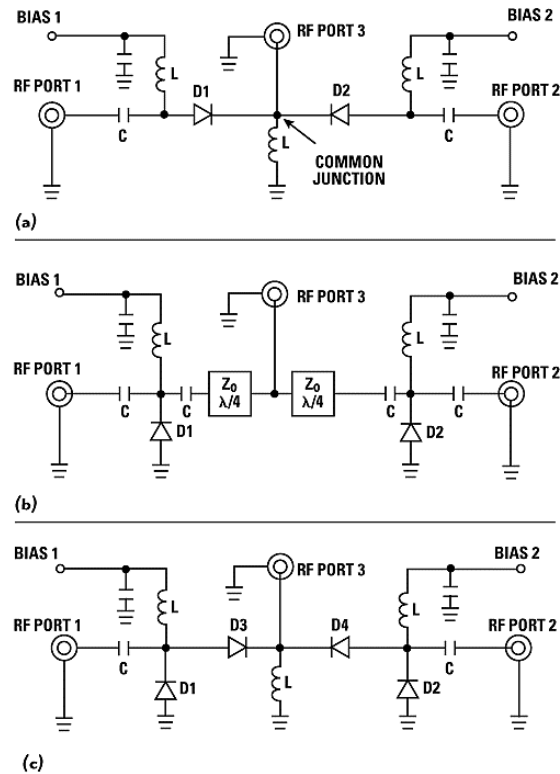


Figure 15. Common PIN diode circuit schematics: (a) SPDT series PIN diode switch; (b) SPDT shunt PIN diode switch; (c) SPDT series-shunt PIN diode switch [51].

Field Effect Transistor (FET)

FET switches use semiconductor devices to control the conductivity of the channels (gate, source, and drain) in the semiconductor material. These switches consume much less current and have excellent isolation at the lower frequency range (decreasing as frequency

increases) but have higher insertion loss, and lower switching speed than the PIN diode switches. FET switches have excellent repeatability but, less isolation due to the drain-to-source resistance and capacitance respectively.

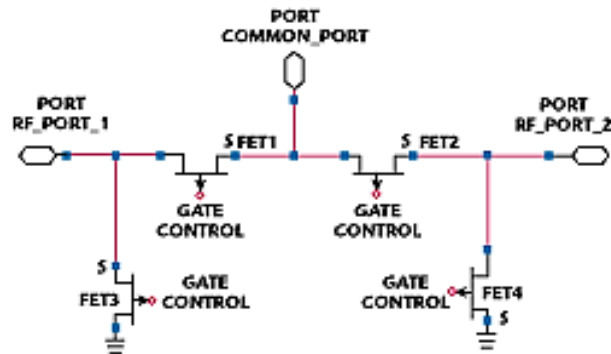


Figure 16. Schematic of a SPDT FET switch configuration [51].

Figure 16 shows a common circuit configuration for a FET switch design similar to PIN diode designs with FETs replacing diodes as the switching device.

RF MEMS Switches

RF MEMS switches are nonconventional semiconductor RF switches that are designed to incorporate the benefits of both electromechanical and traditional solid-state RF switches (PIN diode and FET switches) such as excellent isolation, return loss, and reliability, low insertion loss, large frequency ranges, and high switching speeds [49]. RF MEMS capacitive switches were among the first developed and used an electrostatic actuator as the switch. Electrostatic actuators rely on the force between two electrodes when a voltage is applied to them [54]. These first-generation MEMS switches offer very low insertion loss but typically much lower switching speed. The two means of actuation are ohmic and capacitive switches. With the first generation ohmic switches there are two metal electrodes brought together that create a low

resistance contact. Whereas the capacitive switches use a metal membrane that is pulled down onto a dielectric layer forming a capacitive contact. Figure 17 shows an example of a capacitive type MEMS switch:

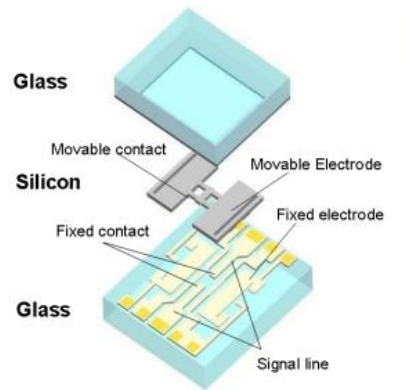


Figure 17. Capacitive RF MEMS switch construction layers used by manufacturing company Omron [51].

In this example you can see that the electrode and contact are made of a special metal composition that will flex downward with an applied voltage to create a capacitive contact turning the switch ON and when the voltage is removed the moveable electrode/contact returns back to its original position breaking contact turning the switch OFF. The usage of electrostatic coupling eliminated many issues plaguing the first generation of ohmic switches that use metal to metal contact such as, contact sticking, and wear [51].

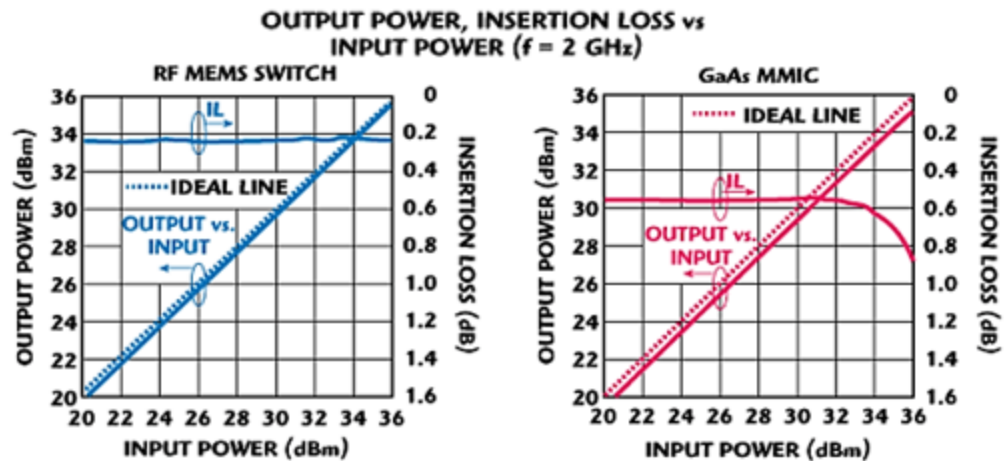


Figure 18. A comparison of output power/insertion loss vs input power performance for a RF MEMS switch and GaAs MMIC FET switch [51].

Here in figure 18, it is shown that RF MEMS switches do not compress up to 36 dBm whereas GaAs MMIC FET switches compression begins around 32 dBm. RF MEMS switches also have very low insertion loss, creating a competitive alternative to other solid-state switch types. Omron and Radant had started manufacturing first generation high isolation and low loss RF MEMS switches up to 20 GHz. Over the years there have been improvements in material refinements, processing improvements, and design choices to follow with less than 0.1 dB insertion loss up to 40 GHz, with low power consumption. Company Radant Technology has tested devices through the Department of Defense and DARPA laboratories and reported RF MEMS switches with lifetimes of over 1 trillion cycles with continuous testing [51].

These breakthroughs in MEMS switch improvements have enabled them to compete in applications like switching arrays for antennas. Another advantage of the RF MEMS switches is that mechanical switches offer very high RF isolation in the OFF state, meaning there is very little leakage current compared to FET switches [51]. Leakage current is a current that flows through the protective ground conductor to ground. Without a proper grounding connection,

leakage current becomes free to flow from any conductive part of a device or surface of a non-conductive part to ground if there is a conductive path available like a human body [55]. With this RF switches are becoming the focus of telecommunication – instrumentation, and cellular/wireless infrastructure and defense – radio systems and phased-array and tunable antenna applications.

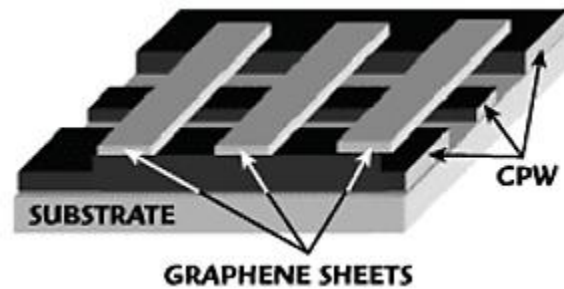


Figure 19. A graphene RF/microwave NEMS switch device design with coplanar waveguide implementation [51].

A counterpart to MEMS technology, nano-electromechanical systems (NEMS), have been researched to possibly overcome the drawbacks of MEMS devices. Works show that graphene sheets can operate as a switch up to 60 GHz with nano second switching speeds. [51,56,57]. Figure 19 shows a simplified design of such a device. It uses a coplanar waveguide (CPW) – a coplanar line structure is where all conductors that support wave propagation are located on the same plane, composed of a middle metallic strip separated by two slits from an infinite ground plane [58], and an array of graphene sheets suspended on the top. The CPW is made from gold strips deposited onto a 500-micron thick silicon (Si) substrate. The graphene sheets stay suspended on the top of the CPW due to van der Waals forces – weak electrostatic forces that define the force of attraction between molecules. If there isn't another force present, there is a distance at which the atoms/molecules become repulsive instead of

attractive called the Van der Waals contact distance [59]. However, this device could also make use of the metallic contact design that MEMS switches employ. The work also notes that the isolation can be improved even further by increasing the electrical conductivity of the graphene sheets by utilizing its unique electric field effect [51,56,57].

This exact device shown in figure 19 is translatable to MEMS and became the second of the two most common electrostatic actuation type MEMS switches for RF/microwave applications. After the electrostatically actuated series switches with metal contacts are the electrostatically actuated switches with a capacitive shunt.

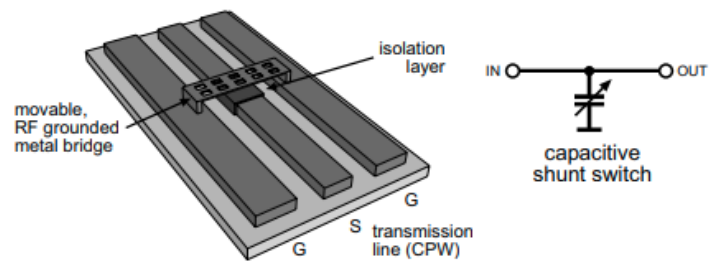


Figure 20. A CPW device design of an electrostatically actuated switch with a capacitive shunt switch using a CPW and RF grounded contact [60].

These two designs are the most common and make up over 80% of the switches presently. There is a moveable metal bridge or membrane that is connected to RF ground and switches ON (down) or OFF (up) above the isolation layer similar to electrostatically actuated series switches with special metal contacts. Naturally the switch is in the ON state, when the bridge is in the down position the membrane capacitively short circuits the signal line to the RF ground. So, in the down position (OFF state) the signal propagates via the bridge to the ground. The isolation is dependent on the parasitic inductance of the entire ground path. This switch

configuration offers the most simplistic design, highest switching speeds (a few μs) and is best suited for high frequency signals [60].

Table 1. Performance and characteristics comparison of electromechanical relay (EMR) vs solid-state PIN diode and FET vs MEMS RF and microwave switches [60].

Parameter	Unit	PIN diode switch [7,70,75-80]	FET switch [7, 70, 75, 81-83]	EMR ^a [84,85]	MEMS switch [7, 70, 75]
actuation voltage	V	$\pm 3-5$	3-5	3-24	20-80
actuation current	mA	3-20	0	150-15	0
power consumption	mW	5-100	0.05-0.1	<400	0.05-0.1 ^b
switching time	μs	0.01-0.1	0.001-0.1	>1000	1-300
off-state capacitance	fF	18-80	70-140	-	1-6
series resistance	Ω	2-4	4-6	<0.1	0.5-2
cutoff frequency	THz	1-4	0.5-2	0.005	20-80
RF isolation (1-10 GHz)	dB	>35	15-25	>40	>40
RF isolation (>10 GHz)	dB	20-35	<20	-	25-40
insertion loss (1-10 GHz)	dB	0.3-0.7	0.4-2	<0.3	0.05-0.2
insertion loss (>10 GHz)	dB	0.7-2	>2	-	0.1-0.2
isolation voltage	-	medium	low	high	low
power handling (1 GHz)	W _{cw}	<10	<5	10	<0.5
signal linearity (IP3)	dBm	27-45	27-53	>60	66-80
size	-	small	very small	large	small
cost — SPDT type [84]	USD	0.9-8	0.5-4.5	0.85-12	8-20
life cycles [84]	-	>10 ⁹	>10 ⁹	0.5-5 \times 10 ⁶	>10 ⁸

^aPCB mounted relays for high-frequency switching applications, such as the OMRON G6 series

^bincludes drive circuitry

Table 2. Advantages and disadvantages of a RF MEMS switch parameters design [60].

Advantages	Disadvantages
very high DC and RF isolation	high actuation voltages needed ^a
very low insertion loss	low switching speed
high signal linearity	limited power handling
almost zero power consumption ^a	lifetime uncertain
very large bandwidth ^b	problematic integration with RF circuits
miniaturization	special packaging necessary
simple control circuits	reliability uncertain
high volume production possible	price uncertain
very resistant to external influences ^c	

In tables 1 and 2 we can again see a summarization of MEMS RF switches and how their research and development made them a competitive option for various RF and microwave applications. The main points of interest in this research are overcoming the lower switching speeds and improving device lifetime avoiding irreversibility and increasing repeatability with a device that has physical/mechanical parts. These improvements are done by choosing a LC-CNT composite to act as the switching mechanism for the RF MEMS device. This ideally avoids any moving mechanical parts that can cause the stiction and contact wear problems. This composite will aim to improve on the already existing performance of RF MEMS switches. Improvements are also made by design choice of the MEMS RF switch based on the application.

2.2.2 Common RF Switch Materials

RF MEMS technology is enabled by MEMS fabrication processes called micromachining that takes advantage of modern semiconductor fabrication processes to enable metal and dielectric film deposition, and different types of etching to achieve unique mechanical device structures which will be discussed in full in chapter 3 [61,62]. The materials used in the full device design process heavily depend on the specific type of desired RF switch, and process capability at the fabrication facility [61]. MEMS switches are typically divided into two categories based on the processing materials – silicon-based and non-silicon-based MEMS switches. Silicon-based MEMS switches are typically fabricated on silicon-on-insulator (SOI) wafers giving the advantage of high structure/design precision and a simplistic process [62-65]. Silicon is also not suited for high impact and high load applications either as a structural layer or as a substrate on its own [63]. As for non-silicon switches, they are commonly fabricated using lithographie, galvanofornung, and abfornung (LIGA) which offers ultra-precision for structure/design

processing. For the metal conductors, deposition is commonly done via micro-electroplating – a process using an electrolyte bath and electrical current where negatively charged ions (anions) are moved onto the anode and positively charged ions (cations) are moved to the cathode where the desired part is covered (plated) evenly in a metal coating [66]. In comparison to silicon-based switches, these metal-based structures have excellent electrical conductivity. Non-silicon-based switches solve the problem of high contact resistance; however, maturity of metal microstructures manufacturing is low (commonly prototype systems and less widespread industrial use). This means during processing the structure is prone to deformation, leading to a low yield of devices [63,67].

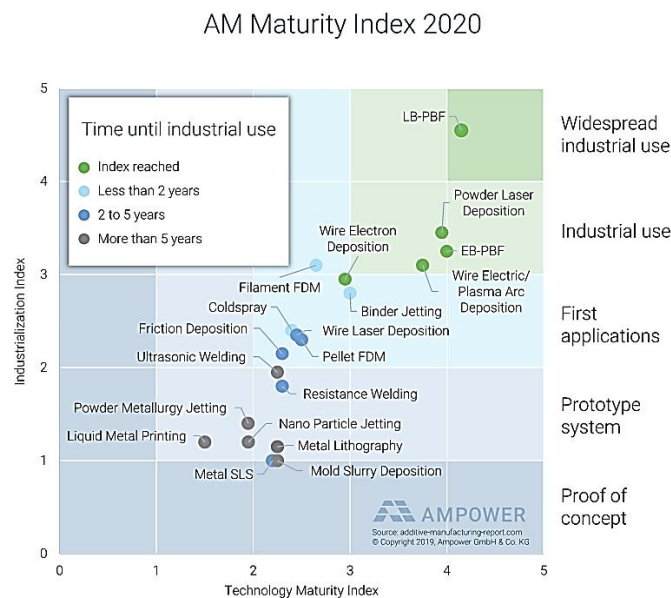


Figure 21. Maturity Index for 2020 showing the maturity level of various metal manufacturing technologies. This diagram shows how commercialized a typical processing technology would be [67].

RF MEMS switches can be made with an antenna design to make the antenna reconfigurable by changing the geometrical structure for different frequencies [68]. It was found that the RF MEMS conductor material has the largest impact on the frequency response of the antenna [68,69].

The Ashby methodology places importance on RF loss and shows that the performance of an antenna depends largely on the RF MEMS switch design and material used. The method has explored the possible materials for RF MEMS switch conductors to be gold (Au), aluminum (Al), platinum (Pt), copper (Cu), nickel (Ni), silicon nitride (Si_3N_4), aluminum oxide (Al_2O_3), and molybdenum (Mo).

In table 3 below we can see the key material parameters, Young's modulus (E), Poisson's ratio (ν), electrical resistivity (ρ), thermal expansion coefficient (α), and thermal conductivity (K) for the possible conductor materials as it relates to their performance for frequency response and general switch performance [68].

Table 3. Key material properties of the possible RF MEMS switch materials showing various material parameters as it relates to performance of RF MEMS switches [68,74].

Material	Young's Modulus E (GPa)	Poisson's Ratio (ν)	Electrical Resistivity ρ ($\Omega\cdot\text{m}$)
Aluminum	69	0.33	2.90×10^{-8}
Gold	77	0.42	2.35×10^{-8}
Copper	115	0.33	1.72×10^{-8}
Platinum	171	0.39	10.60×10^{-8}
Nickel	204	0.31	9.50×10^{-8}
Silicon Nitride	304	0.3	$> 10^{12}$
Molybdenum	320	0.32	5.20×10^{-8}
Aluminum oxide	380	0.22	$> 10^{12}$

Material	Thermal Conductivity K (W/m-K)	Thermal Expansion Coefficient α ($10^{-6} (\text{°C})^{-1}$)	-
Aluminum	222	23.6	-
Gold	388	14.2	-
Copper	315	17	-
Platinum	71	9.1	-
Nickel	70	13.3	-
Silicon Nitride	29	2.7	-
Molybdenum	142	4.9	-
Aluminum oxide	39	7.4	-

Based on Ashby's methodology and material parameters it was determined that gold offers the best device performance in terms of sensitivity and reliability for repeated actions/measurements [68,77-79].

2.3 Coplanar Waveguides

When working with RF signals it is important to properly route and confine the waves to the proper interconnects to provide a low loss and high isolation wave propagation between RF interconnects and other ports of the system when possible. Using a waveguide device is an excellent way to route and confine these signals with the best performance [80]. Coplanar waveguide (CPW) structures are used for high-speed/frequency circuits and interconnect as

planar transmission-line technology. A coplanar line is a structure where all the conductors that support wave propagation are all located in the same plane, commonly on top of the dielectric substrate. The main type of these planar transmission lines is then called a coplanar waveguide or grounded coplanar waveguide (GCPW) [58].

2.3.1 Existing Coplanar Waveguide Devices and Theory

The most conventional CPW design is formed by a single conductor with ground planes on both sides of said conductor separated by narrow gaps, all of which are on the same plane sitting on top of a dielectric medium. Ideally the thickness of the dielectric is infinite, however realistically it is thick enough so the electromagnetic fields (EMFs) die out before they can escape the substrate [81]. EMFs are invisible radiation particles caused from the motion of an electric charge. Making sure there is no EMF leakage is important because there are non-ionizing EMFs (little to no potential to damage cells and DNA) and ionizing EMFs (potential to damage cells and DNA) caused by low and high frequency EMF leakage respectively [82].

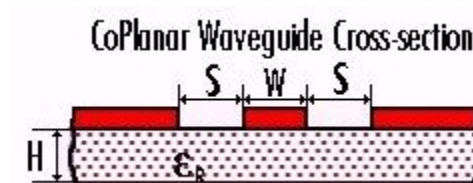


Figure 22. Coplanar waveguide structure showing general dimensions of importance (W , S , H , and ϵ_p) for conductor width, slot/gap width, substrate height, and effective permittivity respectively for EMF mitigation [81].

Typically, there are a few important coplanar waveguide structures. There is the standard CPW, the standard coplanar waveguide with ground (CPWG), the GCPW, then there is

a finite ground plane coplanar waveguide (FG-CPWG). The standard types of coplanar waveguides consist of what are called semi-infinite ground planes that are on either side of the center conductor. The electrical characteristics of CPWs are very good, so the frequency variation of the effective permittivity (ϵ_p) as shown in figure 22 is quite low which simplifies the broadband circuit design. It also allows for multiple variations in characteristic impedance by varying the conductor and gap widths (W & S) respectively [83,84].

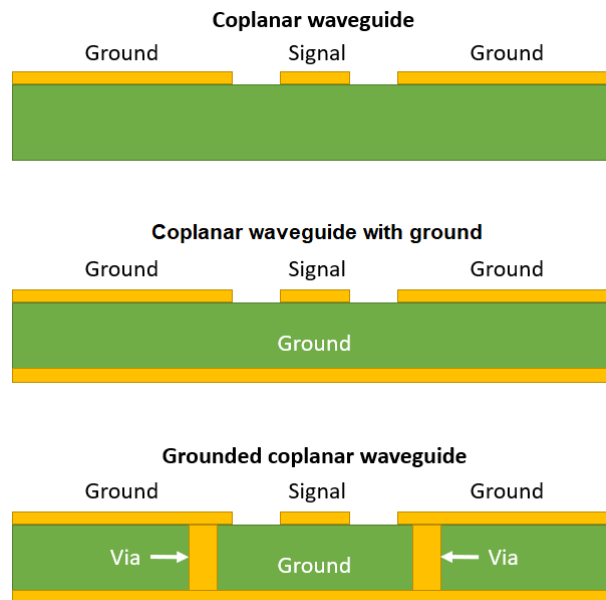


Figure 23. Three common coplanar waveguide configurations – CPW with one signal line and two ground plane conductors; a CPWG with one signal line, two upper layer ground conductors, and one bottom layer ground conductor; a GCPWG same configuration as CPWG with vias connecting the upper and lower ground planes [85].

From figure 23 you can see exactly what each configuration would look like where FG-CPW have the widths of the two ground planes the same or close to the width of the signal line. Whereas the standard CPW has semi-infinite width ground planes.

With a standard CPW typically processing includes a metal base to help with removing heat, prevent EMF leakages, and add mechanical strength to the device. The substrates are also typically thinner by 25 to 100 microns to help more with thermal management. This type of metal backed structure is shown in figure 23 as the CPWG. The CPWG creates a parasitic waveguide mode with lower signal phase velocity than the standard CPW mode over the entire frequency range of the device that causes power leakage between the modes [83,86,87]. To solve this increase in path loss between the CPW/CPWG modes there are several methods available. RF/microwave absorbing materials can be introduced to attenuate the RF/microwave energy at the edges of the dielectric substrate [83,88]. Multiple dielectric layers for the substrate can be used to increase the phase velocity of the transverse electromagnetic (TEM) CPWG mode or vias can be added (figure 23) to short the upper and lower ground planes together, which in turn eliminates the TEM CPWG mode for mode selection, and higher isolation, while increasing the bandwidth [83,86,89]. With this structure the gaps between the signal and ground planes must be greater than the thickness of the dielectric substrate so the EMF is contained between the upper strip/ground plane and lower ground plane [85]. However, the downsides to these methods are in increase in fabrication costs and device design complexity [83].

Another solution was developed that uses finite width ground planes, so the total width of the coplanar transmission line is electrically small. This means that when using the CPWG configuration, lower signal phase velocity, increased power leakage, and path loss doesn't occur [83,90,91].

For a practical approach any of the design structures will offer great performance and allow for high enough bandwidth for large frequency range operation with high isolation. Although CPWs operate on the surface it has lateral isolation thanks to the ground planes, it also

provides EMF/EMI shielding. The CPW advantages also include very low RF loss because the field lines often pass through the region that is above the dielectric substrate preventing much signal loss. The bandwidth is largely tunable just by adjusting the device geometry, and CPW do get bigger to compensate for frequencies above ~ 5 GHz but, can also be confined to the desired frequency range for single-mode operation: transverse electric (TE) or transverse magnetic (TM) modes [85].

2.3.2 Common Coplanar Waveguide Materials

Multi-chip modules (MCMs) combine multiple integrated circuits (ICs) or chips into an even more complex circuit device that is non-hermetically sealed (not airtight) [92]. MCM technologies are typically used for RF MEMS switch devices. There are also hybrid technologies that consist of a substrate with deposited circuitry, and separately processed active and passive components that are later added to complete circuit function. The deposition process and materials are essentially the same as MCMs [93]. The MCM idea is a multi-monolithic/functional design that consists entirely of chips using predominantly silicon (Si) substrates but gallium arsenide (GaAs) or silicon germanium (SiGe) are used based on the application, when needed. The variations in MCMs affect the packaging, deposition process, and substrate configuration, so it is a large indicator of what materials will be used. The modern MCM is typically defined by the substrate technology with the two most important classifications for RF MEMS devices [93]:

MCM-C

This is a ceramic or glass-based substrate technology with a dielectric constant of five or less. Conductor materials are typically fired material i.e., tungsten, molybdenum, or a thick film

metal conductor such as gold, silver, or copper. Vias in this technology are formed during screening by using the same metallurgy as the trace metals [93].

MCM-Si (Silicon Based)

This device type is a silicon-based substrate which is the wafer processing industry standard material which helps to keep costs low, especially for proof of concept/prototype devices. This Si-on-Si fabrication process allows for a high-density interconnects network of which several varieties of bare die may be created. The deposition of a metallic coating to another metallic or non-metallic surface (metallization) is typically Al and Al-Si, while SiO₂ forms the dielectric. The passivation layer on top is usually silicon nitride (Si₃N₄). Silicon based MCM technology provides a unique and perfect temperature coefficient of expansion (TCE) match between the substrate and die which is excellent for high-power applications of MEMS devices [93-95].

Passive Structures

Passive structures used in RF/microwave device applications include planar transmission lines, vias, and airbridges. CPW and microstrips (just the conductor and bottom ground planes) are the most common planar transmission lines as shown in figure 24 [93,96].

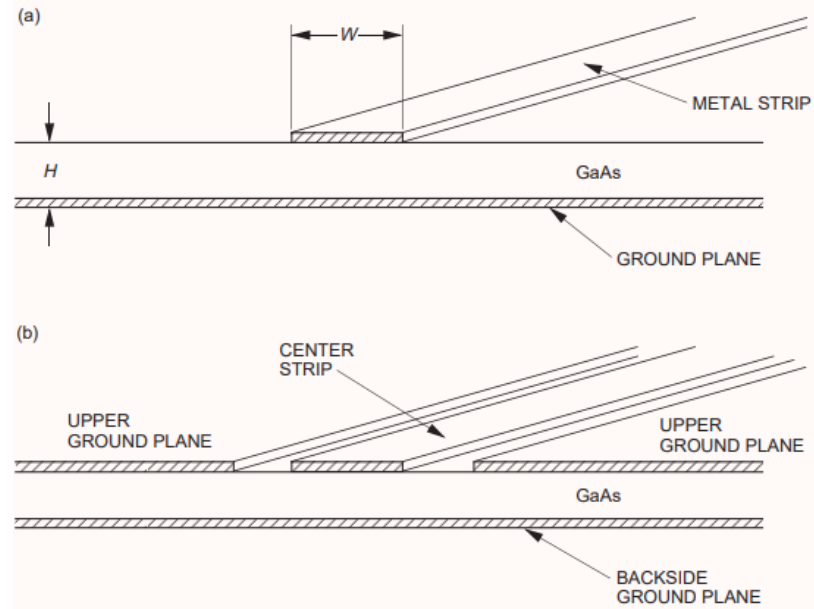


Figure 24. Planar transmission line configurations: (a) microstrip planar transmission line structure; (b) CPWG structure with center signal line and two upper ground planes with one lower ground plane [96].

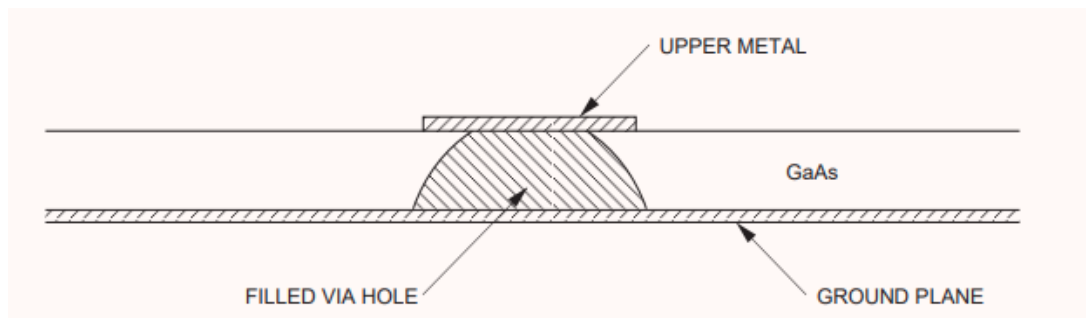


Figure 25. An example of an ideal via hole in a planar transmission line configuration that connects the upper and lower ground planes of a CPW device [96,97].

In figure 25 we can see an example of the via holes used to connect the upper and lower ground planes. GCPWG's require via holes to electrically ground the upper and lower ground

planes together. Via holes are etched through the substrate, typically from the bottom side of the substrate ground plane to minimize the element area on the top plane. The wet or dry etching process (further discussed in sections 2.5 and 2.6) is followed by sputtering or electroplating deposition to fill the hole with Au as shown in figure 25 [96,97]. The reliability of the device becomes a concern because vias that are filled with Au can cause specifically GaAs substrate to crack due to the TCE mismatch. The solution is to use less Au however, this may cause a complication with RF/microwave applications as vias must contain enough Au to create a proper thermal path. This is typically why Si is used over GaAs for this type of configuration and device [96].

2.4 RF and Telecommunication Systems

Telecommunication systems are based on the transmission of information by various technological means such as wired/wireless, optical, or radio transmission. Telecommunication systems are both hardware and software providing the means and capabilities for connected systems to communicate with one another and their users. Modern day transmission paths are divided into multiple telecommunication channels and taking advantage of a method called multiplexing that turns several signals into one in order for them to traverse over a single communication medium. This reduces costs for dedicated networks like fiber optic internets and is largely used for audio/video broadcasting [98,99]. The earliest telecommunication systems used Cu wires as a transmission medium for signals. These networks were the basic landline phone services used since their creation in the late 1800s, which at the time started with telegrams (pre-wireless transmitted texting). Since then, in the 1990s is when the internet largely expanded in popularity and wireless telecommunication became commonplace and the limitations of Cu transmission lines became apparent [100,101].

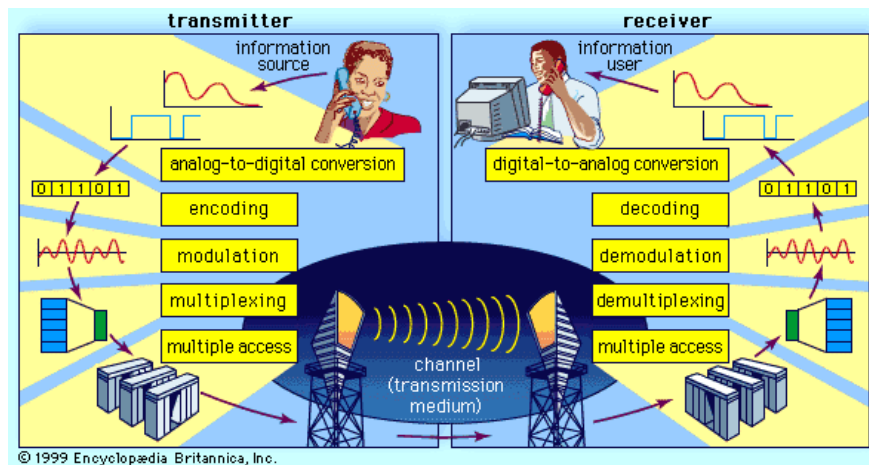


Figure 26. Telecommunication system process flow graph enabled by the semiconductor era. This diagram shows the basic transmitter analog-to-digital conversion process encoding a signal that is transmitted by an antenna. That signal is then received by another antenna, then decoded using the digital-to-analog conversion processes shown [102].

The modern-day usage of wired/wireless telecommunications technology is attributed to the semiconductor era that started around the 1950s and is still in use present day. The research, development, and application of transistor technology allowed for significant advances in telecommunication systems. The development of metal-oxide-semiconductor field-effect transistors (MOSFET or MOS) technology, transistor scaling on an IC, transitioning to RF MOS technology, data compression, and finally digital signal processing (DSP) is what enabled the rapid growth of telecommunication systems with the introduction of digital telecommunications using wireless telecommunication systems into the late 1990s onward. This modern data transmission process is shown in figure 26 and is performed by modern day RF devices [100,101,103].

2.4.1 Applications in Antenna Systems

An antenna system is a vital component in telecommunications and for RF devices. Antennas are defined as an instrument that enables the ability to emit or receive radio waves. This means that an antenna is a transitional device between free-space and a guiding device (i.e., CPWs or microstrips) [104]. Wireless communication systems require antennas to be at the transmitter and receiver in order to operate properly. The design and infrastructure of antennas can make or break wireless telecommunication systems. When there is bad performance from a specific system it is most commonly traced back to poorly implemented antenna infrastructure [105]. The important parameters to describe antenna performance are directivity, gain, antenna efficiency, half-power beam width, bandwidth, polarization and more defined by IEEE standards. However, many of them do not need to be defined for every antenna, and this is based on the application and device used [104]. A simplistic structure of a wireless telecommunication system with transmitter and receiver antennas integrated with a waveguide device (CPW) can be shown in figure 27.

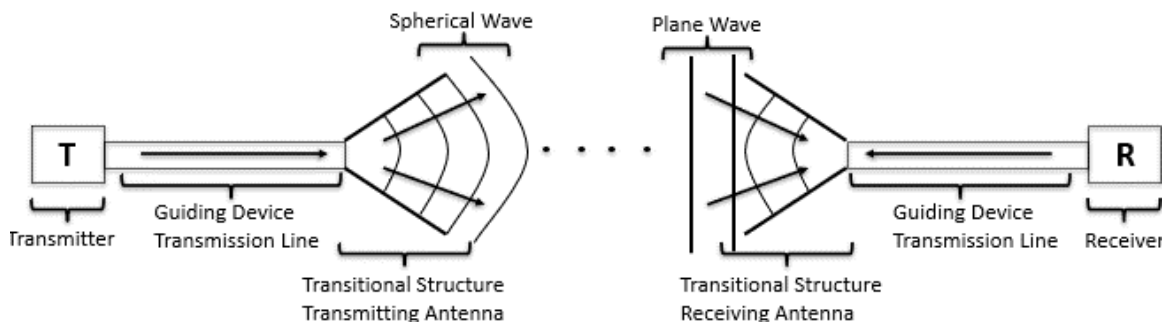


Figure 27. Diagram of an emitting and receiving antenna telecommunication system. In the guiding device transmission line section is where a CPW device would be implemented. The guiding device is the key to a high performing telecommunication system.

Antenna Parameters

The operation of a telecom system depends on the dimensions of the antenna/waveguide devices being used. In figure 28 there is a simplified example of a telecommunication system and its important parameters.



Figure 28. An example diagram of a wireless link telecommunication system between a transmitting and receiving antenna with area and gain of transmitter and receiver labeled. As well as length of the transmission signal between both apertures.

With these parameters the relationship between the transmitted and received power can be calculated and given as

$$\frac{P_r}{P_t} = \frac{A_{er}A_{et}}{r_{TR}^2\lambda^2} = \left(\frac{\lambda}{4\pi r_{TR}}\right)^2 G_r G_t \quad (6)$$

Equation 6 defines the ratio of power received to power transmitted. A_{er} and A_{et} are the aperture area of the receiving and transmitting antenna respectively. r_{TR} is the radius between transmitting and receiving antennas. Then finally, G_r and G_t are the gains of the receiving and transmitting antennas respectively.

This expression is also known as the Friis transmission formula. The Friis transmission formula is an important concept that is used to design the wireless links for telecommunication systems using RF devices. An example of this is, if you know the power sensitivity of the antenna

radio which is denoted as $P_{r.min}$ (minimum power received), and the gain of the transmitting and receiving antennas, then the maximum communication distance and minimal transmitting power can be determined. This is under the condition that the antenna has limited transmitted power and limited communication distance respectively. This is the key for using RF devices in commercial applications and more specifically for applying RF MEMS devices to use and improve 5G technology systems.

2.4.2 RF and 5G Technology Systems

Wireless broadband systems transmit large amounts of data to mobile devices through the air. There is one wireless station that serves a community in its vicinity [101]. However, compared to landlines, wireless telecommunication signals decline much faster at larger distances. A single landline can run many miles and service customers in every direction. Whereas wireless stations that service customers are typically no further than 1-2 miles apart in suburban areas and can be as little as a ¼ mile apart in dense urban areas [101,107]. Another limitation of wireless broadband signals is that they are constrained to how they are transmitted. When the frequency range increases, they have increased bandwidth carrying more information. However, unlike low frequency, higher frequency signals are very prone to absorption and/or scattering. This creates a limit to how far the signal can be transmitted.

The previous technology for wireless broadband 4G had limitations such as latency for long distance and limited data transfer speeds. 5G Improves on this and allows for a similar frequency band of operation from 700 MHz to approximately 5 GHz. Improvements of antenna systems and encoding technology will allow service providers to better use the frequency band based on application and service. Over time, 5G will begin to support broader ranges beyond even RF or microwave frequencies into the millimeter (mmWave) frequency range which is over

20 GHz. Higher frequency signals allow for more user bandwidth and support higher data transfer useful for commercial usage. So, the tradeoff with the mmWave frequency range is transfer speeds will increase, but the higher the frequency the more signal absorption and scattering will occur.

So, 5G telecommunication systems look to increase data volume and rate transfer, increase connected devices, and decrease latency. To realize these specifications, they will have to satisfy multi-node/multi-antenna transmission, or implement a tunable array, proper network dimension and spectrum usage. Given these technical specifications it is important to note how these parameters reflect as characteristics that basic passive RF components must fulfill in order to sustain a proper 5G system. To begin with are wideband RF switches and devices with low loss, high isolation, and very low cross talk between channels from RF to mmWave bands. These devices require characteristics such as reconfigurable filtering, and wideband impedance matching tunability. In more recent years, RF technology has improved on and included wideband phase shifters, and attenuation with antenna arrays integrated with these previous device specifications [107, 108, 109].

2.4.3 LC-CNT Tunable Array Application

The previous 4G technology used omni directional antennas to deliver signals which allowed for a simplistic design and ability to offer service coverage in all directions with moderate radiation [110,111]. To properly take advantage of 5G telecommunication systems the use of mmWave frequency bands is imperative, paired with directional phased array antennas operating at both the service base station and mobile devices [111,112]. The use of mmWave bands provides a challenge because a directional phased array antenna can only deliver service in a single direction. This issue can be overcome through the use of tunable

arrays also known as beam steering, to deliver a service coverage similar to omnidirectional antennas [110,111,113].

Frequency tunable antennas can be realized with the introduction of liquid crystal composites with flexible materials. For a tunable antenna using a flexible LC polymer substrate you can achieve an increased frequency tuning range of 10% up to 35 GHz. These liquid crystal composites as discussed in section 2.1 are controlled through the application of an external electric field [113,114].

Liquid crystals used for beam steering allow for an antenna's main beam to be steered in various directions at a fixed frequency to achieve a signal coverage similar to omni directional antennas. An antenna with an external applied electric field to a LC doped antenna structure achieved a beam tilt of $\pm 10^\circ$. Phased arrays and beam steering research have achieved up to 300° of phase tunability of a unit cell, applying an external bias voltage up to 40 V [113,115]. The integration of an LC-CNT composite in an antenna is achieved by using the LC-CNT in a small portion of the signal line on the waveguide device. LC media can offer a low loss device and up to 5% frequency shifting and adjust the resonance frequency up to the mmWave range [113,116]. The goal of this technology is to create a phased antenna array system which gives the ability to steer multiple antennas allowing for greater signal coverage. As opposed to creating multiple wireless base stations.

All of uses can be realized by implementing the LC-CNT RF switching device investigated in this work, which will allow. To achieve this tunable array the idea is that within the center conductor signal line you would replace a portion of the signal line with the LC-CNT composite in a cell. An example of this device is shown in figure 29 below.

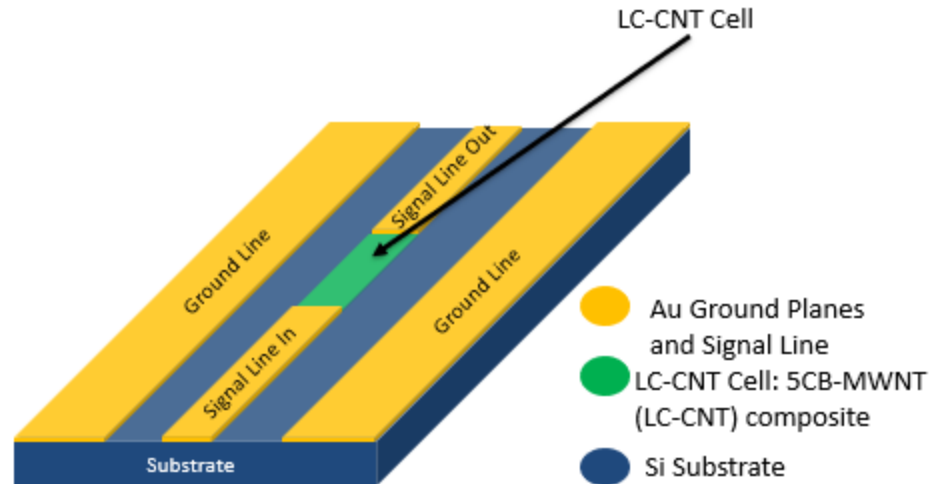


Figure 29. Design of general CPW structure for LC-CNT composite cell used for RF switching device. LC-CNT cell acts as switching mechanism with applied electric field.

The directors of the LC molecules are initially perpendicular to the signal line (OFF state) and then, with an applied electric field the LCs directors align parallel to the signal line (ON state), allowing the signal to pass. The RF field is given by the planar ground and signal lines fundamental mode which would be confined to the LC-CNT cells volume and would be perpendicular to the director. This is how the RF field perceives the effective permittivity $\epsilon_{eff} = \epsilon_{\perp}$. So, applying an increasing external bias voltage the director of the LC molecules begins to rotate at a certain voltage threshold V_{th} . Increasing this external bias voltage even further the LC molecules director will begin to align completely parallel to the applied electric field. Then the RF field and effective permittivity become $\epsilon_{eff} = \epsilon_{\parallel}$. Changing this effective permittivity creates a change in the resonance frequency and shift the phase characteristics shown in figure 30. This is the basis for how the tunable phase array is created [117].

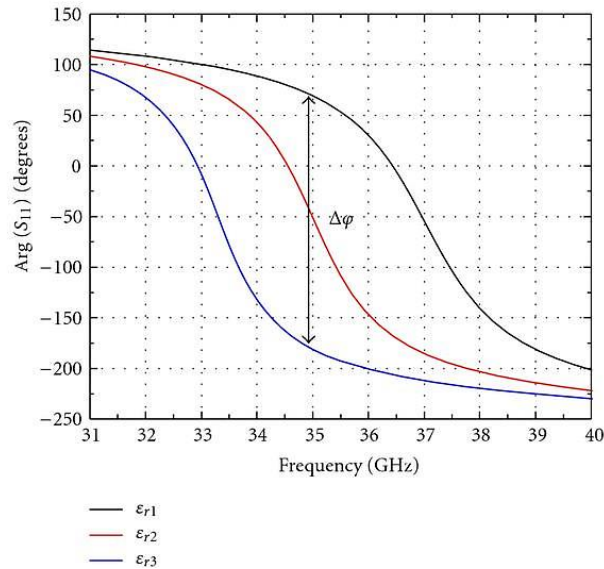


Figure 30. Functioning principle of a LC-CNT doped tunable phase array showing changes in permittivity will create a change in resonance frequency causing the shift in phase you see between ϵ_{r1} and ϵ_{r3} [116].

2.5 Microelectromechanical Systems

MEMS is a processing technology that is used to create micro-scaled integrated devices or systems that use a combination of mechanical and electrical active and passive components. These devices are created using IC batch processing microfabrication techniques that can vary in sizes of a couple millimeters down to a few micrometers. MEMS devices and systems are commonly used as mechanical microstructures, microsensors, micro actuators, and microelectronics in general and have the ability to sense, control and actuate on the micro scale and in turn affect the macro scale. The device's electronic components are fabricated using IC technology (computer chips), while the micromechanical components are fabricated using micromachining processes with various substrates like Si. MEMS commonly takes advantage of

silicon's electrical and mechanical properties, selectively adding or removing parts of Si during micromachining processes to create unique structures for various applications.

Typically, MEMS devices are broken up into two main categories of device types starting with the umbrella term that is transducers – a device that transforms one type of signal/energy into another form of signal/energy. Transducer can be used as a blanket term that includes both sensors and actuators in MEMS. So, the first type is a sensor device – a sensor is a device that gathers information from a surrounding environment as input and outputs an electrical signal in response to the information received. The signals and energies of sensors typically fall into these domains – mechanical, thermal, chemical, radiant, magnetic, and electrical. An example of one of the best sensors in the world is our own eyes. The second type of device are actuators which are devices that converts an electrical signal/energy into an action. These devices have the ability to create a force that can affect itself or other devices, or the environment to achieve a given application. A common example of an actuator device are the brakes on a vehicle. MEMS is known for its extensive range of applications that incorporate unique MEMS devices to achieve high performance across automotive, medical, electronic, communication and defense applications as shown in table 4 [118].

Table 4. Various commercial applications of MEMS devices in various fields [118].

Automotive	Electronics	Medical	Communications	Defence
Internal navigation sensors	Disk drive heads	Blood pressure sensor	Fibre-optic network components	Munitions guidance
Air conditioning compressor sensor	Inkjet printer heads	Muscle stimulators & drug delivery systems	RF Relays, switches and filters	Surveillance
Brake force sensors & suspension control accelerometers	Projection screen televisions	Implanted pressure sensors	Projection displays in portable communications devices and instrumentation	Arming systems
Fuel level and vapour pressure sensors	Earthquake sensors	Prosthetics	Voltage controlled oscillators (VCOs)	Embedded sensors
Airbag sensors	Avionics pressure sensors	Miniature analytical instruments	Splitters and couplers	Data storage
"Intelligent" tyres	Mass data storage systems	Pacemakers	Tuneable lasers	Aircraft control

2.5.1 Fabrication Processes

MEMS fabrication can be divided into three general categories which is bulk micromachining, surface micromachining, and high-aspect-ratio micromachining (HARM), which includes the process mentioned in 2.2.2 called LIGA which means lithography, electroforming, and molding. MEMS fabrication does not follow the typical macroscale fabrication techniques due to the complex high volume IC style devices. Instead, it follows a process of patterning, and chemical etching [118].

Bulk Micromachining

Bulk micromachining involves the formation or creation of device features by removing part of the bulk substrate. It's a subtractive fabrication process that uses a method called wet anisotropic (or isotropic) etching or a dry etching method called deep reactive ion etching (DRIE)

that will be discussed further in section 2.6. These methods are used to create pits, grooves, and channels.

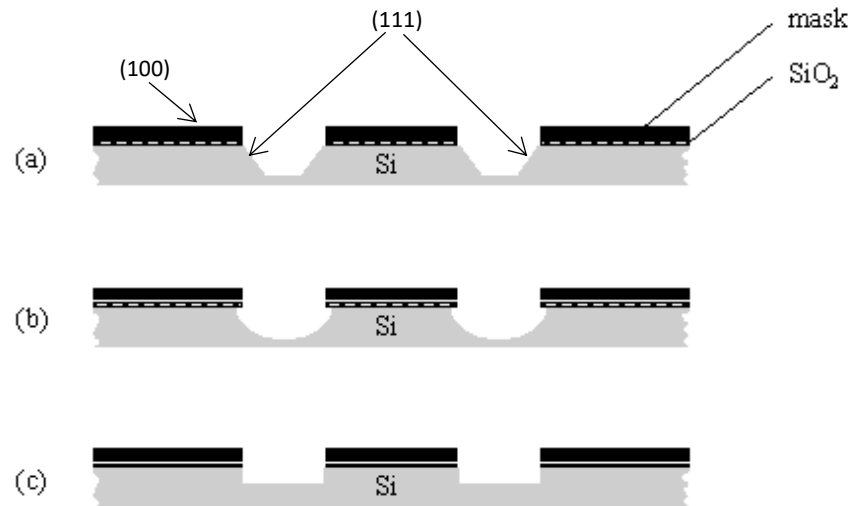


Figure 31. Etching types for bulk micromachining: (a) anisotropic wet etching results; (b) isotropic wet etching; (c) DRIE [119].

Wet etching is a method that removes material through the use of a chemical bath known as a chemical etchant. Isotropic chemical etchants will etch away the material at the same rate in every direction. However, the consequence of this is that the material underneath the etching mask is etched away at that same rate as well which is called undercutting as shown in figure 31b. One of the most common isotropic etchants to Si substrates is hydrofluoric, nitric, acetic (HNA) which is comprised of hydrofluoric acid (HF), nitric acid (HNO₃), and acetic acid (CH₃COOH). Isotropic etches are typically limited by the geometry of the structure being etched and etch rates slow down over time and can even stop. However, this can be avoided by agitating the etchant mixture to evenly etch in every direction for excellent rounded features [118].

Anisotropic chemical etchants will etch faster in a specific and desired direction. A commonly used anisotropic etchant is potassium hydroxide (KOH). Because features that are created on the substrate are dependent on the crystal lattice orientation of the Si substrate, you can control the etch direction. Most anisotropic etchants work quickly in the crystal lattice direction that is perpendicular to the (110) plane, and less quickly in the direction that is perpendicular to the (100) plane, and barely etch if any in the direction that is perpendicular to the (111) plane. An example of this is illustrated above in figure 31a [118,119]. Below in figure 32 are examples of crystal planes that the etchants will etch when fabricating.

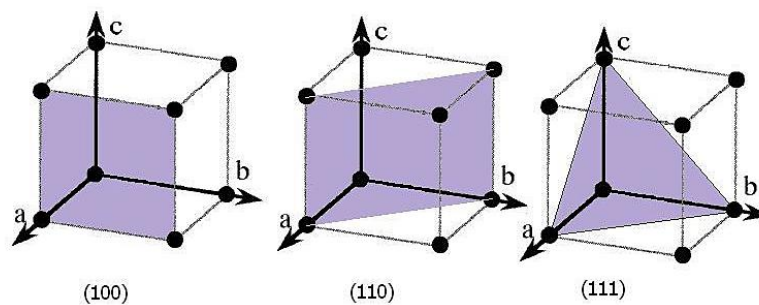


Figure 32. Example of various planes in crystal unit cell used for anisotropic etching [120].

Surface Micromachining

Surface micromachining is the fabrication of features above the substrate instead of subtracting away/into it. It is typically used as the foundational layer that is built upon. Material is added onto the substrate in thin layers on the surface. The layers act as either structural or sacrificial layers to be kept or removed later respectively. The thin layers are deposited one by one and dry etched out progressively with the sacrificial layer being wet etched away to release

the final feature. Every additional layer increases the complexity of the MEMS device greatly. An example of this process is shown in the figure below [118].

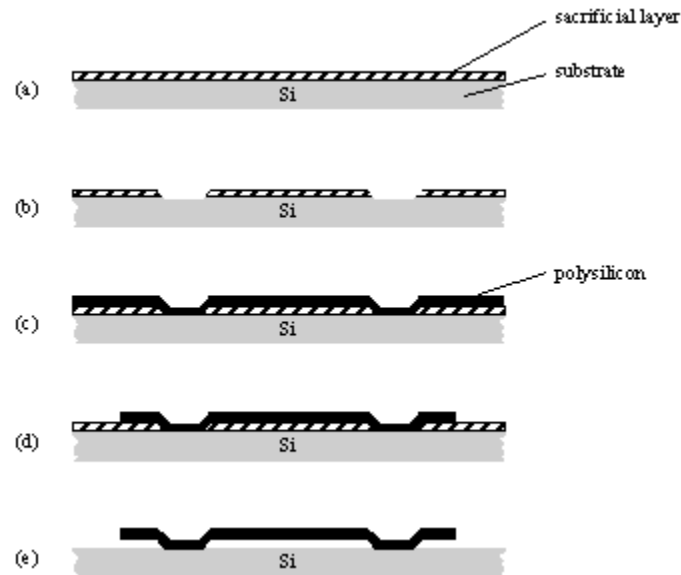


Figure 33. Example of surface micromachining process to create membrane [121].

An oxide sacrificial layer is deposited using a pattern and photolithography in figure 33 parts (a) & (b) that will be discussed further in section 2.6. Next the polysilicon layer is deposited using patterns and DRIE processing as shown in figure 33 parts (c) & (d). The entire substrate and structure are then wet etched to remove the oxide sacrificial layer. The sacrificial layer removal step is crucial to having an acceptable yield of functioning devices per Si wafer and reliability of the device itself. This is due to a common phenomenon in MEMS fabrication called stiction. Stiction is when features stick to one another or the substrate itself. Stiction is also known as static friction which is the amount of force needed to move an object from a

stationary position. Then Van der Waals forces come into effect and can permanently adhere features together after the device is dried [118, 121].

Micromolding

Micromolding or high aspect ratio microstructures (HARM) is a fabricating process that involves a surface micromachined part created through a tooling step done through injection molding or electroforming, to replicate microstructures from molded parts. It's a popular fabricating method to replicate microstructures at a high performance to cost ratio using a method called LIGA. Devices that use HARM are high-aspect ratio devices such as nozzles for inkjet printing or microplates in the medical field. LIGA allows for structures to be fabricated up to 1mm high. Figure 34 below depicts the LIGA process, where an x-ray sensitive photoresist is first deposited onto the structure. Then, an x-ray mask is used to selectively expose the photoresist. The x-ray breaks down the polymer chain of exposed regions and then the exposed resist is developed away.

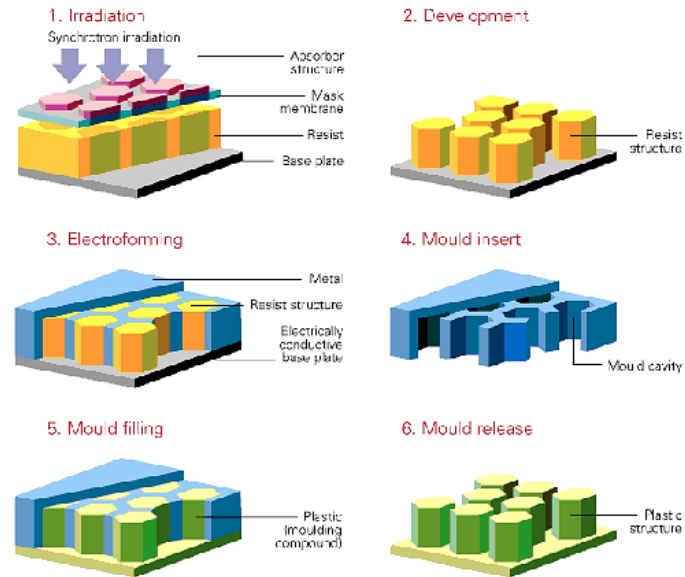


Figure 34. Example of HARM process using LIGA method [118].

2.5.2 Material Selection for MEMS Processing

The materials involved in MEMS processing are important because it decides the reliability and capability of features and etchants to create structures. The most common substrate material for micromachining processes is Si. It's an abundant, and inexpensive resource that can be extremely and finely purified. Another substrate used is GaAs, however due to Si inherent ability to readily oxidize and form a chemically inert and electrically insulated layer of SiO_2 makes silicon's usefulness hard to beat. As described in section 2.5.1 polycrystalline Si (high purity silicon) is used for feature structures. Deposited layer material can be Si_3N_4 , SiO_2 , SiC and more, that can be used as the sacrificial layer or feature layer for processing. Metals and metallic compounds used for conductors are commonly Au, Al, Cu, GaAs, ZnO (Zinc Oxide), IrO_2 (Iridium Oxide), and CdS (Cadmium Sulfide). Ceramics such as Al_2O_3 and organic material such as polymers can be used for depositing layers with specific electrooptic properties [118].

2.6 Fabrication Techniques for Microelectronics and MEMS

2.6.1 Photolithography

Photolithography is a method that transfers a pattern to a substrate to fabricate various features. The substrate is covered in a thin layer of material typically SiO_2 due to it being a very readily available material on Si. Then a thin layer called photoresist is spun on the device. Photoresist is a polymer that is very sensitive to ultraviolet (UV) radiation. Next, a photomask that is made up of a transparent glass plate and a specified pattern made of chromium that is opaque is placed onto the photoresist layer. When the device is exposed to UV light the pattern is transferred onto the photoresist which is then developed to leave the desired feature. This UV light causes one of two special reactions to areas of exposed photoresist that are positive and negative photoresist. Positive photoresist becomes stronger with the UV radiation and negative photo resist becomes weakened.

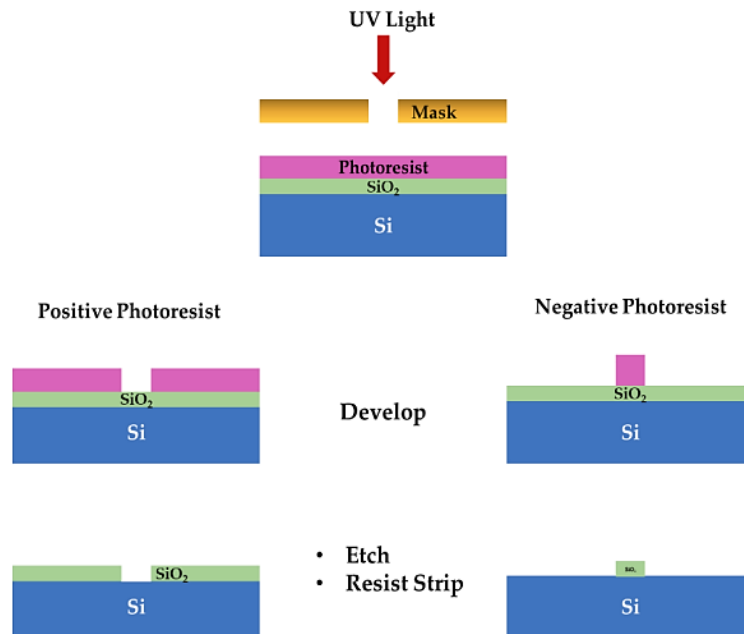


Figure 35. Fabrication method with positive and negative photoresist patterns using photolithography [118].

As shown in figure 35 depending on the type of photoresist the rinsing solution will either remove the exposed or unexposed area of the photoresist which leaves the desired pattern of photoresist coated SiO₂ on top of a substrate. Depending on whether the photoresist is positive or negative the resulting feature will be a 'positive' or 'negative' image of the original photomasks pattern. Hydrofluoric acid (HFL) is typically used to remove the uncovered oxide layer that is exposed from the photoresist layer. The photoresist layer is removed using the lift-off method. Leaving the desired patterned oxide feature intact. Again, this final oxide pattern will either be a positive or negative image of the original photomask pattern and acts as a mask for any following processing steps [118].

2.6.2 Etching

Dry etching uses vapor phase or plasma for etching using the proper reactive gases (or vapors) typically at very high temperatures. Deep reactive ion etching (DRIE) is a common MEMS etching process that actually uses RF energy to start the etching chemical reaction. Ions imparted with RF energy are accelerated towards the device material to be etched done in a plasma phase (very high pressure/temperature gas) that supplies additional energy as needed for the chemical reaction to occur. DRIE unlike wet etching is not limited to specific unit crystal planes in the Si substrate and because of this extremely precise anisotropic (vertical wall) pits/grooves can be created. DRIE is a high-aspect-ratio etching technique that etches using plasma and also depositing a protective polymer layer that prevents etching the sidewalls. This process is called sidewall passivation. The specific etch rate depends on concentration, temperature, material, and time. This calculation is done before fabricating as there is no universal formula to predict every exact etch behavior and outcome [118,122].

2.6.3 Deposition, Bonding, and Packaging

In MEMS devices there are commonly cavity type structures formed by bonding. It can be used as a fabrication technique to create more complex and larger features. Micromachined Si substrates can be bonded to other materials in a process called fusion bonding. It allows for the creating of pre-etched cavities to be covered for various applications or sealing features. It relies on the atomic bonds of each layer of material directly or on a thin SiO₂ layer done with heating and pressure. The resulting structure ends up having quite low residual stress due to Si excellent TCE matching ability. It also creates a very effective bond that results in a sturdy fabrication method for these enclosed cavities, or grooves/channels. Photoresist and

polymethylmethacrylate (PMMA) are used as the fusion bonding media in MEMS and even provide a successful bonding for polyimide [118,122].

Wire bonding, encapsulation and packaging of MEMS devices is one of the most essential steps of a properly operating MEMS device. This is provided by the packaging methods and allows the MEMS devices to be commercialized as shown in figure 36 [118].

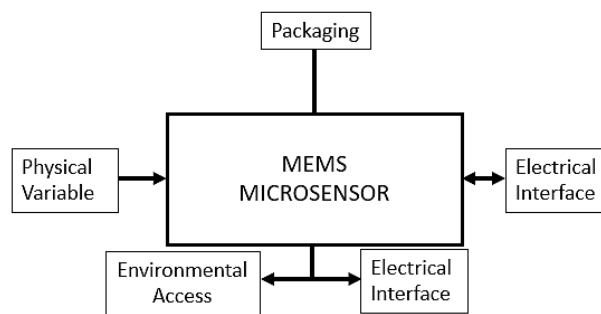


Figure 36. A diagram of the important role that packaging holds for commercial MEMS devices [118].

A proper packaging for a MEMS device should fit the following general criteria – provide protection against and be able to ‘withstand’ its operating environment. Allow for access and connections to a physical environment/domain i.e., optical fibers, fluid feed lines, etc. It should provide EM shielding to prevent electrical interference inside and outside of the device. Provide proper thermal dissipation and withstand operating temperatures. Reduce any stress or strain from external loads, and finally handle power from electrical connections without disrupting any signals [118].

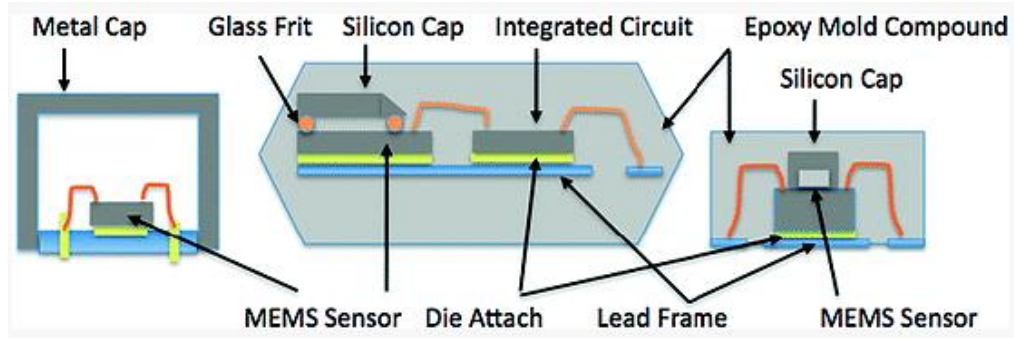


Figure 37. Three common types of packaging for MEMS devices [118].

Figure 37 shows the three most common types of MEMS packaging methods. Each of these package types have been adapted in one form or another for packaging MEMS sensors.

Typically, the substrate for the ICs requires an electrical connection to properly provide an external bias voltage. Sensor dies are mounted to a die attach pad inside the package using a conductive bond. These die pads are joined to a metal lead frame with wiring that provides the necessary electrical connections to the leads shown clearly in figure 37. These electrical connections are called wire bonds. Some of the bond mediums include Au-Si eutectic bonding – essentially a soldering bond between two alloys; epoxy bonding, and glass loaded with silver. The packages themselves are formed by moulding plastic, or airtight sealed ceramic or metal caps (hermetic seal). To electrically connect the die to its environment or domain, wire bonding is the most commonly used method. Wire bonding consists of two types: ultrasonic and thermosonic. The difference between the two methods is the amount of mechanical stress applied to the die, the minimum spacing between wire bonds, the type of wire alloy used, and whether it is possible to adjust the wire bonds. There is another method that is used called flip-chip bonding. This technology does ‘wire’ bonding with the chip face down to a substrate via

bumps. These bumps are made of solder, Au, Cu, or Ni and when heated the bumps melt and simultaneously form all the electrical connections between the chip and die [118].

III. METHODOLOGY

This chapter offers detailed information on sensor and device design selection, parameter selection, simulation technique, and extrapolation. The first section will discuss the coplanar waveguide and RF structure and its parameters discussed for the most optimal geometry to achieve UHF responses with high isolation, reversibility, and switching speeds. The LC-CNT composites and other materials selection criteria as well as the finite element method/analysis (FEM & FEA) will be discussed here as well.

3.1 Device structure

An RF switch is comprised of multiple components and structure elements that carry their own unique importance and purpose. The structure is typically divided into the type of RF planar strip line technology and the specific type of that strip line technology implemented. The first would be the choice to use a CPW instead of a single microstrip planar transmission line device. The CPW is a much better choice to create low insertion, low RF loss, excellent return loss, and isolation. The next choice is the structure of the waveguide device. To prevent parasitic losses and the other disadvantages discussed in section 2.3.2 a GCPW or CPWG structure is best following the MCM-Si device design choice. In figure 38 below the model for this RF switching device is shown. The RF switching mechanism is ideally controlled by a LC-CNT cell in the middle of the signal line.

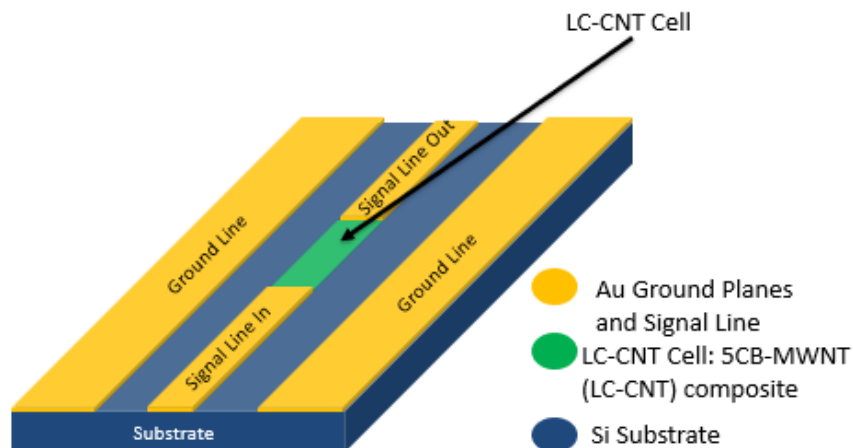


Figure 38. Design of general CPW structure for RF LC-CNT switching device. This device has a LC-CNT cell in the middle of the signal line to control the switching mechanism of the RF device. This is the model that this work is based around.

3.2 Working Principle of Device

The working principle of device operation for an RF switch is essentially two main parts the waveguide, and switch. The waveguide is what will guide RF signals with minimal losses through a device and the switch membrane or bridge is what controls the ON/OFF state. For this device the working principle is to use an LC-CNT composite as the switching mechanism using the unique operating principle of LCs. As discussed in sections 2.1.1 and 2.1.2, the LC molecules are in the 'OFF' state when the molecules director is perpendicular to the signal line and electric field. LC molecules in the 'ON' state will have their directors parallel to the signal line or electric field and allow for the signal to pass.

3.2.1 RF Switch Operation

Waveguide

Typically, for RF applications the waveguide structure will either be a microstrip structure or CPW. In this research a CPW type structure is used. It is most commonly constructed using MCM Si based fabrication with a Si wafer with metal (i.e., Au, Al, Cu etc.) conductors on top in a planar fashion in a ground-signal-ground configuration with gaps in between. There are also grounded configurations of CPW (GCPW or CPWG) that contain a metal backed substrate with the same material used for the conductors. Another configuration can include vias made of the same material used for the conductors that electrically connect the ground planes to the metal bottom. There is one port for the RF signal in and one port for the RF signal out. The transmission of the signal through the dielectric substrate, and air creates modes for how the wave travels. To affect the parameters of an RF switch such as insertion loss, return loss, isolation etc., one would change the dimensions of the waveguide – width of signal and ground conductors, gap between conductors, length, and thickness of substrate, etc. Another option is to also change the conductor and substrate material. So, because the transmission of the signal depends entirely on the material selection, and dimensions of the CPW device there are no universal formulas for CPW transmission since, for example, for any given line impedance there is an infinite number of solutions for the geometry and materials used of a CPW device [123]. An example of the CPWs geometry can be seen below in figure 39. The goal in this research was to use the LC-CNT composite as the switching mechanism and gather the S-parameter results. The geometry of each device type was selected to compare performance between the configuration types.

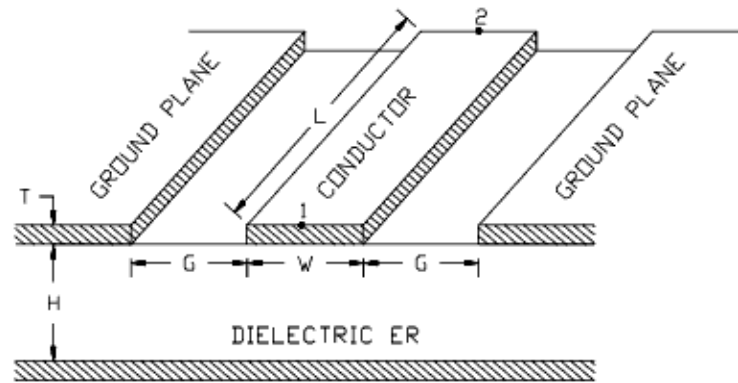


Figure 39. Various constraints of CPW device to alter RF switch parameters with W , L , and T being the width, length, and thickness of the conductors respectively. Where G and H are the width of the gaps between conductors and height of the substrate respectively. Lastly, 1 and 2 represent where the signal is fed through from port 1 to 2. [124].

Switch

The switch is the other portion of the device that determines various RF switch parameters and their performance such as switching speed, reliability, repeatability, and more. The switch's driving principle for RF applications is typically either electrostatic (most common), electromagnetic, electrothermal, or piezoelectric. The contact form for these switches is most commonly either contact or capacitive. This research is based around an RF device using an LC-CNT composite as the switching mechanism as discussed in section 3.2.

3.3 Design

For this design we used a Si substrate. The RF switch is built upon the Si substrate with a waveguide configuration. This device had three variations a CPW, CPWG, and FG-CPWG used for simulations which will be shown in the results section below. The devices used Au conductor

lines and Au metal backed ground. The signal line is either Au or uses the LC-CNT composite material as shown below in figure 40.

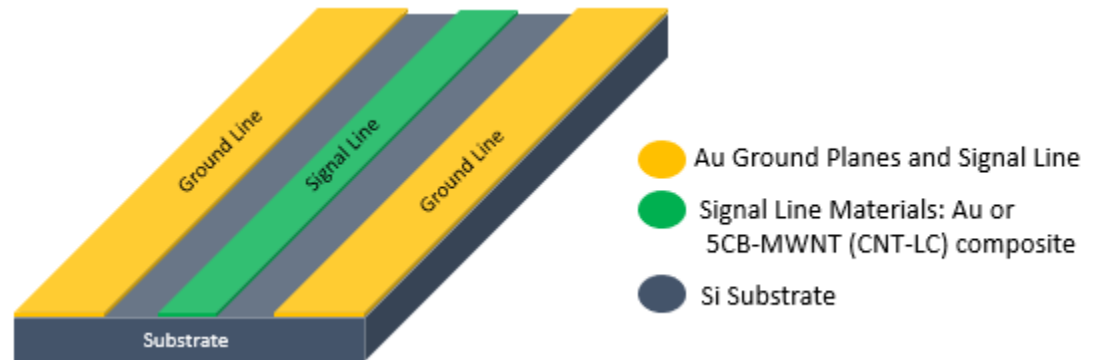


Figure 40. Design of simulated CPW structure for LC-CNT RF switching device with Au ground lines, and Au or LC-CNT composite signal line for measurement comparison.

The LC-CNT composite material chosen for this work is 4-Cyano-4'-pentylbiphenyl multi-walled nanotube (5CB-MWNT). Below in tables 5 and 6 are the material parameter values for various LC media including 5CB. In table 6 we can see material parameter values for both the perpendicular (OFF) and parallel (ON) states used.

Table 5. Characteristics and values for various LC and chiral dopant media as it relates to material selection for 5CB-MWNT in this research [128].

LC	Nematic mesophase	dielectric anisotropy , optical anisotropy n	Reference
EBBA	308.9 - 350.6 K	= -0.13, n = 0.25 at 313 K	Goncharuk et al., 2009
5CB	295.5 - 308.3 K	= 13 , n = 0.177 at 298 K	Blinov & Chigrinov, 1996
MLC6608	clearing point at 363 K	= -4.2 , n = 0.0830 at 293 K	Licristal , 2002
MLC6609	clearing point at 364.5 K	= -3.7 , n = 0.0777 at 293 K	Licristal , 2002

Table 6. Properties and parameter values of various LC and chiral dopant as it relates to material selection for 5CB-MWNT in this research [129].

Samples	Permittivity		Dielectric anisotropy	Loss tangent		Operating frequency
	ϵ_{\perp}	ϵ_{\parallel}	$\Delta\epsilon$	$\tan \delta_{\perp}$	$\tan \delta_{\parallel}$	F (GHz)
K15 (5CB)	2.72	2.90	0.18	0.03	0.03	1–10
BL037	2.35	2.61	0.26	0.06	0.06	1–10
BL006	2.62–2.69	3.11–3.12	0.49–0.43	0.015–0.007	0.035–0.036	4.8–8.7
E7	2.72	3.17	0.45	0.12	0.02	5–6
GT3-23001	2.46–2.50	3.28–3.30	0.82–0.80	0.0143	0.0038–0.004	13.5–19
GT3-24002	2.50	3.30	0.80	0.0123	0.0032	6–10

The information from tables 5 and 6 was used in conjunction with various works to determine a suitable LC-CNT composite and its specific electro optical properties for usage in an LC-CNT RF switching device [130-136]. The environment of transmission is air to keep the relative permittivity simplistic and offer the best performance. The parallel (ON) state of 5CB is the values that were researched and used for this work. The perpendicular (OFF) state was not considered as this is a value given when the device is not functioning. This will be discussed in further detail in chapter 4.

3.4 Simulation Methods HFWorks

Solidworks is a 3D computer-aided design (CAD) software. The technology behind Solidworks is primarily for the use of design, production, and simulation. CAD software's allow for a higher integration of design and manufacturing choices together. It uses computer analysis to create, modify, and analyze various device designs. It allows for the continual improvement of the design, improving documentation, and creating a large database for manufacturing and analysis. CAD software design has important information outputs such as material processes, dimensioning, and tolerancing according to an application's specific conventions [137].

Solidworks has a 3D field simulation program that is fully integrated with Solidworks called HFWorks. HFWorks is used for RF/microwave, and wireless applications. The software includes many solvers that cover antennas, 3D passive structures – using scattering parameters (S-parameters), and many more for resonant structures. HFWorks has a wide variety of specific applications for tuning elements, impedance matching, and most importantly waveguides and antennas. This addon uses the finite element method (FEM) which will be discussed further in the following sections. The program is designed to relate performance of a specific device design to important parameters such as antenna patterns, gain, and directivity, field distributions and scattering parameters. This program is able to integrate planar circuit designs (MCM/MMIC) and antennas and run simulations right from the device model and store simulation information without having to import the data for each design modification made [138].

3.4.1 Finite Element Method

Finite element method (FEM) is used as a numerical solving technique. It is necessary to use these solving techniques to comprehensively understand and quantify very complex

mathematics based around any physical phenomena such as wave/signal propagation. These physical phenomena based around time and space dependent problems are expressed in terms of partial differential equations (PDEs). Typically, PDEs cannot be solved with traditional analytical methods and instead use approximations of these equations. This is commonly achieved through discretization which is the method of taking continuous data and making it individually distinct or discrete, with a finite element. So, the FEM is used to solve these approximated PDEs [139-141].

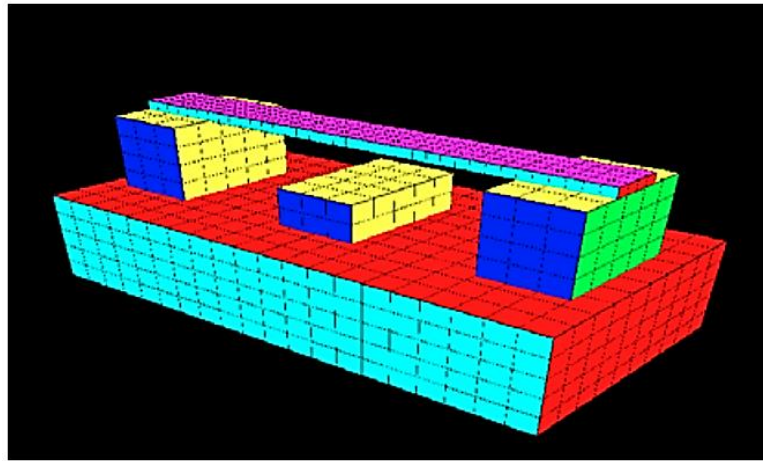


Figure 41. A miniaturized 3D mesh analysis model of an RF coplanar waveguide shunt switch [139].

Discretization is done by creating a 3D mesh – that is creating a finite number of discrete elements (cells) within a numerical domain [141,142]. In figure 41 there is an example of a 3D mesh analysis created for a RF switch with a capacitive shunt.

3.4.2 Finite Element Analysis

The direct practical application of this analysis to a specific field and physical phenomena is known as finite element analysis (FEA). FEA is a computational process that is used in programs like HFWorks. These software's use mesh generations over a domain to create smaller and more simplistic discrete elements to solve. Typically, these software's have an FEM algorithm that can be applied to any unique FEA. For these intricate problems it is most often a complex system with underlying physics principles like wave propagation. FEA's are a great option for solving problems over complex domains, although the model used in this research is a little more simplistic simulation times can still be long depending on how fine the mesh is. Things like the electric/magnetic field, signal loss, and more change throughout the dielectric. Considering simulations can take 5+ minutes it gives good indicator of how fine the mesh for the domain truly is, regardless of the physical systems geometry. This is important in simulating to know what is occurring at each port of planar transmission lines [139-141].

The simulation process was kept as consistent as possible to avoid any variables besides the material selection. As previously stated, the studies were done with high accuracy and a discrete frequency sweep from 0.01 GHz to 25 GHz with 101 points with a Δf step of 0.34999 GHz. Meshing was done with a moderate mesh control with an approximate global tolerance of 0.25 mm, all displayed in figure 42. The boundary conditions to define each waveguide device were a set of implicit boundary conditions of three to four imperfect electrical conductors (IEC) based on the device configuration. The IECs being the three top plane conductors and the one bottom plane conductor. Next was a signal of 5 V sent through the signal line, and then finally 2 ports one on the front face of the substrate and one on the back face which acted as SPST configuration.

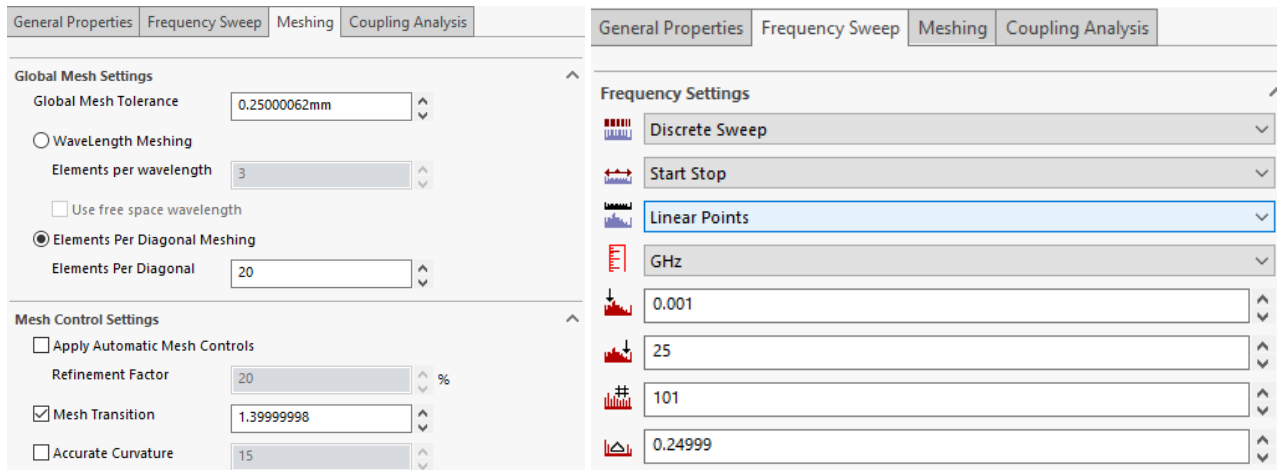


Figure 42. Global mesh tolerance and frequency sweep settings used for s-parameter simulations.

For results a circuits parameter table was added that included s-parameters where S_{11} and S_{21} were selected for return and insertion loss respectively. After the tables were created, the data was then exported as a 2D plot and altered the chart data accordingly.

IV. RESULTS AND DISCUSSION

4.1 Design of Coplanar Waveguide in HFWorks

The simulations done in HFWorks using FEA produced the following results to realize the ability of a LC-CNT composite material to improve the electric conductivity and performance of an LC-CNT RF switching device. The first design is a CPW design configuration that will be comparing S-parameter results. The first CPW using an Au signal line compared to a CPW using the LC-CNT (5CB-MWNT) composite material as the signal line. The same S-parameter results are then collected for the CPWG and FG-CPWG configurations. Simulations performed for the following results were done at a frequency band ranging from 100 MHz to 25 GHz which is the approximate limit needed to achieve mmWave frequency signals for the best performance of modern 5G technologies for large scale operation. The tests included simulations for RF switch parameters such as insertion and return loss through S-parameter measurements.

4.1.1 Material Selection in HFWorks

To keep the constraints for the devices the same so there was no difference of effect based on the material used for conductors and substrate, the same material for each device type was used. The choice of material was based on discussion from sections 2.2.2, 2.3.2, and 2.5.2. Si is used as the substrate, and Au is used for the ground conductors for upper and lower planes based on the design configuration. The signal line used Au or 5CB-MWNT (LC-CNT) composite for simulation.

Table 7. Silicon material parameters used for device substrate.

Property	Value	Unit
Relative Permittivity	11.7	F/m
Dielectric Loss Tangent	0	
Dielectric Strength	3.000E+06	V/m
Relative Permeability	1	N/A ²
Magnetic Loss Tangent	0	
Thermal Conductivity	150	W/(cm·K)
Thermal Expansion Coefficient	2.490E-06	1/K
Elastic Modulus	1.124E+11	Pa
Poisson's Ratio	0.28	

Table 7 show the various material parameters that are important in regard to device performance. The most important device parameters are the relative permittivity also called the dielectric constant which determines how well the material will polarize from an applied electric field. These are electrically insulating materials that essentially store charge. The next most important parameters are thermal conductivity and thermal expansion coefficient (TCE). Having a higher heat resistance and ability to perform better as a heatsink while having a very low TCE is great for high power/frequency applications without affecting device performance due to any deformities. The final parameters of importance are elastic modulus and Poisson's ratio which determine the materials deformation (expansion or contraction) when stress or strain is applied. High elastic modulus and low Poisson's ratio allows the material to resist said deformities.

Table 8. 5CB-MWNT composite material parameters used for Si substrate doping.

Property	Value	Unit
Relative Permittivity	2.9	F/m
Dielectric Loss Tangent	0.03	
Electric Conductivity	1.00E-03	S/m
Dielectric Strength	2.64E+08	V/m
Relative Permeability	1	N/A ²
Magnetic Loss Tangent	0	
Thermal Conductivity	1.25	W/(cm·K)
Thermal Expansion Coefficient	1.10E-03	1/K
Elastic Modulus	1.45E+07	Pa
Poisson's Ratio	0.6	

Table 8 shows the characteristics for the LC-CNT composite material I choose to go with which is a 5CB-MWNT composite. This is the most important material selection choice because it is used in my research to realize an increase in electrical conductivity and RF switch performance. The relative permittivity is really good as a conductor and works well for the region where the RF signal will be switched ON or OFF. This is the resistance to the formation of an electric field within a substance. The electric conductivity is naturally low in LC media however, when MWNT is dispersed into LC media an increase of several orders of magnitude is observed from pure 5CBs naturally low electrical conductivity of $\sim 10^{-9} S/cm$. The dielectric strength is the minimum (or maximum for electrically insulating material) applied electric field that results in electrical breakdown. This breakdown can occur in nanoseconds and results in the formation of an electrically conductive path. When this happens the concentration of charge

carriers in the material increases by several orders of magnitude and it becomes an excellent conductor. This causes an increase in electric field to be realized for the RF device to properly operate, caused by an increase in electrical conductivity which will be shown in section 4.2.2. The thermal conductivity as expected is quite low for a mesophase composite material. The thermal expansion coefficient is higher than most conductors again due to being a mesophase material, however, this is okay because of Si's excellent TCE matching and both Si's and Au's elastic modulus being high the overall structure is not very rigid [130-136].

Table 9. Gold material parameters used for device signal and ground lines.

Property	Value	Unit
Relative Permittivity	1	F/m
Dielectric Loss Tangent	0	
Electric Conductivity	4.10E+07	S/m
Relative Permeability	1	N/A ²
Magnetic Loss Tangent	0	
Thermal Conductivity	318	W/(cm·K)
Thermal Expansion Coefficient	1.44E-05	1/K
Elastic Modulus	7.72E+10	Pa
Poisson's Ratio	0.42	

Table 9 shows the various parameters associated with the devices signal and ground planes. The most important parameter of interest is the electrical conductivity. Good electrical conductivity is essential for any RF switch, especially for higher frequency/power applications.

The thermal conductivity and TCE are important as well for the signal and ground lines, as having high heat resistance, and good heat sink properties is important for the longevity of a RF switching device. Lastly is the elastic modulus and Poisson's ratio which also hold the same importance as the substrate material properties because again longevity, repeatability, and reversability are very important to RF switch performance.

4.1.2 Coplanar Waveguide Design Types

The CPW design is one of the most essential parts for the RF switch's performance. To understand the importance of the various design types for waveguides, the effect of the geometry on return and insertin loss was considered. For this work there are three main configurations starting with the coplanar waveguide with 'infinite' ground planes design structure.

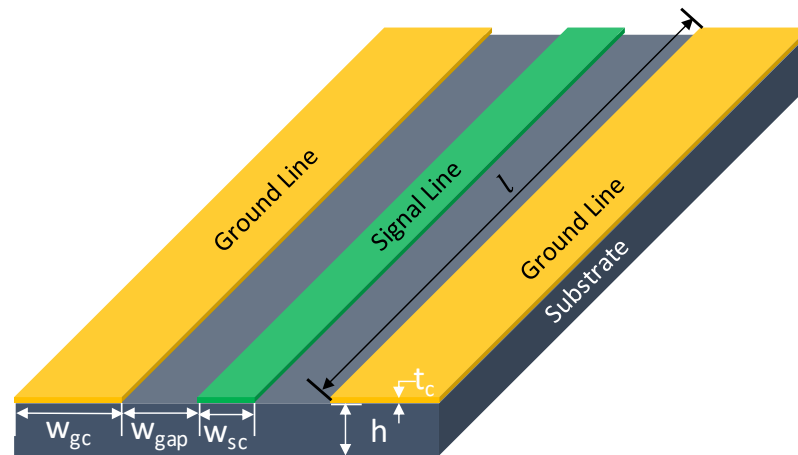


Figure 43. Shows the design structure of the standard simulated CPW configuration with typical dimensions used in this work. ' W_{sc}/W_{gc} , l , and t_c ' includes length, width and thickness of the signal and ground conductors respectively. ' h ' is the height of the substrate, and ' w_{gap} ' is the width of gaps between substrates.

In figure 43 the important dimensions that make up a CPW design are the total length of the device l , the width of the ground conductors w_{gc} , the width of the signal line conductor w_{sc} , the width of the gaps between conductors w_{gap} , the height of the substrate h , and the thickness of any conductors/ground planes t_c .

The second configuration type that was simulated in this research is the CPWG design shown below in figure 44.

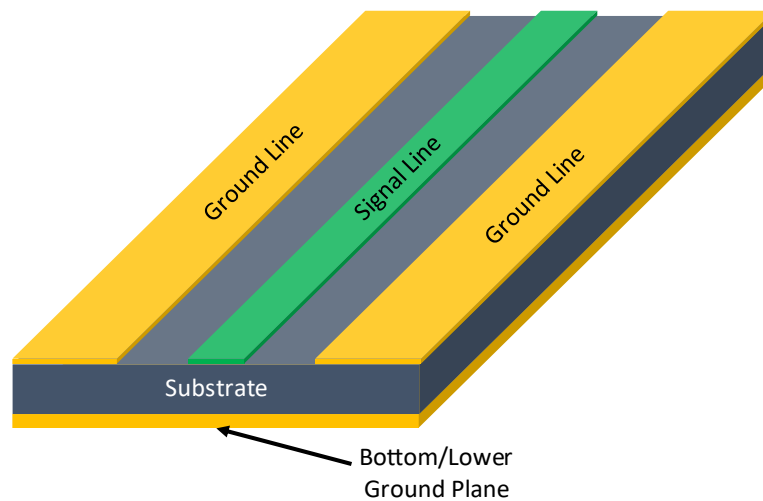


Figure 44. Shows the design structure of the simulated CPWG configuration with the same dimensions as the standard CPW and FG-CPWG devices. This includes the length, width, and thickness of the conductors (top and bottom plane). Width of gaps between conductors, and height of substrate.

The design in figure 44 has the same dimensions as shown in figure 43 including the thickness of ground planes. In this design, the thickness of the lower ground plane is the same thickness as all upper ground plane conductors. The third and final configuration type that was simulated in this research is the FG-CPWG shown in figure 45.

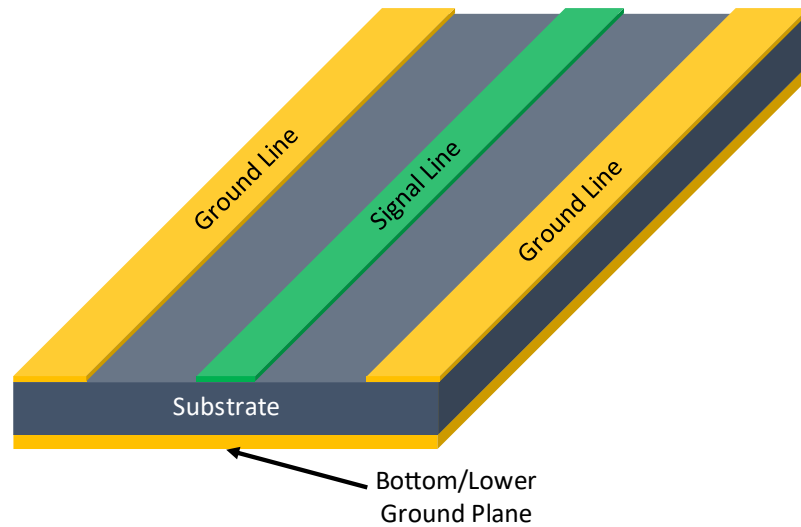


Figure 45. Shows the design structure of the simulated FG-CPWG configuration without vias with different gap and top plane ground conductor widths compared to the CPW and CPWG configurations – dimensions are otherwise the same. This includes the length, and thickness of the conductors (top and bottom plane), and the height of substrate.

The design configuration in figure 45 uses finite ground planes on the top of the device. As discussed in section 2.3.1 the upper finite ground planes and lower ground plane offer several advantages to a RF waveguide to improve device performance. The results showing the FEA data from each design type will be shown in detail in section 4.2.

4.1.3 Coplanar Waveguide Design Dimensions

Using the dimensioning from figure 45 the standard CPW and CPWG structures with theoretically 'infinite' ground planes both have the same dimensions. The conductors are the same length and height (length of substrate/device). The substrate of the device has a length, width, and thickness of 1000 μm , 125 μm , and 25 μm respectively. The ground conductor's width and height are 35 μm and 70 μm respectively. The signal line width is approximately 26 μm . The width of gaps between conductors are approximately 15 μm . This creates a device that

has an area of approximately $125000 \mu\text{m}^2$, with a LC-CNT cell that is approximately $26 \mu\text{m}$ by $50\mu\text{m}$. These dimensions were chosen to maintain the infinite ground plane principle by keeping the ground conductor widths larger than the width of signal line and gaps between conductors.

The FG-CPWG structure has slightly different dimensions as mentioned in figure 47. The conductors are all the same length and height (length of substrate/device). The substrate of the waveguide devices has a length, width, and thickness of $24670 \mu\text{m}$, $2300 \mu\text{m}$, and $400 \mu\text{m}$ respectively. The top plane ground conductor's width and height are $450 \mu\text{m}$ and $20 \mu\text{m}$ respectively. The bottom plane ground conductor's width is the same as the substrate/device width, and the thickness is the same as all top plane conductors. The signal line width is $400 \mu\text{m}$. The width of gaps between conductors are $500 \mu\text{m}$. Finally, the total area of the device is approximately $5.67 \times 10^7 \mu\text{m}^2$. These dimensions were chosen to maintain the finite ground plane principle which keeps the top plane conductors all approximately the same width and the gaps between conductors must be larger than conductor widths. This general geometry allows for an FG-CPWG that avoids too much path loss increase while having good thermal management. As discussed previously there are an infinite number of geometries that can result in the same line impedances and various desired characteristics. The approximations on all feature dimensions for both the CPW and FG-CPWG structures have a $\pm 0.5 \mu\text{m}$ tolerance.

4.2 HFWorks RF Finite Element Analysis

FEA was performed for all types of waveguide devices which includes a CPW, CPWG, and FG-CPWG. The simulation uses high accuracy approximation with a linear and discrete frequency sweep from approximately 0-25 GHz with 101 points of data with a Δf step of 0.34999 GHz. Simulations were done for approximately the same mesh size as follows:

Table 10. General mesh characteristics for waveguide devices.

Mesh Control		
Mesh Density	Global Mesh Tolerance Size (mm)	Mesh Control Global Element Size (mm)
Coarse	> 0.516 (Tolerance)	~1.0002
Moderate	0.5162 (Tolerance)	0.5162
Fine	0.2513 (Tolerance)	0.2513

Table 10 was the general mesh control parameters that each of the three device types followed. A coarse mesh is defined by anywhere the simulation produced inconsistent results and moderate was the threshold between coarse and fine densities. A fine mesh density provided the most accurate and consistent results. The mesh control was a large factor in determining the simulation time for each device. An analysis of exactly how fine the mesh needed to be for the most accurate results are shown in figure 46.

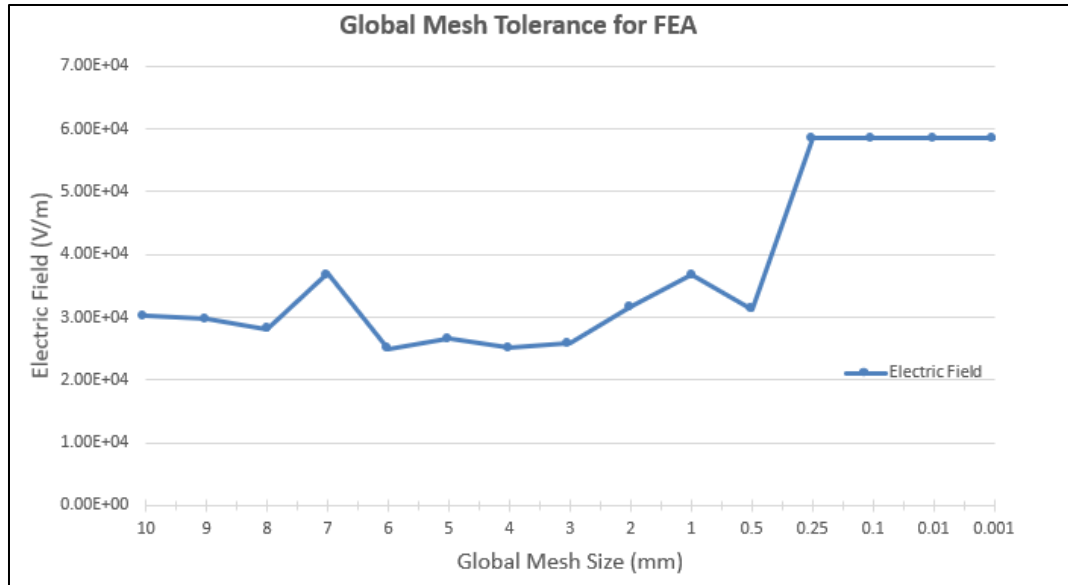


Figure 46. Shows the global mesh tolerance size versus electric field values to find the value where measurements remain consistent to avoid any errors due to too coarse of a mesh.

In figure 46 it is shown that the values for measurements are most consistent at a global mesh size of approximately 0.25 mm or smaller. Between 0.5-0.25 mm is the transition threshold between coarse and fine mesh's also called moderate density. Everything greater than 0.5 was a coarse mesh and would produce the most inaccurate simulation results. The reason this work opted to stay around 0.25 mm global mesh size was because as the global mesh size gets smaller the simulation time increases exponentially. Once the exact global mesh tolerance was determined the mesh control was applied in the gaps between the conductors and the mesh was generated creating a fine mesh for the various CPW configurations as shown in figure 47.

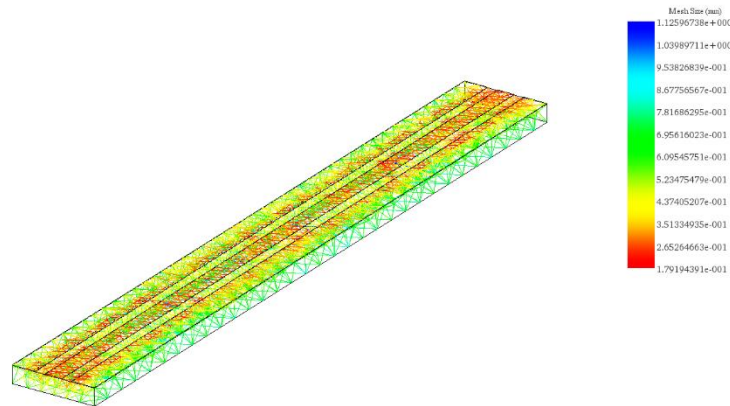


Figure 47. Example of the fine mesh created using 0.25 mm global tolerance for the various CPW device configurations.

4.2.1 S-Parameters

In this section the results and performance of each of the three devices will be shown. Each device type will have data for the return and insertion loss for the standard device configurations and the configurations with 5CB-MWNT (LC-CNT) composite as the signal line. All of the device's operating frequency bands are from approximately 0 to 25 GHz. This is the acceptable and optimal range for 5G applications that range from RF to mmWave frequencies. The purpose of these results is to look for an increase in return loss value from the standard to LC-CNT device. As discussed in section 2.2.1 a larger 'negative' dB value is preferred for return loss (i.e., -20 dB is better than -10 dB), as this means there is less power reflection leading to a more efficient device. For insertion loss, a lower 'negative' dB value is preferred (i.e., closer to 0 dB). An insertion loss value of 0 dB is most ideal to achieve the lowest signal loss during transmission. For the data shown below the peaks represent the local maximum points for each set of data. The local minimums are NULLs and represent discontinuities and noise in the signal.

The s-parameter results for return loss for the CPW with the Au signal line and CPW with the 5CB-MWNT signal line are shown below in figure 48 for comparison.

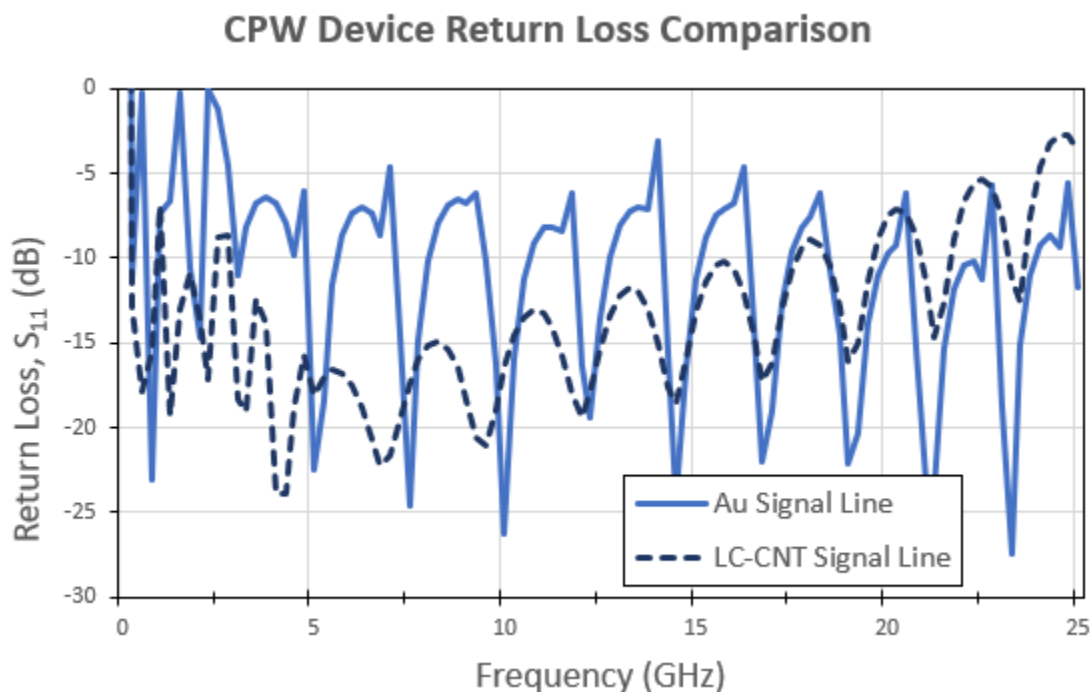


Figure 48. Comparison of return loss for standard Au signal line device and 5CB-MWNT signal line device. S-parameters simulated for CPW configuration.

CPW Return Loss Results

In figure 48 the return loss between the two devices shows a significant improvement most noticeably from the 0-15 GHz range. When comparing the peaks of the device using the Au signal line, we can see the peaks show a value of approximately -7.5 dB consistently from roughly 3-17.5 GHz. In that same frequency range, for the device with the LC-CNT signal line we can see the peak starting around -12.5 dB at 3 GHz decreasing further to -16 dB around 5 GHz and increasing approximately every 2.5 GHz by about 2 dB until roughly 17.5 GHz where it

reaches roughly -9 dB. For the LC-CNT signal line device, from 22.5-25 GHz this is where we can see the return loss increase by about 5 dB when comparing the peaks to the Au signal line device. However, this slight increase here does not change the excellent overall improvement in return loss across the majority of the frequency range.

The following insertion loss s-parameter result comparisons for the CPW device type are shown below in figure 49.

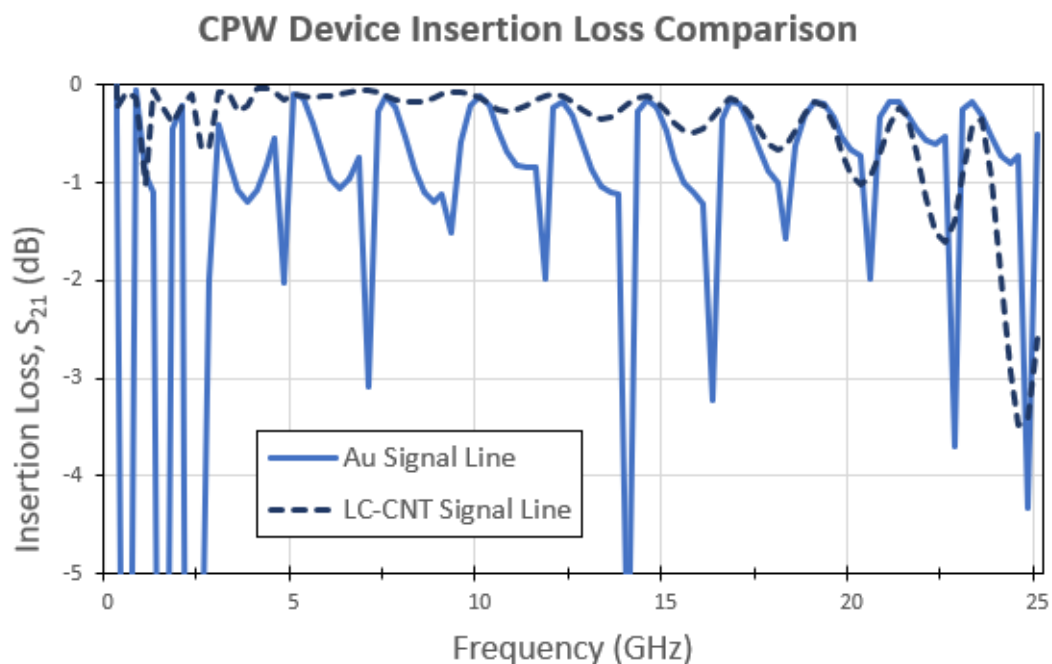


Figure 49. Comparison of insertion loss for standard Au signal line device and 5CB-MWNT signal line device. S-parameters simulated for CPW configuration.

CPW Insertion Loss Results

In figure 49 the insertion loss between the two devices shows a significant overall improvement most noticeably from the 0-17.5 GHz range. When comparing the peaks of the device using the Au signal line to the device using the LC-CNT signal line, it can be seen that the

peak value is relatively the same. However, with the Au signal line there are massive inconsistencies with much more noise. The overall consistency and little to no noise seen in the 5-17.5 GHz range shows the device having more consistent and lower overall insertion loss.

The following return loss s-parameter result comparisons for the CPWG device type are shown below in figure 50.

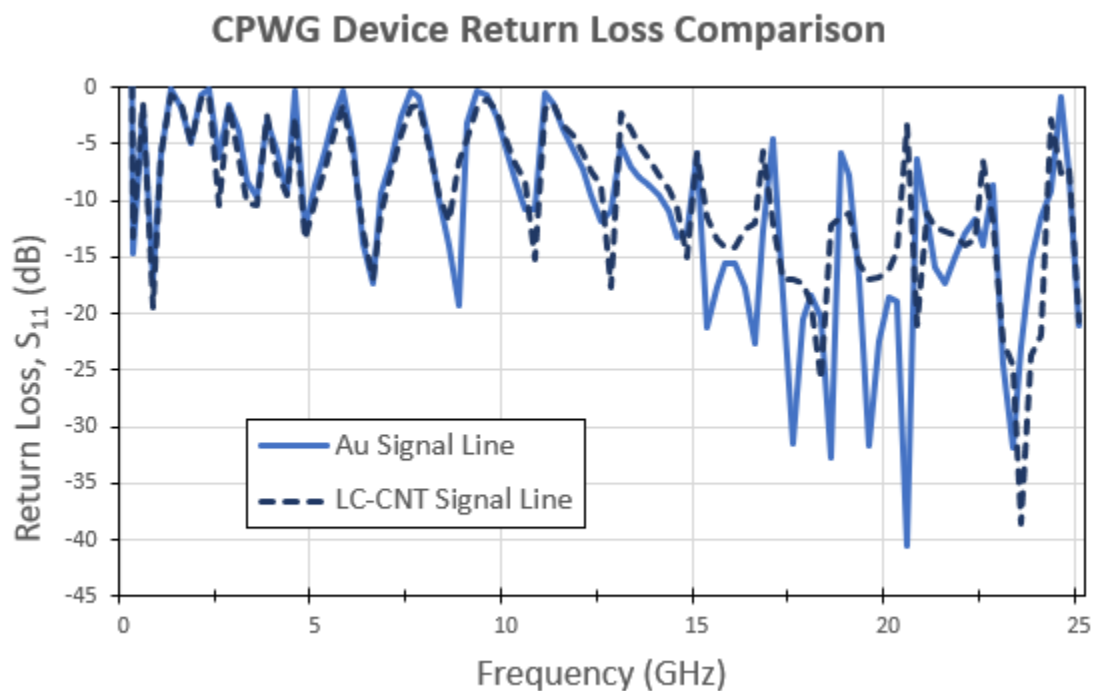


Figure 50. Comparison of return loss for standard Au signal line device and 5CB-MWNT signal line device. S-parameters simulated for CPWG configuration.

CPWG Return Loss Results

In figure 50 the return loss shows little to no overall change in dB across the entire frequency range. The peak values are essentially the same at every peak shown in the data. However, this result is also ideal because it shows that using the LC-CNT composite as a

switching mechanism doesn't reduce the performance of the device by increasing return loss. This means that device reliability can still be improved without loss of actual device performance.

The following insertion loss s-parameter result comparisons for the CPWG device type are shown below in figure 51.

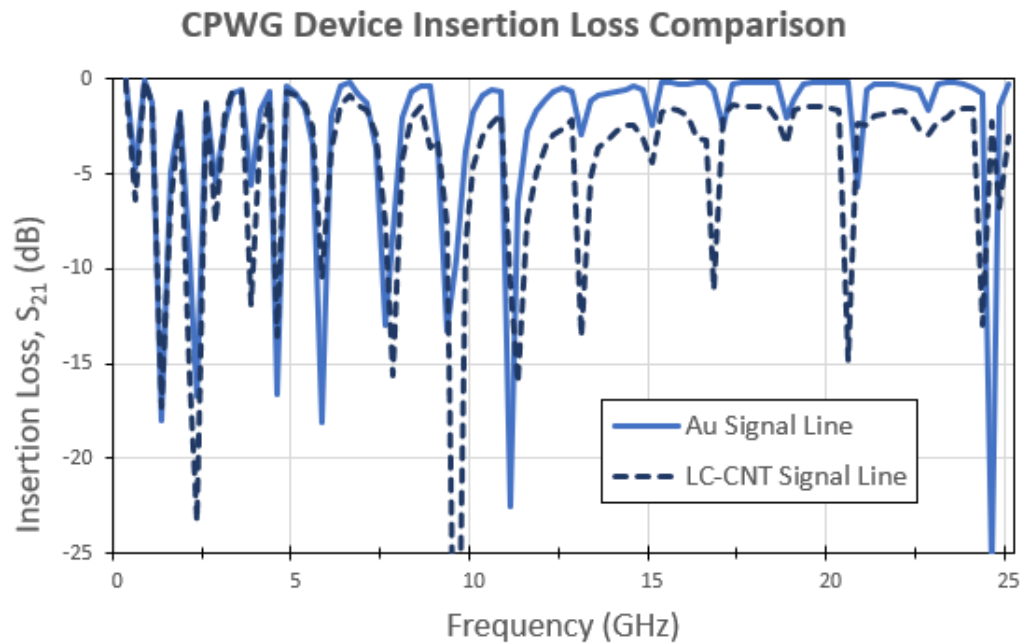


Figure 51. Comparison of insertion loss for standard Au signal line device and 5CB-MWNT signal line device. S-parameters simulated for CPWG configuration.

CPWG Insertion Loss Results

For the insertion loss shown in figure 51 there is a noticeable slight increase in insertion loss most notably from approximately 10-25 GHz. For example, around 14 GHz we can see this shift in dB as a roughly 2 dB increase in insertion loss from the Au signal line device to the LC-CNT signal line device. However, this slight 2 dB shift across a little more than half the frequency

range is still acceptable. The overall difference in insertion loss between the two devices is not large. This means that again, overall performance is not greatly affected for using the LC-CNT switching mechanism, meaning for increased device reliability, there is little tradeoff in the form of insertion loss for the CPWG configuration.

The following return loss s-parameter result comparisons for the FG-CPWG device type are shown below in figure 52.

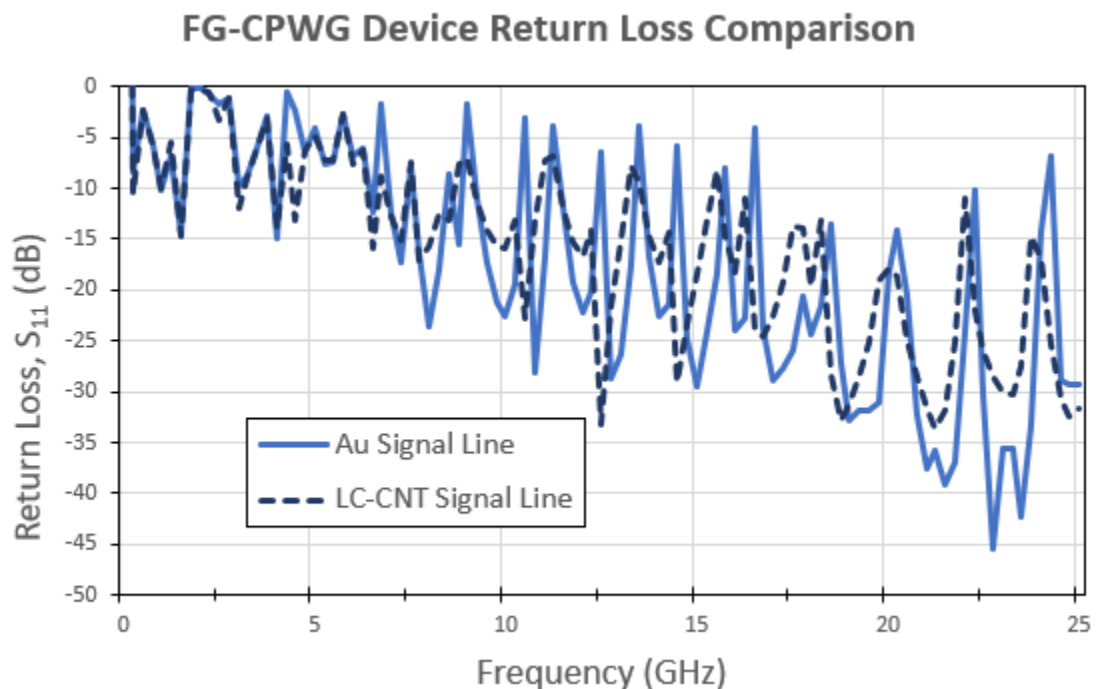


Figure 52. Comparison of return loss for standard Au signal line device and 5CB-MWNT signal line device. S-parameters simulated for FG-CPWG configuration.

FG-CPWG Return Loss Results

In figure 52 similar to the CPWG configuration there is little to no change in overall return loss value across the entire frequency range. The most noticeable change is at peaks

around 7, 9, and 12.5 GHz where the return loss value is larger for the LC-CNT signal line by around 5-10 dB. This shows only a very slight decrease in return loss at these few peaks, meaning overall device performance was relatively the same for return loss. Again, this shows that with similar device performance, return loss wise, the tradeoff for increased device reliability is worthwhile.

The following insertion loss s-parameter result comparisons for the FG-CPWG device type are shown below in figure 53.

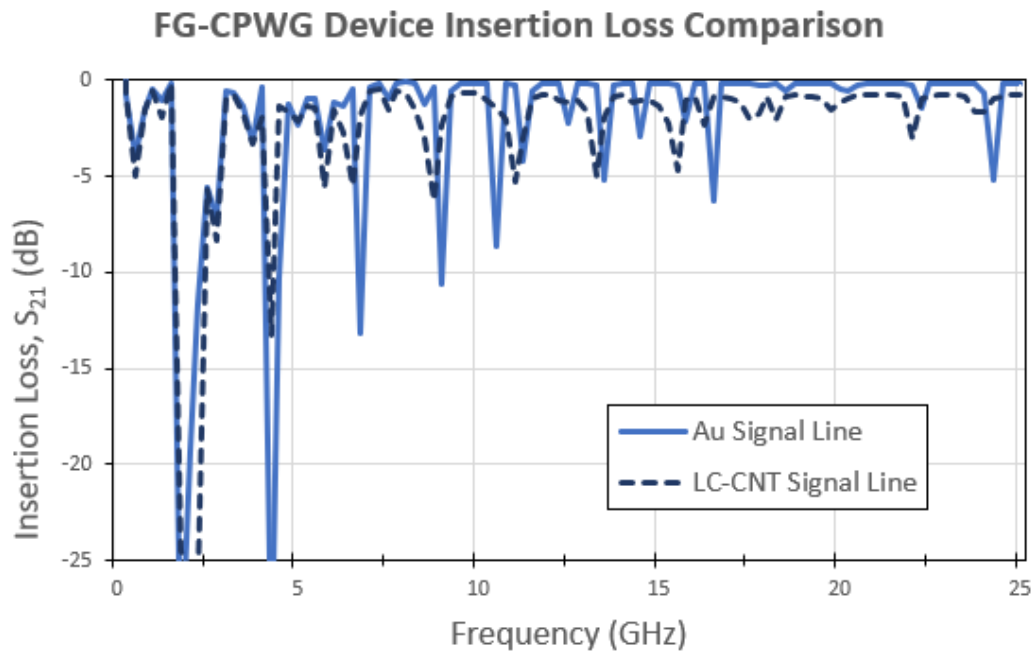


Figure 53. Comparison of insertion loss for standard Au signal line device and 5CB-MWNT signal line device. S-parameters simulated for FG-CPWG configuration.

FG-CPWG Insertion Loss Results

In figure 53 the insertion loss essentially no decrease in performance across the entire frequency range. There is a slight 1 dB shift increase in insertion loss from around 10-25 GHz. However, as previously noted a very slight 1 dB shift is negligible when using the LC-CNT switching mechanism because of the tradeoff between increased device reliability.

The following return and insertion loss data are from the OFF state using the CPW device configuration that showed the best results between the Au and LC-CNT line devices. The OFF state uses the LC molecules parameters from their perpendicular state as shown in table 6. First the return loss data for the CPW configuration in the OFF state will be shown with comparison between the Au signal line and LC-CNT signal line devices.

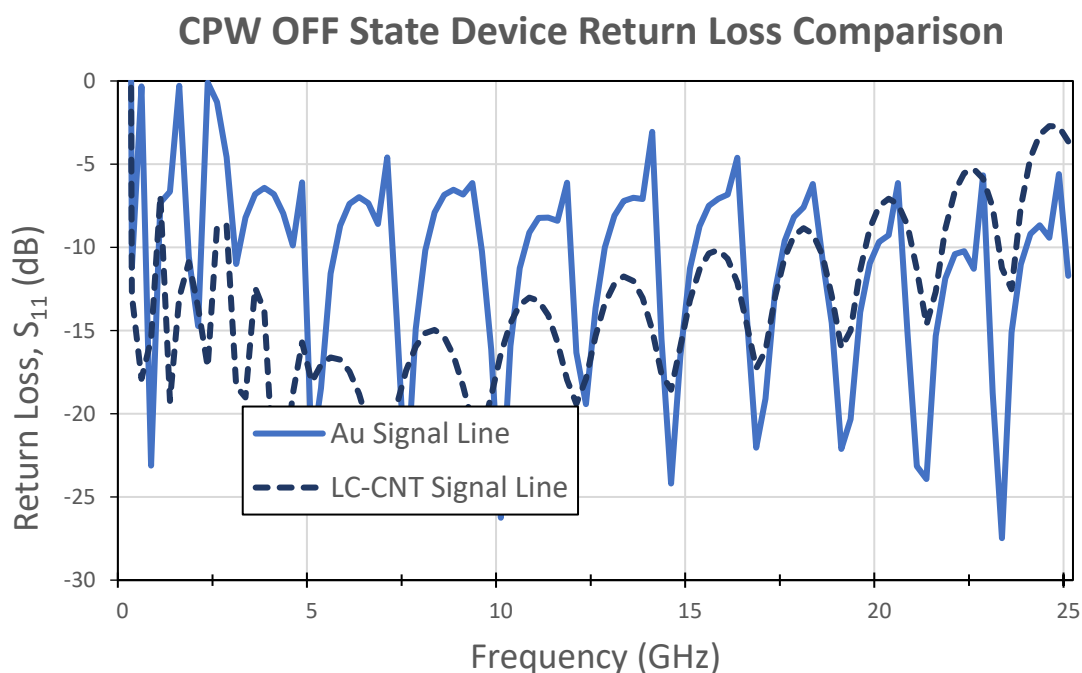


Figure 54. Comparison of return loss for standard Au signal line device and 5CB-MWNT signal line device in OFF state. S-parameters simulated for CPW configuration.

CPW OFF State Return Loss Results

From figure 54 it can be seen that the results are identical to the CPW ON state results shown in figure 48. This is due to limitations in the software that I will discuss in section 4.2.5 below.

Next is the insertion loss data for the CPW configuration in the OFF state, which is shown below in figure 55 with comparison between the Au signal line and LC-CNT signal line devices.

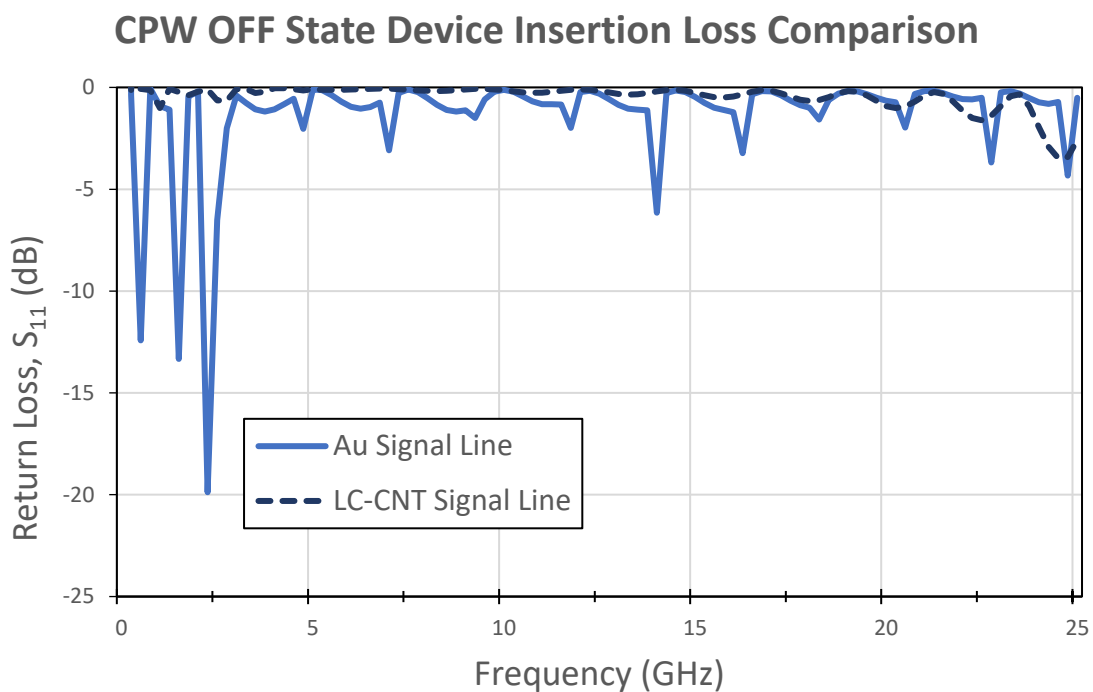


Figure 55. Comparison of insertion loss for standard Au signal line device and 5CB-MWNT signal line device in OFF state. S-parameters simulated for CPW configuration.

CPW OFF State Insertion Loss Results

From figure 55 it can be seen that there is essentially no improvement of insertion loss between the two devices, with the exception of the device using the Au signal line having slightly more noise. The peaks of each of the device's data of the insertion loss value across the entire frequency range is consistent around 0-1 dB.

4.2.4 Design Comparisons

The devices tested had the signal line material altered between Au and the 5CB-MWNT composite to measure changes in device performance. The entire signal line was either Au or 5CB-MWNT for these simulations. Ideally, there would be a cell roughly 25% of the total conductor length in the center of the signal line with the 5CB-MWNT composite as the switching mechanism controlling the transmission of the signal and the rest of the signal line would be Au. In practice and simulation there would be noticeably more signal losses with the signal conductor being entirely 5CB-MWNT. Within the simulation there were fairly large conductor and dielectric losses due to the LC media having larger loss tangents as shown in table 11 below.

Table 11. Average device losses for Au and 5CB-MWNT signal lines. Signal lines were entirely Au or 5CB-MWNT due to simulation constraints discussed in 4.2.5. Overall, the total losses were fairly high between both materials. Enough to contribute to the larger insertion loss results for the antenna study.

Average Device Losses						
Frequency (GHz)	Dielectric Loss		Conductor Loss		Total Loss	
	Au	5CB-MWNT	Au	5CB-MWNT	Au	5CB-MWNT
0	0.000E+00	4.058E+01	5.695E-04	0.000E+00	5.695E-04	4.058E+01
5	0.000E+00	6.671E-04	7.714E-04	0.000E+00	7.714E-04	6.671E-04
10	0.000E+00	3.756E-04	1.683E-03	0.000E+00	1.683E-03	3.756E-04
15	0.000E+00	4.467E-04	2.597E-03	0.000E+00	2.597E-03	4.467E-04
20	0.000E+00	5.206E-04	5.068E-03	0.000E+00	5.068E-03	5.206E-04
25	0.000E+00	7.416E-04	5.173E-03	0.000E+00	5.173E-03	7.416E-04

It is clear that the tradeoff from going from a traditional RF switch with Au signal line to a LC-CNT signal line switching mechanism is excellent. Since the results show overall improvement or overall performance staying consistent, for return and insertion loss between the two different signal line devices, it lends proof to the LC-CNT switching mechanism performing better overall. This means that ideally you would only benefit from using the LC-CNT switching mechanism as there is no tradeoff for device reliability based on device performance.

It is clear from the results that the CPW configuration is the most ideal configuration for best device performance when comparing the Au signal line to the LC-CNT signal line. The FG-CPWG configuration was the next best performing configuration. With the CPWG configuration being last in performance by a small margin. This follows expectations given the limitations for simulating and not being able to achieve the most ideal FG-CPWG structure and geometry we desired.

The key to allowing for the LC switch to operate successfully is avoiding the irreversibility effects caused by the electro-optic memory effect. This is done with mixing concentration, threshold voltage, and sample temperature. This information was previously discussed in section 2.1.2 that the LC molecules operate properly in a 'ON' and 'OFF' state given that there is a proper concentration of the LC mixture used (>0.05 wt. %) to avoid the electro-optic memory effect. A proper threshold voltage of ≥ 5 V, and finally, a proper temperature range (56-64 °C) will decrease the memory effect. Selecting these proper criteria is what will enable the LC molecules to properly follow their parallel and perpendicular switching states that would enable the device to properly turn 'ON' and 'OFF' again for millions of cycles.

4.2.5 Simulation Limitations

The limitations presented by Solidworks and the RF simulation addon HFWorks, were the limited design choices, which is consistent across any simulation software. The main limitation I faced in this research was the design choice for the waveguide device. HFWorks presented a strong selection of devices to do RF simulations with. Using their MiniAtlass creation tool they provide the user with fairly good customizability. However, there were limited options, if any, to alter the device after creation. The assembly was unable to be altered via adding a sketch and extruding or reshaping parts in anyway. In regard to the work presented in this research being unable to add vias made two of the device types in this research unable to realize their full potential in practice. After discussion with a representative and researcher for HFWorks this feature, or limitation was most likely intentional to avoid rendering the device from being unable to be fully integrated and simulated within HFWorks creation tool. This limitation also applies to making the LC-CNT composite only roughly 25% of the signal line instead of the entire conductor. The software was unable to change individual sections of the

device. Another limitation included being unable to fully characterize the RF switch. This meant that certain parameters could not be fully measured, such as switching speeds, power consumption, repeatability, or operating lifetime. All these constraints contribute the reason for creating high conductor losses and dielectric losses.

Additionally, simulations regarding measurements with the LC media in the perpendicular (OFF) state included are not as accurate as the parallel (ON) state measurements. As the OFF-state measurements would consider the device not to be functional when there is no voltage applied, leaving the device inoperable. As shown in section 3.3 in Table 6, there is a value for both OFF and ON states that only varies very slightly with permittivity as 5CB does not have different loss values based on the state it's in. However, this is not applicable as the device will not operate with no voltage applied. The limitations presented by the simulation software would not allow us to measure if any signal is propagating when the device is OFF, as voltage cannot be set below 1 V and 'running' the simulation is considering the device to be turned on. Therefore using 1 V and only slightly changing the permittivity causes almost identical results to the device being in the parallel (ON) state. Ideally, LC media are not perfectly aligned perpendicular to the external field as LC molecules orient themselves randomly without an applied electric field. This would cause an extremely minimal amount of conductivity as some LC molecules would be randomly aligned slightly parallel even when OFF. Again, this effect could not be measured with this software and Table 6 is only given to show the material parameters for when there is no applied electric field for 5CB (which is only a very slight change). If the LC media chosen had a range of permittivity's such as liquid crystal type BL006 as shown in Table 6, then simulations could be run for those values. Exploration into these various LC media is briefly discussed in chapter 5 under the future works section.

V. CONCLUSION

5.1 Summary

A LC-CNT composite material was investigated for creating a novel RF LC-CNT switching device and the various telecommunication applications this device could apply to. It was found that changing the geometry of the device i.e., conductor and gap widths, or device structure was able to alter RF and antenna characteristics. It was discovered that changing the signal conductor material to the LC-CNT composite: 5CB-MWNT would increase the electrical conductivity of an RF waveguide device. The consistent improvement of return and insertion loss when comparing the 5CB-MWNT conductor device to the standard Au signal conductor shows that LC-CNT composites can modulate the electro-optic effect for RF switching extremely well. For this device the 5CB-MWNT composite was found to have excellent electrical conductivity modulation due to its relative permittivity and dielectric strength being a good mixture for an excellent conductor. The main challenges faced in this research were finding a proper LC media and CNT chiral dopant and creating the most ideal device configuration with the given limitations. Beside increased general RF switch performance improvements, an effective RF switch is needed in telecommunication systems with the ever-increasing demand for high performance 5G systems being integrated. High data rate transmission speeds and volume are the key factors for a 5G system. This device can also be used as the base device for a phase tunable array to improve 5G coverage more cheaply and compactly. Currently, 5G systems use multiple antennas to combat the limited transmission range in both distance and phase. Meaning 5G telecommunication systems are costly and take up a great deal of space to provide coverage to urban and rural areas.

5.2 Future Works

To fabricate and test a RF LC-CNT switching device using MEMS fabrication process. Also to further characterize and optimize RF waveguides presented in this research and look into other LC media and CNT chiral dopants to be utilized as the switching mechanism. Various device geometries should be investigated to ascertain the most ideal range of values for the waveguides dimensions. Adding vias to the CPWG or FG-CPWG configuration would in practice produce a device with excellent return and insertion loss and antenna directivity and gain results along with the most ideal waveguide dimensions. In practice without grounding the top and bottom planes with vias there would be EMF leakage that is no longer contained between the top and bottom ground planes and would leak out to the sides of the device. The thermal dissipation would also be much more effective because of the electrical short and dissipating the heat directly through the bottom ground conductor. It would also increase the mechanical strength of the device by adding rigidity throughout the top and bottom of the device. As mentioned virtually all commercial RF simulation software will have similar limitations. In practice after investigating an ideal device geometry, a RF waveguide device should be fabricated to test for the full device characteristics mentioned in 3.2.1.

This type of device fabrication presents a high level of complexity making a working proto-type design difficult to achieve for in-lab and research uses. Work on improving telecommunication systems through LC-CNT composites in RF LC switching devices requires many devices with varying dimensions and materials to be tested, which can make this research very costly and time consuming. Waveguides have an infinite number of possible geometries and characterizations, so it is hard with limited time and resources to theorize the most ideal RF switch and antenna structure using a CPW device configuration.

BIBLIOGRAPHY

- [1] I. Lysenko, A. Tkachenko, E. Sherova, and A. Nikitin, "Analytical Approach in the Development of RF MEMS Switches," *Electronics*, vol. 7, no. 12, p. 415, 2018.
- [2] M. Munna, F. Anwar, and R. Coutu, "Nematic liquid crystal composite materials for DC and RF switching," *Technologies*, vol. 7, no. 2, p. 32, 2019.
- [3] Chien-Wen Chiu and Ruey-Beei Wu, "A moment method analysis for coplanar waveguide discontinuity inductances," in *IEEE Transactions on Microwave Theory and Techniques*, vol. 41, no. 9, pp. 1511-1514, Sept. 1993, doi: 10.1109/22.245669.
- [4] Dehghani, Mohammad Reza, et al. "Liquid Crystals: A Power and Cost-Efficient Electronically Steerable Antenna Solution for 5G." *Microwave Journal* 63.5 (2020).
- [5] C. Culbreath, "Artificial Microscopic Structures in Nematic Liquid Crystals Created by Patterned Photoalignment and Controlled Confinement: Instrumentation, Fabrication and Characterization," Ph.D. dissertation, Dept. Chem. Phys., Kent State University, Kentucky, United States, 2015.
- [6] Liquid Crystals. Simon Fraser University, 15 Aug. 2020, [Online]. Available: <https://chem.libretexts.org/@go/page/3584>.
- [7] Debnath A, Mandal PK, Sarma A, Gutowski O. Effect of silver nanoparticle doping on the physicochemical properties of a room temperature ferroelectric liquid crystal mixture. *Journal of Molecular Liquids* 2020;319:1–4. doi:10.1016/j.molliq.2020.114185.
- [8] "Chemical Properties of Liquid Crystals." *Chemical Properties*, [Online]. Available: <https://web.archive.org/web/20160716115311/http://plc.cwru.edu/tutorial/enhanced/files/lc/chem/chem.htm>.
- [9] "liquid crystals - liquids and intermolecular forces - chemistry the central science." *Educational Materials*, [Online]. Available: <https://schoolbag.info/chemistry/central/105.html>.
- [10] Ciattoni, Alessandro, Gabriella Cincotti, and Claudio Palma. "Angular momentum dynamics of a paraxial beam in a uniaxial crystal." *Physical Review E* 67.3 (2003): 036618.
- [11] Rego, James A., et al. "Asymmetric synthesis of a highly soluble 'trimeric' analogue of the chiral nematic liquid crystal twist agent Merck S1011." *Liquid crystals* 37.1 (2009): 37-43.
- [12] Castellano JA (2005). *Liquid Gold: The Story of Liquid Crystal Displays and the Creation of an Industry*. World Scientific Publishing. ISBN 978-981-238-956-5.

- [13] Barron, Andrew R. Pavan, M. Raja, V. "Physical methods in chemistry and nano science." (2015).
- [14] Duda, Łukasz, et al. "Helical twisting power and compatibility in twisted nematic phase of new chiral liquid crystalline dopants with various liquid crystalline matrices." *Liquid Crystals* 46.12 (2019): 1769-1779.
- [15] Fraccia, T.P.; Smith, G.P.; Clark, N.A.; Bellini, T. Liquid Crystal Ordering of Four-Base-Long DNA Oligomers with Both G–C and A–T Pairing. *Crystals* **2018**, *8*, 5.
<https://doi.org/10.3390/cryst8010005>
- [16] Achard, M. F., et al. "Switching of banana liquid crystal mesophases under field." *The European Physical Journal E* 10.2 (2003): 129-134.
- [17] Schadt, Martin. "Nematic liquid crystals and twisted-nematic LCDs." *Liquid Crystals* 42.5-6 (2015): 646-652.
- [18] Jacobson, Ted. *Phys104 Notes, Demos and Supplements - Fall 2008*, 20 Nov. 2008, [Online]. Available: <http://www.physics.umd.edu/grt/taj/104a/104anotessupps.html>.
- [19] Gray, George W., and Stephen M. Kelly. "Liquid crystals for twisted nematic display devices." *Journal of Materials Chemistry* 9.9 (1999): 2037-2050.
- [20] Dolgov, Leonid, et al. "Electro-optical memory of a nematic liquid crystal doped by multi-walled carbon nanotubes." *arXiv preprint arXiv:1210.1431* (2012).
- [21] Dolgov, L., O. Yaroshchuk, and M. Lebovka. "Effect of electro-optical memory in liquid crystals doped with carbon nanotubes." *Molecular Crystals and Liquid Crystals* 496.1 (2008): 212-229.
- [22] I. Dierking, G. Scalia, P. Morales, Liquid crystal – carbon nanotube dispersions, *J. Appl. Phys.* 97 (2005), 044309
- [23] Cîrtoaje, Cristina, Emil Petrescu, and Cornelia Moțoc. "Electric field effects in nematic liquid crystals doped with carbon nanotubes." *Physica E: Low-Dimensional Systems and Nanostructures* 54 (2013): 242-246.
- [24] Jackson, John David. "Classical electrodynamics." (1999): Wiley 841-842.
- [25] Griffiths, David J. *Introduction to electrodynamics*. New Jersey: Prentice Hall, 1962.
- [26] Chow, Tai L. *Introduction to electromagnetic theory: a modern perspective*. Jones & Bartlett Learning, 2006.
- [27] Electronics Tutorials: Capacitance in AC Circuits. Available. Online: https://www.electronics-tutorials.ws/capacitor/cap_8.html

- [28] Guralnik, I. R., et al. "Interdependence of the electrical and optical properties of liquid crystals for phase modulation applications." *Journal of Applied Physics* 87.9 (2000): 4069-4074.
- [29] De Gennes, Pierre-Gilles, and Jacques Prost. *The physics of liquid crystals*. No. 83. Oxford university press, 1993.
- [30] Natarajan, L. V., et al. "Electro-optical switching characteristics of volume holograms in polymer dispersed liquid crystals." *Journal of Nonlinear Optical Physics & Materials* 5.01 (1996): 89-98.
- [31] Kasap, Safa, Cyril Koughia, and Harry E. Ruda. "Electrical conduction in metals and semiconductors." *Springer handbook of electronic and photonic materials*. Springer, Cham, 2017. 1-1.
- [32] Heilmeyer, George H., and L. A. Zanoni. "guest-host interactions in nematic liquid crystals. a new electro-optic effect." *Applied Physics Letters* 13.3 (1968): 91-92.
- [33] Zakri, Cecile. "Carbon nanotubes and liquid crystalline phases." *Liquid Crystals Today* 16.1 (2007): 1-11.
- [34] Chen, Hui-Yu, Wei Lee, and Noel A. Clark. "Faster electro-optical response characteristics of a carbon-nanotube-nematic suspension." *Applied physics letters* 90.3 (2007): 033510.
- [35] Jeon, Sang Youn, et al. "Effects of carbon nanotubes on electro-optical characteristics of liquid crystal cell driven by in-plane field." *Applied physics letters* 90.12 (2007): 121901.
- [36] Baik, In-Su, et al. "Local deformation of liquid crystal director induced by translational motion of carbon nanotubes under in-plane field." *Journal of applied physics* 100.7 (2006): 074306.
- [37] Efros, A. L., and Boris I. Shklovskii. "Critical behaviour of conductivity and dielectric constant near the metal-non-metal transition threshold." *Physica status solidi (b)* 76.2 (1976): 475-485.
- [38] Ponevchinsky, V. V., et al. "Cluster self-organization of nanotubes in a nematic phase: The percolation behavior and appearance of optical singularities." *JETP letters* 91.5 (2010): 241-244.
- [39] Lisetski, L. N., et al. "Spectrophotometry and electrical conductivity studies of multiwall nanotubes dispersed in nematic liquid crystals." *Functional Materials* (2007).
- [40] *What Are High Aspect Ratio Nanoparticles (HARN)?*, [Online]. Available: [https://www.safenano.org/knowledgebase/resources/faqs/what-are-high-aspect-ratio-nanoparticles-\(harn\)/](https://www.safenano.org/knowledgebase/resources/faqs/what-are-high-aspect-ratio-nanoparticles-(harn)/).
- [41] Steffen, John E. "The Optics of Life: A Biologist's Guide to Light in Nature. Sönke Johnsen." (2012): 331-331.

- [42] Basu, Dipak. *Dictionary of pure and applied physics*. CRC press, 2018.
- [43] Cross, Jason. "Digital Displays Explained." *PCWorld*, 18 Mar. 2012, [Online]. Available: <https://www.pcworld.com/article/469152/digital-displays-explained.html>.
- [44] Davis, Chris. "What Is an IPS Monitor? Monitor Panel Types Explained." *ViewSonic Library*, 25 Mar. 2021, [Online]. Available: <https://www.viewsonic.com/library/photography/what-is-an-ips-monitor-panel/>.
- [45] Demus, D. "Plenary lecture. One hundred years of liquid-crystal chemistry: thermotropic liquid crystals with conventional and unconventional molecular structure." *Liquid Crystals* 5.1 (1989): 75-110.
- [46] "Liquid Crystal Hot Spot Detection." *Procedure - Liquid Crystal Hot Spot Detection*, Internet Archive, 3 Feb. 2001, [Online]. Available: https://web.archive.org/web/20090211050934/http://www.acceleratedanalysis.com/LC_hotspotdetection_procedure.html.
- [47] Bragg's Law. 15 Aug. 2020, [Online]. Available: <https://chem.libretexts.org/@go/page/313>.
- [48] Ge, Jia, and Mable P. Fok. "Ultra high-speed radio frequency switch based on photonics." *Scientific reports* 5.1 (2015): 1-7.
- [49] "RF Switches Information." *RF Switches Selection Guide: Types, Features, Applications | Engineering360*, [Online]. Available: https://www.globalspec.com/learnmore/telecommunications_networking/rf_microwave_wireless_components/rf_switches.
- [50] S. Germain, D. Deslandes and K. Wu, "Development of substrate integrated waveguide power dividers," *CCECE 2003 - Canadian Conference on Electrical and Computer Engineering. Toward a Caring and Humane Technology (Cat. No.03CH37436)*, 2003, pp. 1921-1924 vol.3, doi: 10.1109/CCECE.2003.1226289.
- [51] Hindle, Pat. "The state of RF/microwave switches." *microwave journal* 53.11 (2010): 20-36.
- [52] Blair, Ed, Kalyan Farrington, and Kelvin Tubbs. "Selecting the right RF switch." *Microwave Journal* 32.6 (1989): 161-166.
- [53] "Bias Tee." *Microwaves101*, [Online]. Available: <https://www.microwaves101.com/encyclopedias/bias-tee>.
- [54] Johnstone, Robert W., M. Parameswaran, and Ash Parmaswaran. *An introduction to surface-micromachining*. "Electro-static actuators". Springer Science & Business Media, 2004.
- [55] Amin, Muhammad, Salman Amin, and Muhammad Ali. "Monitoring of leakage current for composite insulators and electrical devices." *Rev. Adv. Mater. Sci* 21.1 (2009): 75-89.

- [56] Dragoman, M., et al. "Microwave switches based on graphene." *Journal of applied physics* 105.5 (2009): 054309.
- [57] Sharma, Pankaj, Julien Perruisseau Carrier, and Adrian M. Ionescu. "Nanoelectromechanical microwave switch based on graphene." *2013 14th International Conference on Ultimate Integration on Silicon (ULIS)*. IEEE, 2013.
- [58] Jahn, Stefan. *Coplanar Waveguides (CPW)*, 30 Dec. 2007, [Online]. Available: <http://qucs.sourceforge.net/tech/node86.html>.
- [59] Margenau, H. "Van der Waals forces." *Reviews of Modern Physics* 11.1 (1939): 1.
- [60] Oberhammer, Joachim. *Novel RF MEMS switch and packaging concepts*. Diss. KTH, 2004.
- [61] Nordquist, Christopher. Olsson, Roy H. *Radio Frequency Microelectromechanical Systems (RF MEMS)*. United States: N. p., 2013.
- [62] Madou, Marc J. *Fundamentals of microfabrication and nanotechnology, three-volume set*. CRC Press, 2018.
- [63] Cao, Tongtong, Tengjiang Hu, and Yulong Zhao. "Research status and development trend of MEMS switches: A review." *Micromachines* 11.7 (2020): 694.
- [64] Kageyama, Tomoaki, et al. "An ohmic contact type RF-MEMS switch having Au-Au/CNTs contacts." *2017 IEEE 12th International Conference on Nano/Micro Engineered and Molecular Systems (NEMS)*. IEEE, 2017.
- [65] Joshitha, C., et al. "Fabrication and investigation of low actuation voltage curved beam bistable MEMS switch." *Microsystem Technologies* 23.10 (2017): 4553-4566.
- [66] "Electroplating 101: How Metal Plating Works." *Formlabs*, [Online]. Available: <https://formlabs.com/blog/electroplating-metal-plating/>.
- [67] How mature is metal manufacturing AMPower maturity index. [Online]. Available: <https://additive-manufacturing-report.com/wp-content/uploads/2020/04/m20-additive-manufacturing-maturity-index-2020.svg>
- [68] Sharma, Ashish Kumar, and Navneet Gupta. "Material selection of RF-MEMS switch used for reconfigurable antenna using ashby's methodology." *progress in electromagnetics research letters* 31 (2012): 147-157.
- [69] Cheng, Chih-Chieh, Balaji Lakshminarayanan, and Abbas Abbaspour-Tamijani. "A programmable lens-array antenna with monolithically integrated MEMS switches." *IEEE Transactions on Microwave Theory and Techniques* 57.8 (2009): 1874-1884.

- [70] Puyal, V., D. Dragomirescu, C. Villeneuve, J. Ruan, P. Pons, and R. Plana, "Frequency scalable model for MEMS capacitive shunt switches at millimeter-wave frequencies," *IEEE Trans. Microw. Theory Tech.*, Vol. 57, No. 11, 2824–2833, 2009.
- [71] Ekkels, P., X. Rottenberg, R. Puers, and H. A. C. Tilmans, "Evaluation of platinum as a structural thin film material for RF-MEMS devices," *J. Micromech. Microeng.*, Vol. 19, 065010–065018, 2009.
- [72] Palego, C., J. Deng, Z. Peng, S. Halder, J. C. M. Hwang, D. I. Forehand, D. Scarbrough, C. L. Goldsmith, I. Johnston, S. K. Sampath, and A. Datta, "Robustness of RF MEMS capacitive switches with molybdenum membranes," *IEEE Trans. Microw. Theory Tech.*, Vol. 57, No. 12, 3262–3269, 2009.
- [73] Alam, A. H. M. Z., M. R. Islam, S. Khan, N. B. Mohd Sahar, and N. B. Zamani, "Effects of MEMS material on designing a multiband reconfigurable antenna," *Iranian Journal Of Electrical and Computer Engineering*, Vol. 8, No. 2, 112–118, 2009.
- [74] Callister, W. D., *Material Science and Engineering: An Introduction*, 7th edition, John Wiley & Sons Inc., New York, 2007.
- [75] Rebeiz, G. M., *RF MEMS: Theory, Design, and Technology*, 3rd Edition, John Wiley & Sons Inc., New Jersey, 2003.
- [76] Palego, C., J. Deng, Z. Peng, S. Halder, J. C. M. Hwang, D. I. Forehand, D. Scarbrough, C. L. Goldsmith, I. Johnston, S. K. Sampath, and A. Datta, "Robustness of RF MEMS capacitive switches with molybdenum membranes," *IEEE Trans. Microw. Theory Tech.*, Vol. 57, No. 12, 3262–3269, 2009.
- [77] Kingsley, N., D. E. Anagnostou, M. Tentzeris, and J. Papapolymerou, "RF MEMS sequentially reconfigurable sierpinski antenna on a flexible organic substrate with novel DC-biasing technique," *J. Microelectromech. Syst.*, Vol. 16, No. 5, 1185–1192, 2007.
- [78] Reines, I., B. Pillans, and G. M. Rebeiz, "Thin-film aluminum RF MEMS switched capacitors with stress tolerance and temperature stability," *J. Microelectromech. Syst.*, Vol. 20, No. 1, 193–202, 2011.
- [79] Dai, C.-L. and J.-H. Chen, "Low voltage actuated RF micromechanical switches fabricated using CMOS-MEMS technique," *Microsyst. Technol.*, Vol. 12, 1143–1151, 2006.
- [80] Peterson, ZM. "Waveguide Cavity Design in Your RF PCB Layout." *Northwest Engineering Solutions LLC*, Northwest Engineering Solutions, 22 Sept. 2020, [Online]. Available: <https://www.nwengineeringllc.com/article/waveguide-cavity-design-in-your-rf-pcb-layout.php>.
- [81] "Coplanar Waveguide." *Microwaves101*, 4 Nov. 2021, [Online]. Available: <https://www.microwaves101.com/encyclopedias/coplanar-waveguide>.

- [82] "Electric & Magnetic Fields." *National Institute of Environmental Health Sciences*, U.S. Department of Health and Human Services, [Online]. Available: <https://www.niehs.nih.gov/health/topics/agents/emf/index.cfm>.
- [83] Ponchak, George E., Linda PB Katehi, and Emmanouil M. Tentzeris. "Finite ground coplanar (FGC) waveguide: Its characteristics and advantages for use in RF and wireless communication circuits." *3rd International Wireless Communications Conference (WCC'98) Digest*, San Diego, CA. 1998.
- [84] J. B. Knorr and K.-D. Kuchler, "Analysis of coupled slots and coplanar strips on dielectric substrate," *IEEE Trans. Microwave Theory Tech.*, Vol. MTT-23, No. 7, pp. 541-548, July 1975
- [85] Peterson, ZM. "Coplanar Waveguide Design for Your RF PCB." *Northwest Engineering Solutions LLC*, Northwest Engineering Solutions, 22 Oct. 2020, [Online]. Available: <https://www.nwengineeringllc.com/article/coplanar-waveguide-design-for-your-rf-pcb.php>.
- [86] R. W. Jackson, "Considerations in the use of coplanar waveguide for millimeter-wave integrated circuits," *IEEE Trans. Microwave Theory Tech.*, Vol. MTT-34, No. 12, pp. 1450-1456, Dec. 1986.
- [87] M. Riazat, R. Majidi-Ahy, and I.-J. Feng, "Propagation modes and dispersion characteristics of coplanar waveguide," *IEEE Trans. Microwave Theory Tech.*, Vol. 38, No. 5, pp. 245-251, March 1990.
- [88] K. Jones, "Suppression of spurious propagation modes in microwave wafer probes," *Microwave Journal*, pp. 173-174, Nov. 1989.
- [89] M. Yu, R. Vahldieck, and J. Huang, "Comparing coax launcher and wafer probe excitation for 10-mil conductor-backed CPW with via holes and airbridges," *IEEE Int. Microwave Symposium Digest*, Atlanta, GA, June 14-18, 1993, pp. 705-708
- [90] C. Sinclair, "A coplanar waveguide 6-18 GHz instantaneous frequency measurement unit for electronic warfare systems," *1994 IEEE Int. Microwave Symposium Digest*, San Diego, CA, May 23-27, pp. 1767-1770, 1994.
- [91] F. Brauchler, S. Robertson, J. East, and L. P. B. Katehi, "W-band finite ground plane coplanar (FGC) line circuit elements," *1996 IEEE Int. Microwave Symposium Digest*, San Francisco, CA, June 17-21, pp. 1845-1848, 1996.
- [92] "Packaging." *Microwaves101*, 4 Nov. 2021, [Online]. Available: <https://www.microwaves101.com/encyclopedias/packaging>.
- [93] MCM & Hybrid Technologies. [Online]. Available: https://www.navsea.navy.mil/Portals/103/Documents/NSWC_Crane/SD-18/PDFs/Products/MCMs/McmTech.pdf

- [94] Anguera, Jaume, et al. "Metallized foams for fractal-shaped microstrip antennas." *IEEE Antennas and Propagation Magazine* 50.6 (2008): 20-37.
- [95] Harris, Jonathan, and M. Matthews. "Selecting die attach technology for high-power applications." *Power Electronics Technology* 35.11 (2009): 18-23.
- [96] S. Kayali, G. E. Ponchak, Resistors, A. "VII. Passive Elements." *GaAs MMIC Reliability Assurance Guideline for Space Applications* (1996): 56.
- [97] Griffin, Donald W., and Andrew J. Parfitt. "Electromagnetic design aspects of packages for monolithic microwave integrated circuit-based arrays with integrated antenna elements." *IEEE Transactions on Antennas and Propagation* 43.9 (1995): 927-931.
- [98] Gantz, Stephen D., and Daniel R. Philpott. *FISMA and the risk management framework: the new practice of federal cyber security*. Newnes, 2012.
- [99] Stewart, James M. "What Is Multiplexing?" *Worldwide IT Training*, Global Knowledge a Skillsoft Brand, 22 Aug. 2013, [Online]. Available: <https://www.globalknowledge.com/us-en/resources/resource-library/articles/what-is-multiplexing/>.
- [100] National Research Council. *Renewing US Telecommunications Research*. National Academies Press, 2006.
- [101] Cyphers, Bennett. "The Case for Fiber to the Home, Today: Why Fiber Is a Superior Medium for 21st Century Broadband." *Electronic Frontier Foundation*, 16 Oct. 2019, [Online]. Available: <https://www.eff.org/wp/case-fiber-home-today-why-fiber-superior-medium-21st-century-broadband>.
- [102] Stark, Wayne Eric , Lehnert, James S. and Borth, David E.. "telecommunication". *Encyclopedia Britannica*, 1 Mar. 2019, <https://www.britannica.com/technology/telecommunication>. Accessed 4 November 2021.
- [103] Łukasiak, Lidia, and Andrzej Jakubowski. "History of semiconductors." *Journal of Telecommunications and information technology* (2010): 3-9.
- [104] Bellavista, Paolo, ed. *Telecommunication systems and technologies-Volume I*. Vol. 5. EOLSS Publications, 2009.
- [105] Uttamchandani, Deepak, ed. *Handbook of MEMS for wireless and mobile applications*. Elsevier, 2013.
- [106] "Vector." *Merriam-Webster*, Merriam-Webster, [Online]. Available: <https://www.merriam-webster.com/dictionary/vector>.

- [107] Bernard Prkić, Understanding Small-Cell Wireless Backhaul, *ElectronicDesign* (Apr. 3, 2014), [Online]. Available: <https://www.electronicdesign.com/communications/understanding-small-cell-wireless-backhaul>
- [108] Wi-Fi Alliance, Wi-Fi Certified WiGig: Multi-gigabit, Low Latency Connectivity, [Online]. Available: <https://www.wi-fi.org/discover-wi-fi/wi-fi-certified-wigig>
- [109] Persano, Anna, et al. "Thin film encapsulation for RF MEMS in 5G and modern telecommunication systems." *Sensors* 20.7 (2020): 2133.
- [110] Ojaroudiparchin, Naser, et al. "A switchable 3-D-coverage-phased array antenna package for 5G mobile terminals." *IEEE Antennas and Wireless Propagation Letters* 15 (2016): 1747-1750.
- [111] Y. Azar et al., "28 GHz propagation measurements for outdoor cellular communications using steerable beam antennas in New York city," 2013 IEEE ICC, pp. 5143–47, 2013.
- [112] D. -G. Yang, D. -O. Kim, and C. -Y. Kim, "Design of internal multi-band mobile antenna for LTE700/WCDMA/UMTS/WiMAX/WLAN operation," PIERS Proceedings, 27-30 March, Kuala Lumpur, pp. 1490-1493, 2012.
- [113] Yaghmaee, Pouria, et al. "Electrically tuned microwave devices using liquid crystal technology." *International Journal of Antennas and Propagation* 2013 (2013).
- [114] C. Fritzsche, S. Bildik, and R. Jakoby, "Ka-band frequency tunable patch antenna," in Proceedings of the IEEE Antennas and Propagation Society International Symposium, pp. 1–2, 2012.
- [115] W. Hu, M. Y. Ismail, R. Cahill et al., "Tunable liquid crystal reflectarray patch element," *Electronics Letters*, vol. 42, no. 9, pp. 509–511, 2006.
- [116] Martin, Noham, et al. "Patch antenna adjustable in frequency using liquid crystal." *33rd European Microwave Conference Proceedings (IEEE Cat. No. 03EX723C)*. Vol. 2. IEEE, 2003.
- [117] Gaebler, A., et al. "Liquid crystal-reconfigurable antenna concepts for space applications at microwave and millimeter waves." *International Journal of Antennas and Propagation* 2009 (2009).
- [118] Partnership, Prime Faraday. "An introduction to MEMS (Micro-electromechanical Systems)." *Wolfson School of Mechanical and Manufacturing Engineering, Loughborough, England* (2002).
- [119] Bulk Micromachining. *Microengineering -- Bulk Micromachining*, [Online]. Available: https://terpconnect.umd.edu/~sandborn/research/JPL_MEMS/microeng_bulk.html.

- [120] Mustafa, Sheelan Muhamed. *Nanoscale Size Dependent Lattice Volume for Si Nanoparticles and Nanowires*. Diss. Salahaddin University-Erbil, 2011.
- [121] Surface Micromachining. *Microengineering –Surface Micromachining*, [Online]. Available: https://terpconnect.umd.edu/~sandborn/research/JPL_MEMS/microeng_surface.html
- [122] Kovacs, G.T.A., *Micromachined Transducers Sourcebook*, McGraw-Hill, New York, NY, 1998.
- [123] Ma, Li-Ya, et al. "Comprehensive study on RF-MEMS switches used for 5G scenario." *IEEE Access* 7 (2019): 107506-107522.
- [124] Miller, Greg. "CPWG (Coplanar Waveguide with Lower Ground Plane)." *Keysight Knowledge Center*, Keysight, 14 Oct. 2008, [Online]. Available: <https://edadocs.software.keysight.com/pages/viewpage.action?pagelid=5928544>.
- [125] Greaves, G. N., Greer, A. L., Lakes, R. S., and Rouxel, T., "Poisson's Ratio and Modern Materials", *Nature Materials*, 10, 823-837 Nov. (2011).
- [126] Hidnert, Peter, and Wilmer Henry Souder. *Thermal expansion of solids*. No. 486-487. US Government Printing Office, 1950.
- [127] Thermal Conductivity. University of Victoria, 9 Sept. 2020, [Online]. Available: <https://phys.libretexts.org/@go/page/7230>.
- [128] Dolgov, L., et al. *Liquid crystal dispersions of carbon nanotubes: dielectric, electro-optical and structural peculiarities*. IntechOpen, 2010.
- [129] James, Richard, et al. "Characterisation and applications of nematic liquid crystals in microwave devices." *Molecular crystals and liquid crystals* 542.1 (2011): 196-718.
- [130] Ponevchinsky, V. V., et al. "Self-organized composites of multiwalled carbon nanotubes and nematic liquid crystal 5CB: optical singularities and percolation behavior in electrical conductivity." *Ninth International Conference on Correlation Optics*. Vol. 7388. International Society for Optics and Photonics, 2009.
- [131] Basu, Rajratan, and Germano S. Iannacchione. "Nematic anchoring on carbon nanotubes." *Applied physics letters* 95.17 (2009): 173113.
- [132] Coluci, Vitor R., et al. "Modeling the auxetic transition for carbon nanotube sheets." *Physical Review B* 78.11 (2008): 115408.
- [133] Zhang, Wei, et al. "Electromagnetic characteristics of carbon nanotube film materials." *Chinese Journal of Aeronautics* 28.4 (2015): 1245-1254.
- [134] Takenaka, Y., and T. Yamamoto. "Light-induced displacement of a microbead through the thermal expansion of liquid crystals." *Soft matter* 13.6 (2017): 1116-1119.

- [135] Yang, Cheng, Yuanhua Lin, and C. W. Nan. "Modified carbon nanotube composites with high dielectric constant, low dielectric loss and large energy density." *Carbon* 47.4 (2009): 1096-1101.
- [136] Zheng, Jinbao, et al. "Nematic liquid crystal 4-cyano-4'-pentylbiphenyl functionalization of MWNTs for improved thermal and mechanical properties of silicone pressure sensitive adhesives." *International Journal of Adhesion and Adhesives* 98 (2020): 102457.
- [137] Groover, Mikell, and E. W. J. R. Zimmers. *CAD/CAM: computer-aided design and manufacturing*. Pearson Education, 1983.
- [138] "HFWorks: EMWorks Inc." *SOLIDWORKS*, 4 Nov. 2021, [Online]. Available: <https://www.solidworks.com/partner-product/hfworks>.
- [139] Pande, Rajesh S., and Rajendra M. Patrikar. "Modeling and Simulation of RF MEMS devices." *WSEAS transactions on electronics* 5.4 (2008): 155-165.
- [140] Harish, Ajay. "What Is FEM & FEA Explained: Finite Element Method." *SimScale*, 20 Dec. 2020, [Online]. Available: <https://www.simscale.com/blog/2016/10/what-is-finite-element-method/>.
- [141] "Multiphysics Cyclopedia." *COMSOL, The Finite Element Method (FEM)*. [Online]. Available: <https://www.comsol.com/multiphysics/finite-element-method>.
- [142] "Discrete." *Merriam-Webster*, Merriam-Webster, [Online]. Available: <https://www.merriam-webster.com/dictionary/discrete>.